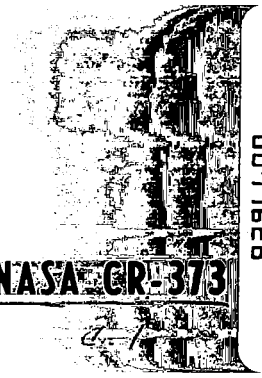

NASA CONTRACTOR REPORT

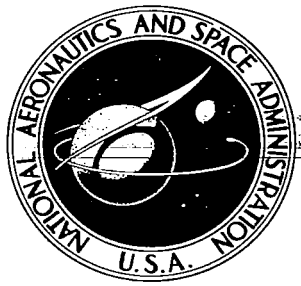

NASA CR-373

EXHAUST JET WAKE AND THRUST CHARACTERISTICS OF SEVERAL NOZZLES DESIGNED FOR VTOL DOWNWASH SUPPRESSION

TESTS IN AND OUT OF GROUND EFFECT WITH 70° F AND 1200° F NOZZLE DISCHARGE TEMPERATURES

by C. C. Higgins, D. P. Kelly, and T. W. Wainwright

Prepared under Contract No. NASw-908 *by*
THE BOEING COMPANY
Renton, Wash.
for

NATIONAL AERONAUTICS AND SPACE ADMINISTRATION - WASHINGTON, D. C. - JANUARY 1966

EXHAUST JET WAKE AND THRUST CHARACTERISTICS OF SEVERAL NOZZLES DESIGNED FOR VTOL DOWNWASH SUPPRESSION

TESTS IN AND OUT OF GROUND EFFECT WITH 70° F AND 1200° F NOZZLE DISCHARGE TEMPERATURES

By C. C. Higgins, D. P. Kelly, and T. W. Wainwright

Prepared under Contract No. NASw-908 by
THE BOEING COMPANY
Renton, Wash.

for

NATIONAL AERONAUTICS AND SPACE ADMINISTRATION

For sale by the Clearinghouse for Federal Scientific and Technical Information
Springfield, Virginia 22151 – Price $3.00

EXHAUST JET WAKE AND THRUST CHARACTERISTICS OF SEVERAL NOZZLES DESIGNED FOR VTOL DOWNWASH SUPPRESSION — TESTS IN AND OUT OF GROUND EFFECT WITH 70°F AND 1200°F NOZZLE DISCHARGE TEMPERATURES

By C. C. Higgins, D. P. Kelly, and T. W. Wainwright

SUMMARY

The jet wake degradation and thrust characteristics of eleven exhaust nozzle models designed for dynamic pressure and temperature reduction in the jet were evaluated statically, using both hot gases and unheated air, and similar tests were conducted with a reference circular nozzle. Additional tests of selected nozzles were conducted to determine effects of fuselage and/or proximity of a ground plane upon thrust and jet wake characteristics.

Results show significant jet wake degradation for all suppressor nozzles tested, both in and out of ground effect and with various fuselage configurations. Most rapid jet wake degradation was achieved with nozzle designs having widely spaced and/or high aspect ratio nozzle elements. Except for regions very close to the nozzle exit, increasing exit wall divergence angles provided only a small improvement in jet wake degradation characteristics.

Thrust losses were a function of nozzle geometry, with losses minimized for nozzles having small exit wall divergence angles and moderate values of aspect ratio of the discharge openings. The effect upon thrust of varying spacing between nozzle elements was not clearly established by these tests. Combining the nozzles with a fuselage resulted in additional thrust losses; these losses further increased when operating in proximity with a ground surface. Ventilation of the fuselage reduced thrust losses, particularly with suppressor nozzles, but all nozzle and fuselage configurations exhibited large losses when tested in proximity to a ground surface. These thrust losses were associated with the large projected fuselage area used in the present tests, and it is concluded that the projected area must be minimized if excessive losses are to be avoided during operation in ground effect.

INTRODUCTION

Ground impingement of the downwash from VTOL aircraft can produce operational problems of varying degree, depending upon the type of landing site and the disc-loading of the lift system. With jet powered VTOL aircraft built to date, operations have been conducted primarily from prepared sites, thereby avoiding problems of surface deterioration from impingement of high velocity, high temperature exhaust gases on unprotected natural surfaces. Some success has been achieved with operational techniques which reduce exposure time of the surfaces to jet impingement, and ways of rapidly preparing the sites with surface coatings are being investigated. Other solutions to the jet impingement problem have been proposed, but no solution appears to be completely satisfactory at this time. Many of the proposed solutions involve some operational or logistic penalties, and other approaches to the problem must be investigated if VTOL aircraft are to achieve maximum utilization. In practice, a combination of the best elements of a number of solutions may be required to achieve the desired operational capability.

In an effort to reduce the severity of the fundamental problem, particularly with jet-lift aircraft with high disc loadings, a program to evaluate various exhaust nozzle design factors which could lead to a reduction of dynamic pressures and temperatures at the ground surface was undertaken (reference 1). The current effort represents a follow-on to the program reported in reference 1; emphasis in the current tests was directed toward an evaluation of the nozzle performance and jet wake degradation characteristics of suppressor nozzle designs under representative jet engine nozzle discharge temperatures and pressures. Effects of a simulated fuselage upon installed nozzle performance, together with the effects of an adjacent ground plane, were evaluated. Significant thrust losses due to adverse pressure fields induced on the undersurface of the fuselage (i. e. , suck-down losses) have been reported by other investigators, references 2, 3, and 4, and it was anticipated that the higher rates of mixing associated with suppressor nozzles would result in proportionately larger thrust losses.

Twelve nozzle configurations were evaluated in the current tests, designated as Phase II tests to distinguish the present efforts from those reported in reference 1, which are designated as Phase I tests. Of the twelve nozzle configurations tested, three nozzles duplicated Nozzles No. 1, No. 8, and No. 12 of the Phase I tests. Nine additional nozzles, each with four parallel rectangular discharge ports, were designed to investigate in greater detail the range of nozzle design parameters applicable to VTOL jet lift aircraft. The principal design parameters were:

1) spacing between nozzle elements

2) internal exit wall divergence angle

3) aspect ratio of the elements forming the nozzle exit

All nozzle designs were evaluated without fuselage or ground plane at both 70° F and 1200° F nozzle discharge temperatures. Surveys of the pressures and temperatures in the jet wake of each nozzle were made at a nozzle pressure ratio of 2.0, while thrust measurements were made over a range of nozzle pressure ratios from 1.3 to 2.5. Following these tests, the thrust and jet wake degradation characteristics of the circular nozzle and two suppressor nozzles were evaluated with a large simulated fuselage out of ground effect in which varying degrees of fuselage ventilation were provided. Testing was completed with these three nozzles and various fuselage configurations while operating at a distance of five equivalent nozzle diameters from a ground plane. Thrust measurements and surveys of jet wake pressures and temperatures in the efflux over the surface of the ground plane were obtained in these tests. Except for differences of procedure and equipment necessitated by the tests at 1200° F exhaust gas temperatures, the current tests were conducted in a manner similar to those of the Phase I tests.

This research was sponsored by the National Aeronautics and Space Administration through the Office of Grants and Research Contracts under Contract NASw-908.

SYMBOLS

A_e	exit area of the nozzle, square inches
A_f	projected area of the fuselage on the ground plane, square inches
AR	aspect ratio, D^2/Area or length/width
C_F	mass flow coefficient, actual mass flow/ideal mass flow
C_p	static pressure coefficient, $p_{s\ measured} - p_o / p_{t_n} - p_o$
C_{v_e}	effective velocity coefficient, effective exit velocity/ideal exit velocity. Effective velocity = $(\text{thrust/mass flow})_{actual}$
ΔC_{v_e}	incremental change of effective velocity coefficient
D_a	diameter of nozzle exit, inches
D_e	diameter of a circular nozzle with exit area equal to that of a non-circular nozzle, inches
L	length of an element of rectangular exit planform, inches
W	width of an element of rectangular exit planform, inches

R	radial distance from center of ground plane, inches
S	distance between centerlines of nozzle elements, inches
X, Y, Z	axes of a right hand coordinate system with the Z axis in the direction of flow. Also designates distances along each respective axis from center of nozzle exit, inches
X	distance from core or "apparent core" to any point in the mixing region, measured parallel to the X axis, inches (ref. figure 29).
$X_{.25q_{z_{max}}}$	distance from core or "apparent core" to reference contour at twenty-five per cent dynamic pressure, inches (ref. figure 29).
$X_{.50\tau_{z_{max}}}$	distance from core or "apparent core" to reference contour at fifty per cent differential temperatures, inches (ref. figure 29, by analogy).
Y	distance from core or "apparent core" to any point in the mixing region, measured parallel to the Y axis, inches (ref. figure 29).
$Y_{.25q_{z_{max}}}$	distance from core or "apparent core" to reference contour at twenty-five per cent dynamic pressure, inches (ref. figure 29).
$Y_{.50\tau_{z_{max}}}$	distance from core or "apparent core" to reference contour at fifty per cent differential temperatures, inches (ref. figure 29, by analogy).
h	height above the ground plane, inches
h_c	distance from ground plane to the end of the jet core, inches
ΔL	load induced on plate, lb.
n	number of exit segments
p_o	atmospheric pressure, lbs/sq ft
p_{s_f}	static pressure measured by orifices in the fuselage surface, lbs/sq ft
p_{s_g}	static pressure measured by orifices in the ground plane, lbs/sq ft

p_{s_z}	static pressure at any specified point in the jet wake, lbs/sq ft
p_t	total or stagnation pressure, lbs/sq ft
p_{t_n}	total or stagnation pressure at the nozzle exit, lbs/sq ft
p_{t_z}	total or stagnation pressure at any specified point in the jet wake, lbs/sq ft
$p_{t_{gr}}$	total or stagnation pressure at any specified point on, or over the ground plane, lbs/sq ft
q	compressible dynamic pressure, $p_t - p_o$, lbs/sq ft
q_n	compressible dynamic pressure at the nozzle exit, $p_{t_n} - p_o$, lbs/sq ft
q_z	compressible dynamic pressure at any specified point in the jet wake, $p_{t_z} - p_o$, lbs/sq ft
$q_{z_{max}}$	maximum compressible dynamic pressure measured at any specified transverse plane perpendicular to the Z axis, $p_{t_{z_{max}}} - p_o$, lbs/sq ft
q_g	compressible dynamic pressure at any specified point on, or adjacent to, the ground plane, $p_{t_{gr}} - p_o$, lbs/sq ft
$q_{g_{max}}$	maximum compressible dynamic pressure measured on, or adjacent to, the ground plane at specified distances of the ground plane from the nozzle, $p_{t_{gr_{max}}} - p_o$, lbs/sq ft
q_{g_s}	local dynamic pressure measured on, or adjacent to the ground plane $p_{t_{gr}} - p_{s_g}$, lb/sq ft
$q_{g_{s_{max}}}$	maximum local dynamic pressure measured on, or adjacent to the ground plane $p_{t_{gr_{max}}} - p_{s_g}$, lb/sq ft
T	jet thrust, lbs

t_o	ambient temperature, °F
t_t	total or stagnation temperature, °F
$t_{t_{gl}}$	total temperature measured in the boundary layer immediately adjacent to the ground plane, °F
$t_{t_{gl_{max}}}$	maximum total temperature measured in the boundary layer immediately adjacent to the ground plane, °F
$t_{t_{gr}}$	total temperature measured in the jet efflux over the ground plane, °F
$t_{t_{gr_{max}}}$	maximum total temperature measured in the jet efflux over the ground plane, °F
t_{t_n}	total temperature at nozzle exit, °F
t_{t_z}	total temperature measured at any specified point in the jet wake, °F
$t_{t_{z_{max}}}$	maximum total temperature measured at any transverse plane perpendicular to the Z axis, °F
Z_c	length of unmixed jet core, measured from nozzle exit, inches
β	nozzle wall divergence angle, referred to the longitudinal axis of the nozzle, degrees
Γ	nozzle wall convergence angle, referred to the longitudinal axis of the nozzle, degrees
τ_g	differential temperature at any specified point on, or adjacent to, the ground plane $t_{t_{gl}} - t_o$ or $t_{t_{gr}} - t_o$, °F
$\tau_{g_{max}}$	maximum differential temperature at any specified point on, or adjacent to, the ground plane $t_{t_{gl_{max}}} - t_o$ or $t_{t_{gr_{max}}} - t_o$, °F
τ_n	differential temperature at the nozzle exit, $t_{t_n} - t_o$, °F
τ_z	differential temperature at any specified point in the jet wake, $t_{t_z} - t_o$, °F
$\tau_{z_{max}}$	maximum differential temperature measured at any specified transverse plane perpendicular to the Z axis, $t_{t_{z_{max}}} - t_o$, °F
θ	angle subtended by a nozzle sector, degrees

APPARATUS AND PROCEDURE

Models

The nozzle models used in this program are described in figures 1 through 4 while figure 5 gives details of the fuselage configurations used with nozzles 1.1, 2.1, 2.5, 2.6, and 2.8. The circular and twelve segment nozzles shown in figure 1 were the same nozzles (designated as nozzles Nos. 1 and 12 during the Phase I tests, reference 1) previously tested, while the delta nozzle shown in figure 1 was a new nozzle of stainless steel which duplicated the contours of the previous fiberglass delta nozzle.

The circular nozzle provided a reference standard to which the performance of the remaining nozzles could be compared, while the delta and twelve segment nozzles provided correlation with previous Phase I tests at lower pressures and temperatures. Basic characteristics of these nozzles are shown in the following table:

Nozzle No.	Configuration
1.1	Circular Nozzle
1.2	Delta Nozzle $AR = 5$, $\beta = 5°$
1.3	Twelve Segment Suppressor Nozzle, $\theta = 6°$

The additional nine nozzles shown in figure 2 consisted of four rectangular discharge elements which were designed to cover the probable range of nozzle geometry applicable to jet-lift VTOL aircraft. Nozzle design parameters for the four-element suppressor nozzles were (1) nozzle internal wall divergence angle, β ; (2) spacing to width ratio of the nozzle elements, S/W; and (3) aspect ratio of the nozzle element, AR . The dimensions of the four-element suppressor nozzles 2.1 through 2.9, are shown in figure 3. Configurations were selected so that a systematic variation of each of the nozzle design parameters was obtained for at least three nozzles. The nozzles selected are shown in the following table:

Nozzle No.	Variable Investigated	Variables Held Constant
2.1 2.2 2.5 2.7	β = 0° to 30°	AR = 5.0 S/W = 3.0
2.3 2.4 2.5 2.6	S/W = 1.5 to 4.0	AR = 5.0 β = 15°
2.8 2.5 2.9	AR = 3.0 to 10.0	S/W = 3.0 β = 15°

All nozzles were designed to have the same physical exit area as that of the three-inch-diameter circular nozzle. The four-element suppressor nozzles were designed with internal contours which provided similar cross-sectional area distributions as shown in figure 4. All nozzles, except Nos. 1.1 and 1.3, were fabricated of stainless steel for dimensional stability at the 1200° F exhaust gas temperatures. Circular nozzle No. 1.1 was fabricated with thick walls of mild steel, and distortion did not appear to be a problem. However, thermal distortion and failure of a weld occurred with the twelve segment nozzle, and only a limited number of tests were conducted.

The fuselage incorporated large orifices on the "upper" side of the fuselage which would permit ambient air to flow from the upper fuselage surface into the fuselage cavity; for some of the tests these orifices were covered with solid plates to prevent the flow of ventilating air through the fuselage. The lower surface of the fuselage also incorporated removable plates which permitted variation in the clearance between the nozzle and the lower surface of the fuselage. With these plates, clearances of 0, 0.5, and 1.5 inches were tested with circular nozzle 1.1 and suppressor nozzles 2.1 and 2.5. Combining variation of lower fuselage clearance space with upper fuselage ventilation openings provided six fuselage and nozzle configurations; of these, the two extreme configurations were investigated in greatest detail; i.e., sealed nozzle and fuselage for minimum ventilation in one case, and maximum nozzle clearance with upper fuselage open for maximum ventilation in the other case. The fuselage was constructed primarily of aluminum, but the plates used to vary the clearance between the nozzles and the lower fuselage surface were fabricated from stainless steel. For the plates which reduced the clearance space between the nozzles and fuselage to zero, a perfect seal was not achieved and spaces on the order of 0.02 inches existed between the nozzles and the fuselage at some points.

Nozzle Test Rig

A schematic of the test facility is shown in figure 6. Additional details of the instrumentation are shown in figure 7, and photographs of the rig and instrumentation are shown in figure 8.

As in the Phase I tests, the nozzle models were installed on a bellmouth transition section at the end of a twenty-inch inside diameter plenum chamber. Three internal baffle plates and a screen were used to provide uniform flow at the entrance to the bellmouth section. The plenum was suspended by means of four flexures which minimized resistance to fore and aft movement. Thrust loads were balanced only by the strain-gaged thrust ring and a small force resulting from deflection of the flexible inlet air pipe. Direct calibration of the installed strain-gaged thrust ring by means of dead weights effectively isolated nozzle thrust forces from any mechanical loads imposed by the inlet air pipe and other service connections.

Airflow was measured with an ASME long radius flow nozzle upstream of the air preheater, and a dual valve arrangement permitted a constant Mach number to be maintained through the flow nozzle. Filtered air for the nozzle tests was obtained from a laboratory supply system at approximately 70° F with a dew point of -40° F or less. For hot gas testing a propane-fired preheater was installed upstream of the plenum chamber.

Pressure measurements in the jet wake were obtained with a remotely-controlled pitot-static probe which could be traversed along each coordinate axis of the model. Pressures were sensed by means of transducers. Pressures obtained in wake surveys were recorded directly as a function of probe position on Moseley X-Y plotters; other pressure data were recorded either manually or automatically on IBM punch card equipment.

Temperature measurements in the jet wake were obtained with a forty-one element chromel-alumel thermocouple rake installed on the mast of the probe traversing mechanism; the thermocouples were of the shielded stagnation type shown in figure 7. For the hot gas tests, operating conditions were based upon the maximum temperature found with the forty-one element thermocouple rake when positioned at the nozzle exit plane; this nozzle discharge temperature was then maintained throughout the jet wake surveys or other tests by means of a reference thermocouple just upstream of the nozzle exit. For the 1200° F nozzle discharge condition of the present tests, the average nozzle discharge temperature was found to be 1161° F. A thermal profile was present at the nozzle exit, apparently the result of non-uniform temperature distribution generated within the propane fired preheater.

A 24 inch by 36 inch translating ground plane was instrumented as shown in figures 7 and 8 to measure pressures and temperatures at the surface. Pressure and temperature surveys in the boundary layer above the ground plane were obtained using traversing five-element total pressure and stagnation temperature rakes of the type shown in figure 7. Surveys along the major and minor

axes were obtained by rotating the nozzles (and fuselage when used) 90 degrees at a quick-disconnect nozzle flange.

Data Accuracy

Repeated calibrations and checks on the rig instrumentation and read-out equipment were made during the program, and it is believed that all data, with the exception of the temperatures, were accurate within ± 0.5 per cent of full scale values. Temperatures were repeatable within ± 15° F, or in the case of differential temperature ratios, ± 1.0 per cent. Shielded thermocouples were used, where possible, to minimize radiation effects at the thermocouple junctions, and it is believed that the accuracy of these readings was within ± 2.0 per cent of full scale value

RESULTS

Method of Data Presentation

Because of uncertainties associated with static pressure measurements in an intensely turbulent stream, all dynamic pressure measurements are presented as differentials between indicated probe total pressure and atmospheric pressure. Static pressures are presented as differential pressures with respect to atmospheric pressures. Presentation of dynamic pressure data in this form introduces effects of compressibility, but the treatment is consistent with previous investigations. The use of dimensionless ratios further minimizes possible errors due to compressibility effects. Sign conventions have been taken as positive for values where the measured pressure was greater than atmospheric, and negative when the pressure was less than atmospheric.

In the case of dynamic pressures determined with respect to a ground surface, it has been found advantageous in some analyses to use the differential pressure between total pressure measured above the ground and a local static pressure measured at the surface of the ground plane, rather than a differential between the total pressure above the ground plane and atmospheric. Wherever this procedure has been followed, the resultant dynamic pressure has been designated as a local dynamic pressure, to distinguish from dynamic pressures referenced to atmospheric pressure. Data obtained for the tests in ground effect have been presented in both forms; consequently, care must be used in making comparisons between various sections or figures of this report.

Nozzle Performance Evaluation

Effective velocity and mass flow coefficients were determined for all basic nozzles using unheated air; a typical test configuration is shown in figure 8a. Results for the three Phase I nozzle configurations previously evaluated in reference 1 are shown in figure 9a. Other results obtained in these tests have been grouped according to the suppressor nozzle design parameters of exit wall angle β, aspect ratio of the elements AR, and spacing to width ratio S/W, figures 9b, 9c and 9d. It may be seen from these results that, in general, both effective velocity and mass flow coefficients increased with increasing nozzle pressure ratio. In general, effective velocity and mass flow coefficients decrease progressively with increasing exit wall angle, increasing aspect ratio of the nozzle elements, and increasing spacing to width ratio. However, the mass flow coefficients for nozzle 2.3 show a reversal of trend at low nozzle pressure ratios. This effect is believed to be related to internal flow separation due to local high velocities and unfavorable pressure gradients associated with exit wall divergence angle $\beta = 15°$ and the small exit wall convergence angle $\Gamma = 8.4°$. The other nozzles in this series (nozzles 2.4, 2.5, and 2.6) had larger values of exit wall convergence angle Γ, thus providing more favorable pressure gradients and lower velocities at any specified cross section prior to the nozzle exit.

Following evaluation of the basic nozzles, tests were conducted with nozzles Nos. 1.1, 2.1, 2.5, 2.6, and 2.8 in conjunction with an unventilated fuselage, similar to that shown in figure 8c. The effect of a ground plane on effective velocity and flow coefficients was evaluated in this series of tests. Results obtained in ground effect and out of ground effect for both the basic nozzle and the unventilated fuselage configurations are shown in figure 10 for nozzles Nos. 1.1, 2.1, and 2.5. These results indicate that effective velocity coefficients were reduced by either the presence of a fuselage or ground plane, and largest reductions were found when the fuselage and ground plane were tested together. These effects are caused by reduced static pressures acting over the projected area of the fuselage and plenum, rather than changes in the effective velocity coefficient of the basic nozzles. No significant effects upon mass flow coefficients were noted for any configuration of fuselage or ground plane evaluated in the present program.

The effects of variation of the clearance between the nozzle exit and fuselage lower surface upon thrust were evaluated for two conditions of fuselage cavity ventilation; i.e., upper fuselage inlets were either both open or both closed. The results for tests out of ground effect are shown in figure 11, while results obtained in ground effect are shown in figure 12 for the circular nozzle 1.1 and suppressor nozzles 2.1 and 2.5. These results indicate that increased clearance between the nozzle and fuselage improves effective velocity coefficient, while mass flow coefficients remain essentially unchanged in all cases. Largest benefits of clearance between the nozzles and fuselage were obtained with the suppressor nozzles, and it was found that a clearance of 0.5 inches was nearly as effective as a clearance of 1.5 inches. Ventilating the fuselage cavity resulted in only minor improvement in effective velocity coefficients.

Similar, but less extensive, data were obtained for suppressor nozzles 2.6 and 2.8, figure 13. In this figure, the effect of the ground plane upon effective velocity and mass flow coefficients is shown for two fuselage configurations; namely, (a) non-ventilated fuselage cavity with no clearance between nozzle exit and fuselage lower surface, and (b) ventilated fuselage cavity with maximum clearance of 1.5 inches between the nozzle exit and the fuselage lower surface. The first configuration of fuselage described in (a) is designated as the non-ventilated fuselage, while the second configuration of fuselage described in (b) is designated as a ventilated fuselage. These designations will apply to figure 13 and all subsequent figures of this report in which effects of fuselage configuration are being presented. Although testing only two fuselage configurations with each nozzle of interest eliminates some fuselage/nozzle interactions, it was felt that the two extremes of fuselage/nozzle clearance and cavity ventilation would bracket reasonably well the range of effects which would be encountered in practical applications.

From the results shown in figures 9 through 13, it is apparent that overall thrust of the various nozzle and fuselage configurations is influenced significantly by (1) internal nozzle geometry, (2) fuselage to nozzle clearance, and (3) proximity to a ground surface. Additional results which may be of assistance in further evaluating these factors will be presented in subsequent sections of this report.

Free Jet Wake Surveys

Typical results of pressure surveys of four-element suppressor nozzles are shown in figure 14 for nozzle 2.1. The data obtained from the surveys of the jet wake of several basic nozzles were cross-plotted as shown in figure 15 in order to provide "contour maps" of dynamic pressure and differential temperature, along the major axes of the nozzles. From these plots, the relative rate of mixing of the various jet wakes is readily apparent, as are the subsequent growth and merging patterns of the jets from each discharge opening of the multiple-element suppressor nozzles. The point at which merging of these individual jets occurs is largely determined by the spacing between the nozzle elements. Because the relative rate of mixing of the overall jet wake is also strongly influenced by the merging characteristics of the individual jets, it is apparent that spacing between the nozzle elements is an important factor in determining the pressures and temperatures imposed upon a ground surface during VTOL aircraft operations.

Maximum values of dynamic pressure and differential temperature in the jet wake at selected distances downstream of the nozzle exit are shown in figures 16 and 17 for each of the basic nozzles tested. Maximum values of dynamic pressure and differential temperature, rather than average values, have been used as a criterion of erosion characteristics of the nozzles by other investigators and, as shown in reference 5, correlation between maximum values of jet wake dynamic pressure and erosion characteristics of various ground

surfaces has been obtained experimentally. In addition, the maximum values of dynamic pressure and differential temperature provide a valid indication of the rapidity of mixing of the entire jet, inasmuch as the central regions of the jet will be the last regions to be affected by the shear generated turbulence originating on the perimeter of the jet.

The data of figures 16 and 17 show that the suppressor nozzles produced significantly greater decay of the pressures and temperatures in the jet wake, compared with the decay characteristics of the circular nozzle. The suppressor nozzles were less effective in reducing differential temperatures in the jet wake than in reducing dynamic pressures. The differences in jet wake degradation characteristics shown in figures 16 and 17 for nozzles 2.3 and 2.4 are due to differences in the merging of the individual jets.

Differences in the jet wake degradation characteristics of the various nozzles at discharge temperatures of 70°F and 1200°F may be determined also from the data of figures 16a and 16b. In general, the decay of the jet wakes occurred more rapidly at the higher nozzle discharge temperatures, with the largest changes found in tests of the circular nozzle. The effect of temperature upon the decay characteristics of the suppressor nozzles is similar to that of the circular nozzle, but is much less evident because of the masking effect of the high mixing rates inherent with the suppressor nozzle configurations.

Results obtained from surveying the jet wake dynamic pressures and temperatures in various locations removed from the central axes of the nozzle, figure 18, show that the two outer jets of the four slot suppressor nozzles decay much more rapidly than the two inner jets. The results of figure 18 indicate that total pressures less than ambient will be found in the regions between the individual nozzle discharge elements. These negative pressure regions represent a thrust loss which cannot be separated from the internal flow losses with the test rig force measurements obtained.

Fuselage and Ground Plane Effects

Figure 19 shows maximum values of the dynamic pressure ratio and differential temperature ratio on or above the ground plane for various nozzle and fuselage configurations. The dynamic pressure and differential temperature degradation curves for the basic nozzles provide a comparison with mixing rates previously determined in the free jet tests. For the circular nozzle, values of pressures and temperatures over the ground surface were less than measured in the free jet wake at $Z/D_e = 5$. Conversely, values of pressures and temperatures over the ground surface were somewhat higher for the suppressor nozzles. For the distance of five nozzle diameters maintained between the ground surface and the nozzle exit in the present tests, the results indicate that the ground plane did not greatly disturb the degradation of the jet wake prior to impingement with the ground surface.

Additional results obtained from the dynamic pressure and differential temperature surveys over the ground plane are shown in figures 20 and 21. The dynamic pressure profiles (referenced to ambient pressure) of the suppressor nozzles are smaller in value and show less variation with height above the ground

than do the profiles produced by the circular nozzle. This result is attributable to the greater mixing in the jet wakes of the suppressor nozzles. The values of dynamic pressures and differential temperatures over the ground plane were slightly higher in tests of the basic nozzles, compared with non-ventilated fuselage and nozzle configurations. Surveys over the ground plane indicated that larger values of dynamic pressure were present along the major axis (X axis) of the nozzles and fuselage than along the minor axis (Y axis). A similar but much smaller effect of nozzle and fuselage orientation with respect to the ground plane was observed in the differential temperatures measured in the jet efflux over the ground plane. Because effects of orientation were observed in tests with and without the fuselage, it is believed that these effects are related to nozzle geometry.

Some of the dynamic pressures measured in the surveys of the efflux over the ground plane were found to be lower than the static pressures measured on the surface of the ground plane at corresponding radial locations from the center of the ground plane; these data have been indicated by broken lines in figures 20b and 20c. It is believed that these data are an indication that the efflux over the ground plane at these locations was flowing radially toward the center of the ground plane rather than radially away from the center of the ground plane. Radial inflow direction over the ground plane may be caused by merging of the jets impinging at points not located at the center of the ground plane. Further evidence of this behavior may be seen in the free jet wake surveys of nozzle 2.1, figure 14a.

Contour maps of static pressure coefficients and local gas temperatures on or immediately above the ground plane are presented for the circular nozzle and suppressor nozzles 2.1 and 2.5 with non-ventilated fuselage configurations, figure 22. These data were obtained using the instrumented traversing ground plane, details of which are shown in figures 7 and 8b. The contours obtained in the circular nozzle tests were nearly symmetrical with respect to the center of the ground plane, but the contours developed for the suppressor nozzles contained distinct "islands" of high static pressures displaced 1.0 to 1.5 nozzle diameters from the center of the ground plane. A large region of nearly uniform temperature was found at the center of the ground plane during the suppressor nozzle tests.

While it is difficult to obtain meaningful measurements near the point of jet impingement, it is believed that some useful interpretation of the flow field may be made from the difference between total pressure measurements just above the ground plane boundary layer and the static pressures measured on the surface of the ground plane. Figure 23 shows the radial distribution of maximum local dynamic pressures ($q_{g_{s\ max}}/q_n$) along the major and minor axes of the ground plane, together with the corresponding radial variation of the maximum differential temperature ratios ($\tau_{g\ max}/\tau_n$). For the circular nozzle, figure 23a, the local dynamic pressure is very low near the center of the ground plane. The local dynamic pressure increases to a maximum at approximately one diameter from the center, and then decreases in an exponential manner with radial distance beyond that point. The radial distribution of maximum differential

temperature above the ground plane exhibited highest values at the center of the ground plane, and these values decreased non-linearly with radial distance from the center.

Local dynamic pressures over the ground plane in the suppressor nozzle tests acted in a manner similar to that of the circular nozzle; however, the highest values were found at radial distances of 1.5 to 2.0 nozzle diameters from the center of the ground plane. These results are due to merging characteristics of the jets, as noted above for figures 20b and 20c. The "negative" values of local dynamic pressures in figures 23b and 23c are also an indication of the radial inflow toward the center of the ground plane. Surveys parallel to the major and minor axes of the suppressor nozzles and fuselage (X and Y axes) show that higher values of the local dynamic pressure and differential temperature ratios are found along the major axis, both with and without fuselage; consequently, it was concluded that the primary factor which produces the effects noted is nozzle geometry.

The radial distribution of flow from the point of impingement of a circular jet has been investigated in references 5 and 6, and results similar to that shown in figure 23a were obtained. However, the nozzles used in these investigations exhibited differences in the jet core length which were reflected in differences in the magnitude of local dynamic pressures measured over the ground surface. It has been suggested that the distance from the end of the jet core to the ground plane constitutes a reference parameter of jet wake mixing characteristics. Figure 24 shows the correlation between the results of references 5 and 6 and the present tests.

Figure 25 shows the distribution of static pressure coefficients over the lower fuselage surface, while figure 26 shows the variation of these fuselage static pressure coefficients with distance radially from the nozzle exit. Increased static pressure differentials ($p_{s_f} - p_o$) were found in ground effect. Largest static pressure differentials were found to occur very near the nozzle exit. These differentials were both large and non-uniform in the region between elements of the suppressor nozzles. Static pressure differentials found between outermost suppressor nozzle elements were much larger for nozzle 2.5 than 2.1, indicating a strong influence of wall divergence angle β upon local jet entrainment. The largest values of static pressure differentials were located near the outer ends of the suppressor nozzle elements, as indicated by the "islands" in figure 25. The static pressure differentials between the outermost nozzle elements were larger than the corresponding static pressure differentials between the two most centrally located elements.

Temperature distributions on the lower fuselage surface are shown in figure 25. Measurements were made with the ground plane at a distance of five diameters from the nozzle exit. At the nozzle discharge temperature of 1200° F, temperatures on the fuselage were less than 200° F.

DISCUSSION

Free Jet Characteristics of Basic Nozzles

In order to be effective, suppressor nozzle designs must substantially reduce the dynamic pressures and temperatures of the jet wake prior to impingement on the ground surface. A primary consideration in the program has been the evaluation of those factors which could alter the mixing rates in the jet wake. The objective of Phase II of the program has been the evaluation of VTOL nozzle design parameters and configurations which promise significant reduction of the dynamic pressures and temperatures imposed upon a ground surface, consistent with minimum thrust reduction. The effects of a fuselage and of a ground plane upon jet mixing and nozzle thrust were investigated.

Effects of nozzle wall discharge angle, discharge aspect ratio, and spacing to width ratio upon dynamic pressure and differential temperature degradation of free jets of the basic nozzles are shown in figures 27 and 28. The gains due to increasing nozzle wall divergence angle and aspect ratio are shown to be minor, except at small distances from the nozzle exit. Variation of the spacing between the nozzle elements was found to be an important parameter in determining jet wake degradation (figures 27 and 28); maximum degradation was achieved with the largest values of the spacing ratio.

Data obtained from the jet wake surveys were used to determine the rate of spreading of the jet wake and the progression of the mixing process in a manner similar to that used in the Phase I tests, reference 1. By non-dimensionalizing the respective dynamic pressures and differential temperatures against selected reference values, it was possible to collapse the dynamic pressure and differential temperature distributions across the jet wake onto "universal" profiles as shown in figure 29. The results presented in figure 29 indicate that the shear-generated turbulent mixing processes remain generally similar throughout the fully developed jet wake region. However, the rate of spreading of the jet appears to be influenced by factors related to nozzle geometry, and the general observation may be made that those jets which spread most rapidly also decay most rapidly with distance from the nozzle exit. Because of the interrelationship between nozzle geometry and the subsequent spreading characteristics of the jet wake from suppressor nozzles, methods of predicting the location of the reference dynamic pressures and differential temperatures appear to be less than satisfactory at this time.

In order to investigate changes in the mechanics of mixing as a function of nozzle design, the maximum dynamic pressure ratio at several locations downstream from the nozzle exit of each basic nozzle was compared with the maximum differential temperature ratios at corresponding locations, figure 30a. Maximum values of dynamic pressures and temperatures maintain a well established relationship along the jet for all nozzle configurations in which merging between individual jets does not occur. Figure 30a shows that temperature

degradation lags dynamic pressure degradation in the fully developed mixing region of the jets. For jets in which merging occurred, the decay of differential temperatures was inhibited to a greater degree than the decay of dynamic pressures. Turbulent energy dissipation continues during the merging process, but only small amounts of external air can enter the mixing zone between the jets to reduce the temperatures.

Figure 30b shows that the distance from the nozzle exit at which a specific ratio of dynamic pressure to differential temperature occurs is distinctly different for various basic nozzle configurations. The suppressor nozzles, because of the rapid rates of dynamic pressure degradation achieved, quickly reach ratios of dynamic pressure to differential temperature which correspond to similar ratios found much farther downstream in the jet wake of a circular nozzle. The principal effect achieved by the suppressor nozzles is a compression of the distance scale in which the mixing occurs.

Comparisons of the free jet maximum dynamic pressure and differential temperature degradation of the various nozzles with that of the circular nozzle have been made in figure 31. These curves were determined by finding the differences between the respective quantities for the suppressor and circular nozzles for various distances downstream from the nozzle exit. These curves represent an incremental gain (in terms of nozzle exit values) which can be obtained by use of each suppressor nozzle as contrasted with that of the circular nozzle. It is seen that gains on the order of 70 per cent in dynamic pressure reduction and 50 per cent in differential temperatures may be obtained by using suppressor nozzles. For the nozzles tested, maximum gains occur at approximately five to six nozzle diameters from the exit. Because of the nature of the circular nozzle degradation curve, the distance from the ground surface for maximum gains will always occur in the range of four to six equivalent circular nozzle diameters.

Data from figure 31, when combined with the effective velocity coefficients of each nozzle, can be used to show the trades between jet wake degradation characteristics and nozzle thrust performance. Figure 32 shows the trades for a distance of five equivalent nozzle diameters from the nozzle exit. The results indicate that dynamic pressure and differential temperature degradation are nearly independent of nozzle thrust coefficient. Maximum degradation with minimum thrust losses were achieved with nozzles 2.1, 2.2, 2.6, 2.8, and 1.3, and it was found that best results from the Phase II tests correspond well with the best results of the Phase I tests. It should be noted that thrust losses were largest with nozzles 2.7, 2.9, 2.3, and 2.5, i.e., nozzles with large wall divergence angles ($\beta \geq 15°$), small spacing to width ratio (S/W = 1.5), and high aspect ratio ($AR = 10$).

Nozzle 2.4 showed somewhat better thrust performance than would be anticipated on the basis of the performance of nozzles 2.3, 2.5, and 2.6. The value of effective velocity coefficient shown for nozzle 2.4 in figure 32 was verified by several check runs. In comparison with the performance of nozzle

2.4, nozzle 2.3 exhibits a markedly lower effective velocity coefficient. The low effective velocity coefficient of 2.3 is attributed to large internal losses. Consequently, it is possible to visualize nozzle designs with small spacing to width ratios (i.e., $S/W < 2.0$) which have high velocity coefficients. If a point is visualized with an effective velocity coefficient of approximately 0.96 to 0.97 instead of the 0.94 found with nozzle 2.3, then the curve connecting nozzles of variable S/W in figure 32 would assume a shape similar to that of the envelope curve from the Phase I tests.

Fuselage and Ground Effects

The above discussion has summarized thrust and dynamic pressure degradation characteristics of basic nozzles; other effects are introduced when the nozzle is installed in a fuselage and when operating in the proximity of a ground surface. The principal effect, as shown in figure 33, was a reduction in available thrust of the combined nozzle and fuselage. Only minor changes were noted in the jet wake degradation characteristics. These effects are presented for a nozzle height of five diameters from the ground. As indicated by references 2 and 3, the thrust losses would be expected to increase rapidly with smaller distances between the nozzle and ground surface.

The effect of fuselage ventilation upon thrust losses in and out of ground effect is shown in figure 34. These curves show that gains to be made by ventilating the fuselage are relatively insensitive to nozzle pressure ratio. Maximum gain in effective velocity coefficient by ventilating the fuselage appears to be about 2 to 3 percent for the suppressor nozzles, and less than 1 percent for the single circular nozzle. Fuselage ventilation is most helpful with nozzles which have the greatest base pressure losses.

An unexpected result of the tests in ground effect is shown in figure 35. The presence of a ground plane increased the suckdown losses by very nearly a constant amount, regardless of the nozzle or fuselage ventilation. This loss, which approximates 5 to 7 per cent of nozzle thrust for all nozzle pressure ratios, constitutes the largest single loss found during the tests. This loss is associated with large scale circulation under the fuselage, and can be minimized by reduction of projected fuselage area.

Thrust losses determined from static pressure measurements on the fuselage are shown in figure 36 in and out of ground effect. Figure 36 shows that base losses of suppressor nozzles are concentrated largely in the regions immediately adjacent to the nozzles when out of ground effect, while large losses are caused by static pressure reductions over the entire lower fuselage surface when operating in ground effect. Large losses with suppressor nozzle 2.5 appear to be associated with a small fuselage area adjacent to the divergent side of the nozzle. As an explanation for this effect, it appears that increased turbulence in the jet existed with nozzles having exit wall divergence, thus leading to greater entrainment of external air near the nozzle. To obtain a more

positive explanation of this behavior would require extensive measurements of the flow in the nozzle, as well as more complete surveys of the jet wake and entrainment region near the nozzle exit.

The results obtained in tests with various fuselage and nozzle configurations were found to agree with that of other investigators, reference 2. These results, with the ratio of projected model area to nozzle exit area as a primary parameter, are shown in figure 37. Although only a single large fuselage was used in the current tests, it is apparent from figure 37 that small fuselage projected areas will be required to avoid significant suckdown effects, particularly when operating in ground effect. Figure 37 also shows that fuselage ventilation assists materially in maintaining competitive effective velocity coefficients for the suppressor nozzle configurations. Thrust losses due to suckdown effects associated with suppressor nozzles vary from 0.5 to 2.0 percent greater than those of the circular nozzle.

A summary of all thrust losses for the various nozzle and fuselage configurations are shown in figure 38. The losses are shown to be cumulative. Nozzles which had greatest losses in the tests of the basic nozzles also exhibited higher suckdown losses with the fuselage and ground plane.

CONCLUDING REMARKS

Several exhaust nozzle models designed to achieve downwash suppression of the exhaust jets of VTOL aircraft have been evaluated for jet wake degradation and thrust characteristics with both hot gases and unheated air.

1) For the best suppressor nozzle and fuselage configuration tested, dynamic pressures were reduced by 60 to 70 per cent, differential temperatures were reduced by nearly 50 per cent, and thrust losses increased by less than 2 per cent compared with a reference circular nozzle at five nozzle diameters above the ground surface.

2) A large thrust loss resulted from small negative pressure differentials acting over the lower fuselage surface in ground effect, and this loss was nearly constant for all nozzle configurations. This loss is related to projected area of the model on the ground surface.

3) Jet wake degradation characteristics were strongly influenced by the merging characteristics of the multiple jets. Merging of the jets was primarily related to the spacing between the nozzle elements. Increasing the aspect ratio of the nozzle elements was effective in increasing jet wake degradation. Increasing the exit wall divergence angle was effective in increasing jet wake degradation for the region less than three diameters away from the nozzle exit, but related

thrust losses result in an optimum nozzle having small exit wall divergence angles, moderate aspect ratio of the elements, and a large spacing between the elements.

4) Base area of the nozzle and fuselage immediately adjacent to the nozzle contributes significantly to the thrust losses with suppressor type nozzles. Providing clearance between the suppressor nozzles and fuselage was found to be an effective way to minimize these losses. Ventilation, in the sense of providing large open areas around the nozzle exit, will be necessary for best thrust performance with suppressor nozzles. Openings on the upper fuselage surface did not reduce thrust losses.

5) At a distance of five diameters from the nozzle exit, the ground plane had only small effects upon jet wake degradation prior to impingement. Effects of a fuselage upon the mixing processes were minor.

Airplane Division, The Boeing Company
Renton, Washington
June 22, 1965

REFERENCES

1. Higgins, C. C., and Wainwright, T. W.: Dynamic Pressure and Thrust Characteristics of Cold Jets Discharging from Several Exhaust Nozzles Designed for VTOL Downwash Suppression. NASA TN D-2263, April 1964

2. Gentry, Garl L., Margason, Richard J., and Kuhn, Richard E.: Jet-Induced Base Losses on VTOL Configurations Hovering In and Out of Ground Effect. NASA TN D-3166

3. Spreemann, Kenneth P., and Sherman, Irving R.: Effects of Ground Proximity on the Thrust of A Simple Downward-Directed Jet Beneath a Flat Surface. NACA TN 4407, September 1958

4. Davenport, Edwin E., and Spreeman, Kenneth P.: Thrust Characteristics of Multiple Lifting Jets in Ground Proximity. NASA TN D-513, September 1960

5 Kuhn, Richard.: An Investigation to Determine Conditions Under Which Downwash from VTOL Aircraft will Start Surface Erosion From Various Types of Terrain. NASA TN D-56, September 1959

6. Tani, Itero, and Komatsu, Yasuo: Impingement of A Round Jet on a Flat Surface. Presented at Eleventh International Congress of Applied Mechanics, Munchen, 1964

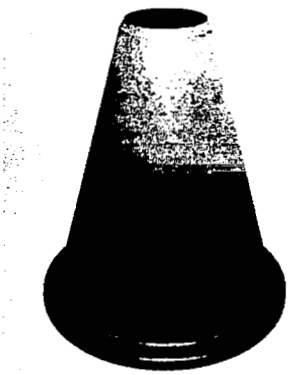

(a) CIRCULAR NOZZLE 1.1

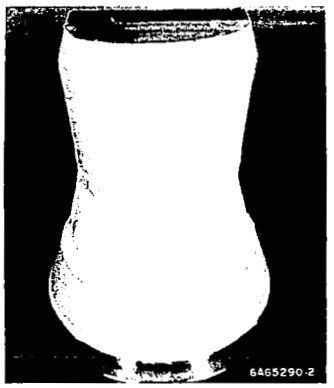

(b) DELTA NOZZLE 1.2

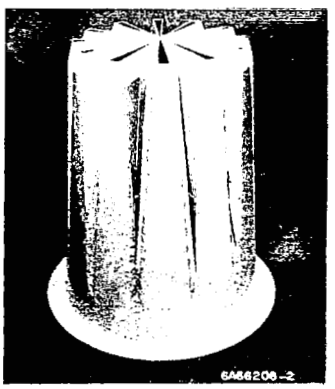

(c) TWELVE SEGMENT NOZZLE 1.3

Figure 1. - Phase I nozzles evaluated under phase II.

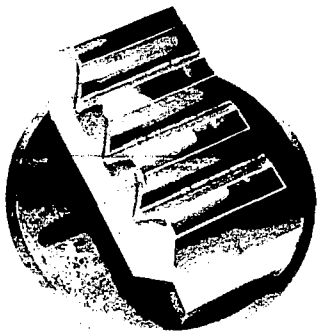

NOZZLE 2.1

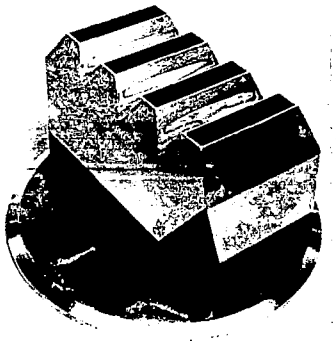

NOZZLE 2.2

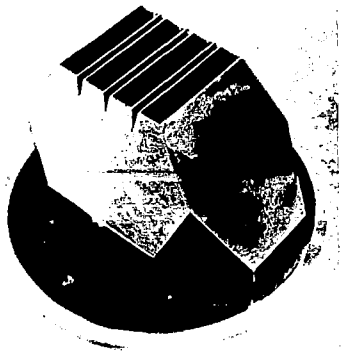

NOZZLE 2.3

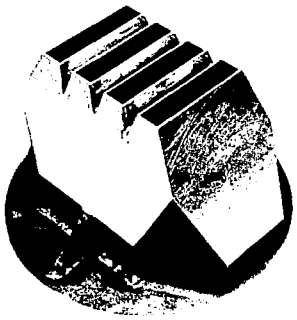

NOZZLE 2.4

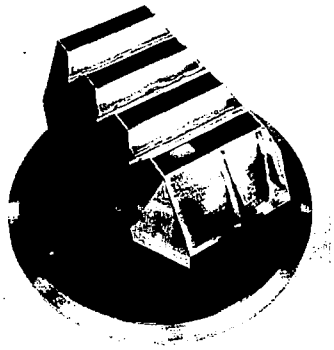

NOZZLE 2.5

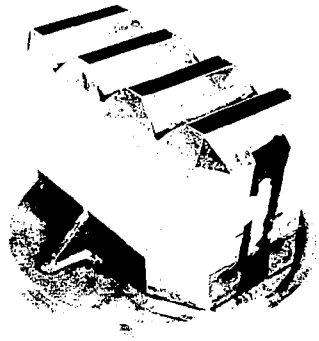

NOZZLE 2.6

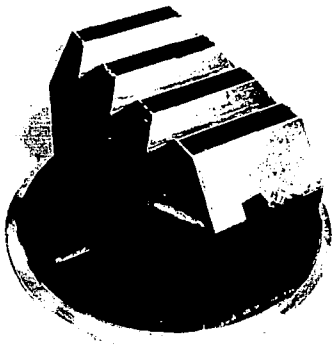

NOZZLE 2.7

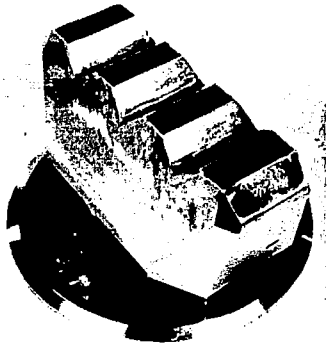

NOZZLE 2.8

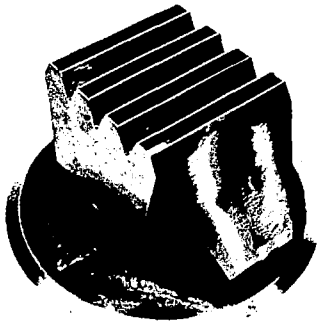

NOZZLE 2.9

Figure 2. - Non-circular nozzle configurations for phase II.

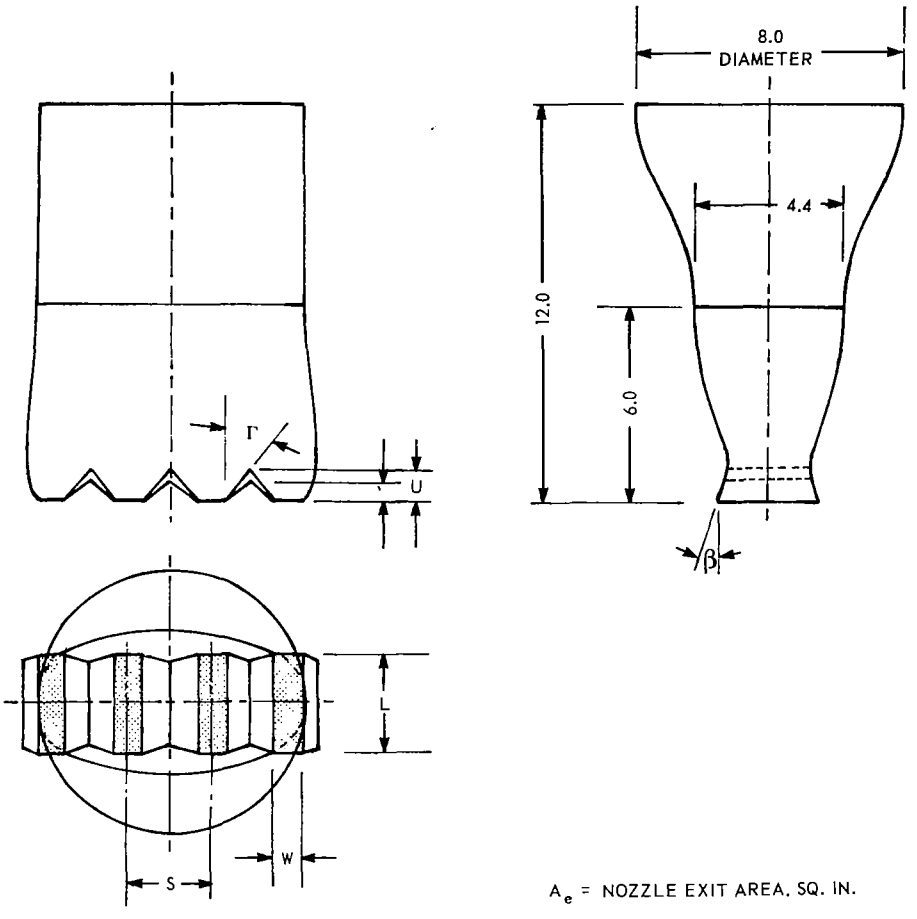

Nozzle No.	A_e	L	W	S	V	U	β	r	AR	S/W
2.1	7.1336	2.975	0.595	1.785	1.144	1.250	0	25°27'	5	3.0
2.2	7.0534	2.975	0.595	1.785	1.053	1.150	5	27°21.5'	5	3.0
2.3	7.1119	2.975	0.595	0.8925	0.567	1.000	15	8°28.5'	5	1.5
2.4	7.0300	2.975	0.595	1.190	0.785	1.000	15	16°34'	5	2.0
2.5	7.1151	2.975	0.595	1.785	0.915	1.000	15	30°45'	5	3.0
2.6	7.1465	2.975	0.595	2.380	0.943	1.000	15	41°45'	5	4.0
2.7	7.0407	2.975	0.595	1.785	0.854	0.930	30	33°28'	5	3.0
2.8	7.0640	2.298	0.766	2.298	0.934	1.000	15	37°27'	3	3.0
2.9	7.0900	4.200	0.420	1.260	0.847	1.000	15	22°47'	10	3.0

Figure 3 - Four-element suppressor nozzle configurations

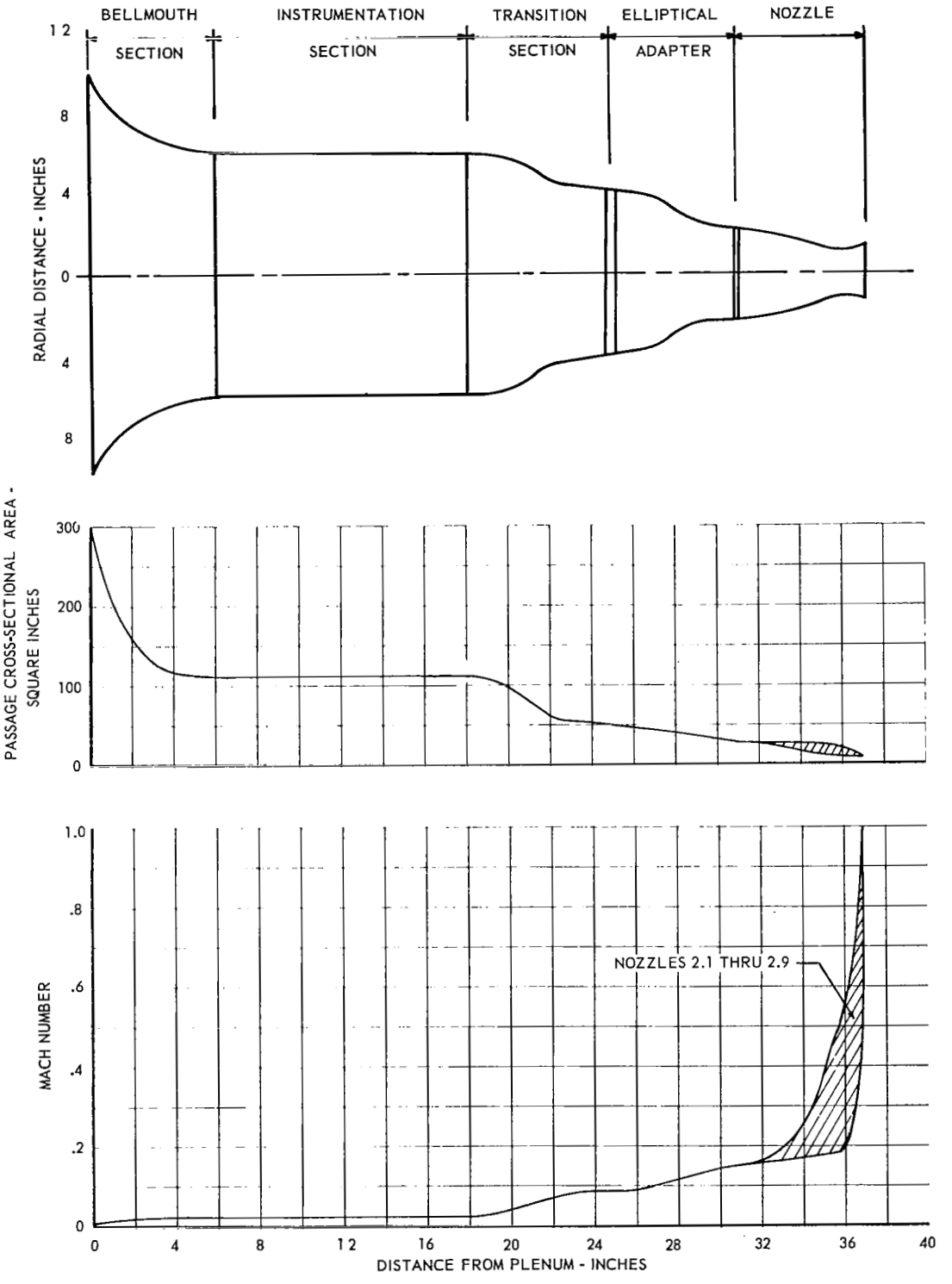

Figure 4 - Typical four-element suppressor nozzle cross-sectional area and Mach number progression

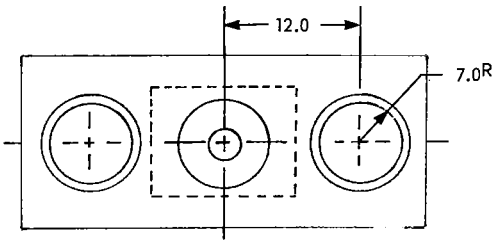

TOP VIEW SHOWING INLETS

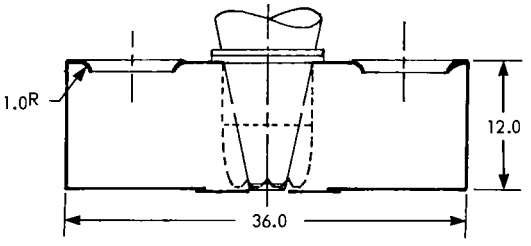

SIDE VIEW

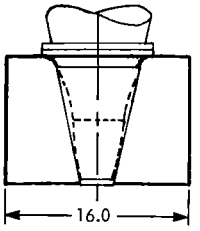

END VIEW

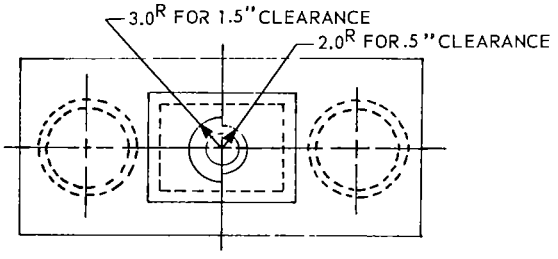

BOTTOM VIEW SHOWING CLEARANCE BETWEEN FUSELAGE AND CIRCULAR NOZZLE

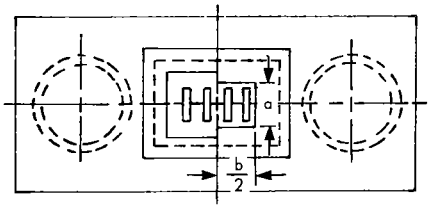

BOTTOM VIEW SHOWING CLEARANCE BETWEEN FUSELAGE AND FOUR-ELEMENT SUPPRESSOR NOZZLES

NOZZLE 2.1 & 2.5	NOZZLE CLEARANCE 0.5"	1.5"
a	4.0	6.0
b/2	3.5	4.5

Figure 5 - Fuselage configurations

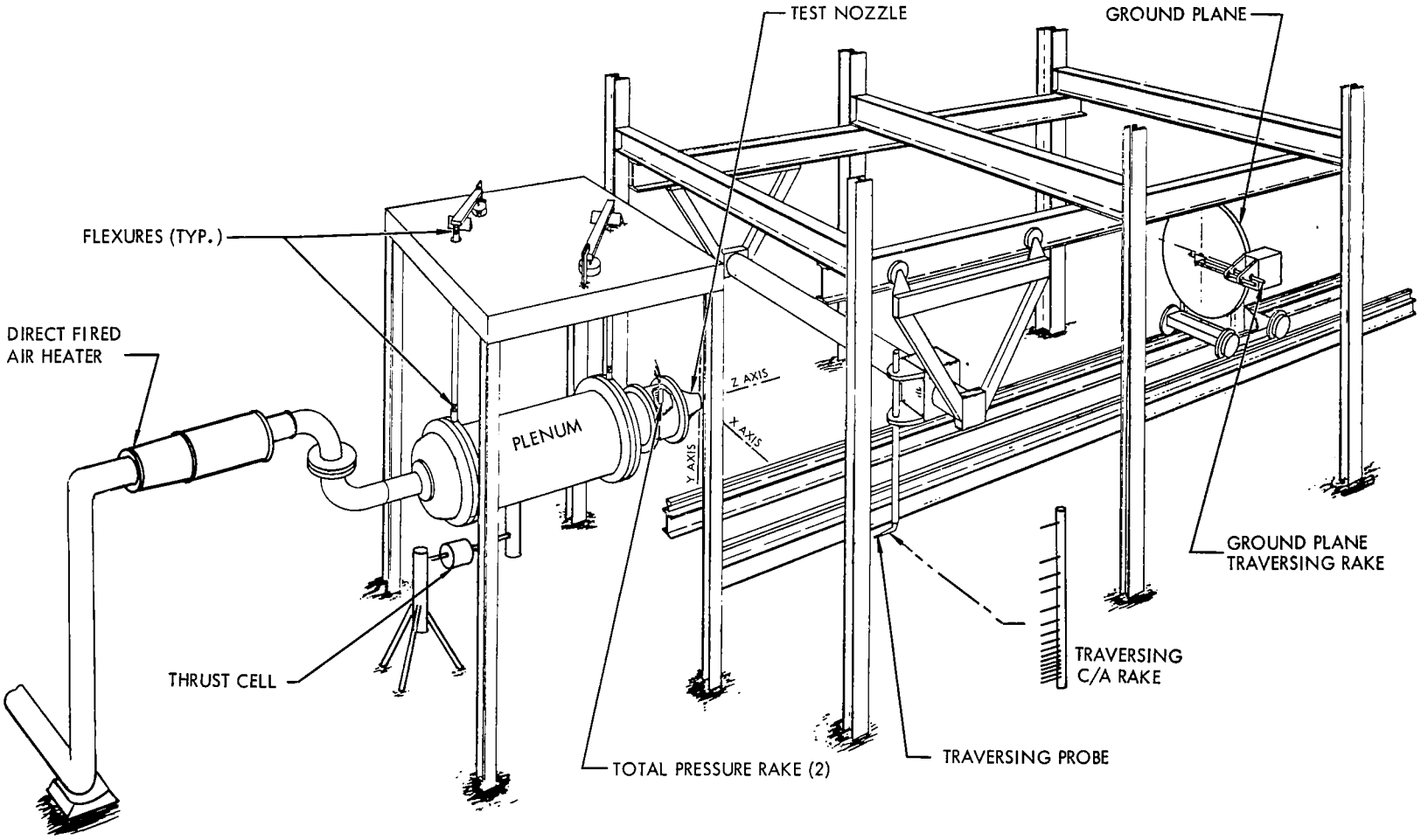

Figure 6 - Schematic of test rig and facilities

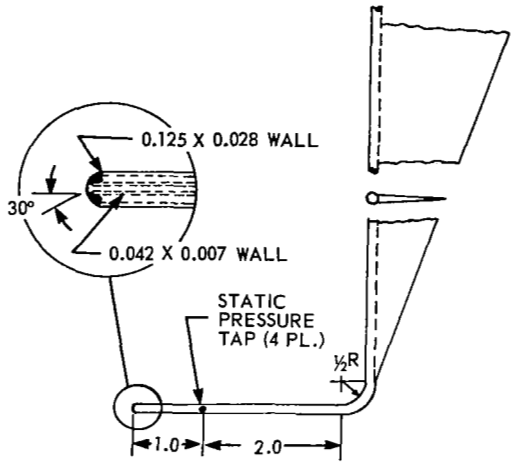

(a) TRAVERSING PITOT PROBE

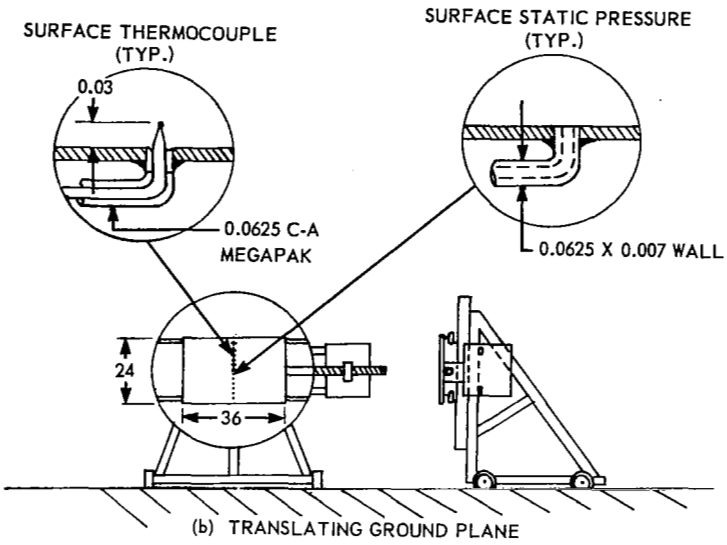

(b) TRANSLATING GROUND PLANE

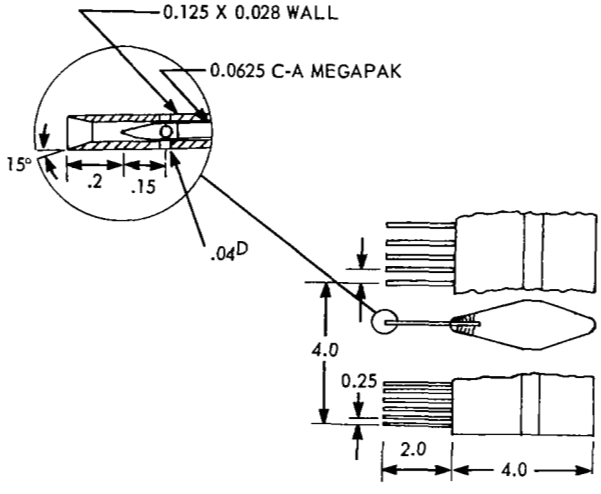

(c) FORTY-ONE ELEMENT TRAVERSING THERMOCOUPLE RAKE

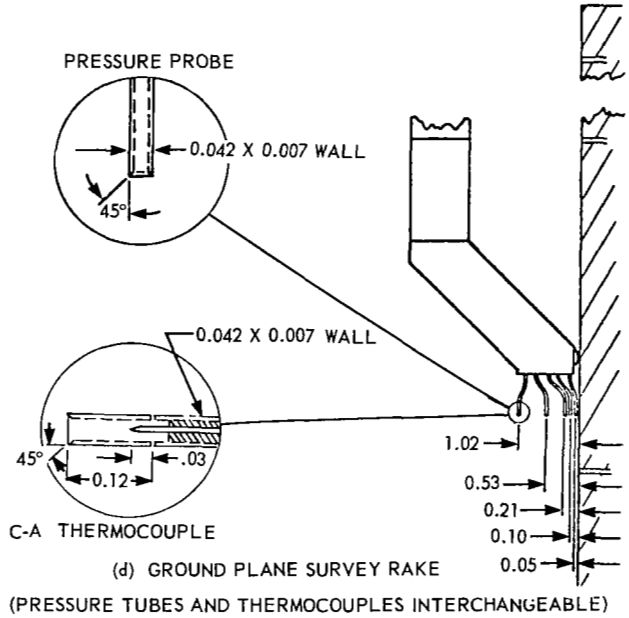

(d) GROUND PLANE SURVEY RAKE

(PRESSURE TUBES AND THERMOCOUPLES INTERCHANGEABLE)

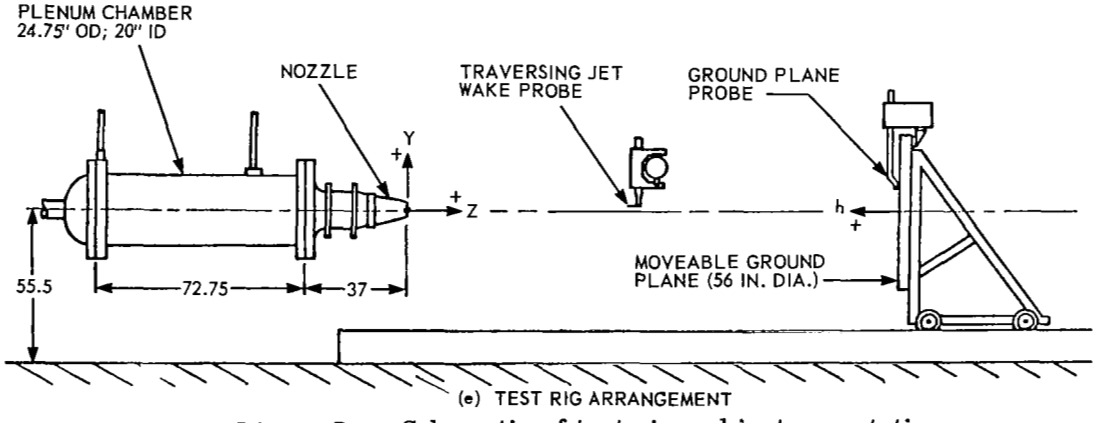

(e) TEST RIG ARRANGEMENT

Figure 7 - Schematic of test rig and instrumentation

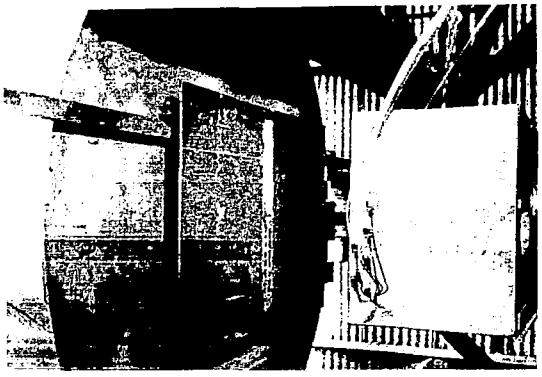

(a) TEST RIG

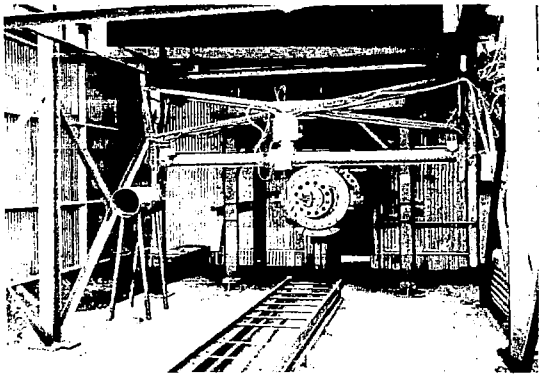

(b) TRAVERSING GROUND PLANE

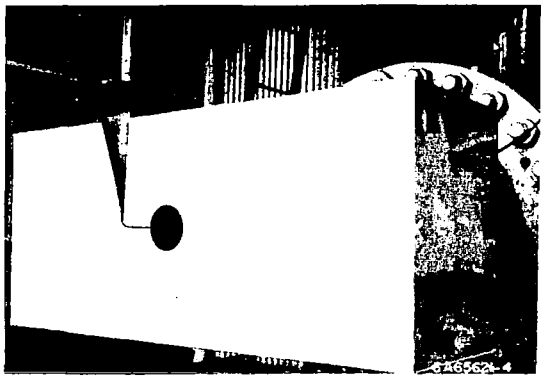

(c) CIRCULAR NOZZLE WITH NON-VENTILATED FUSELAGE

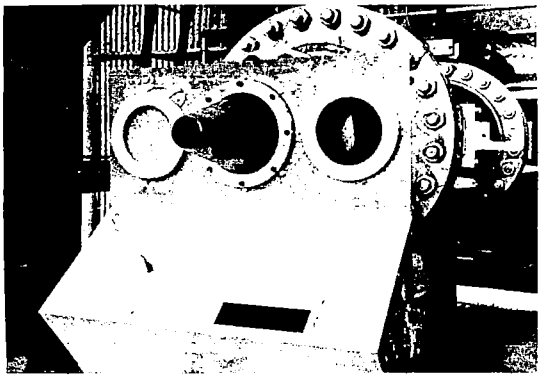

(d) INTERIOR OF FUSELAGE

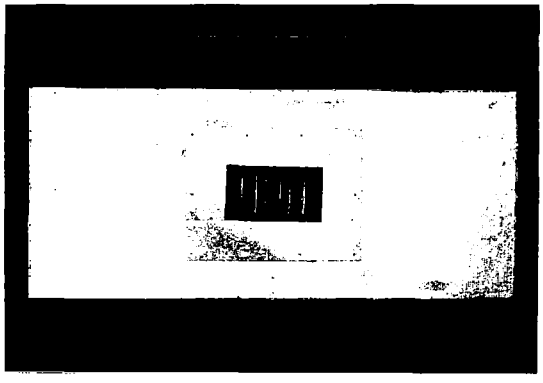

(e) NOZZLE 2.5 WITH VENTILATED FUSELAGE

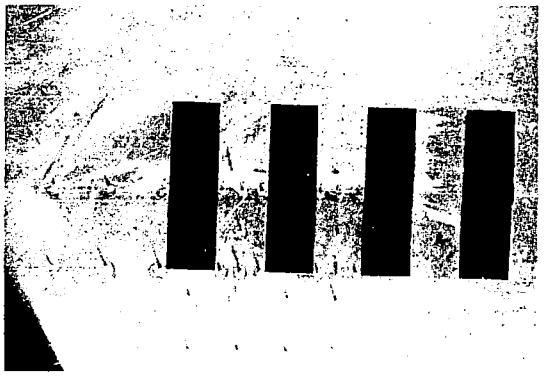

(f) NOZZLE 2.5 WITH INSTRUMENTED FUSELAGE

Figure 8. - Photographs of test rig for various nozzle and fuselage configurations

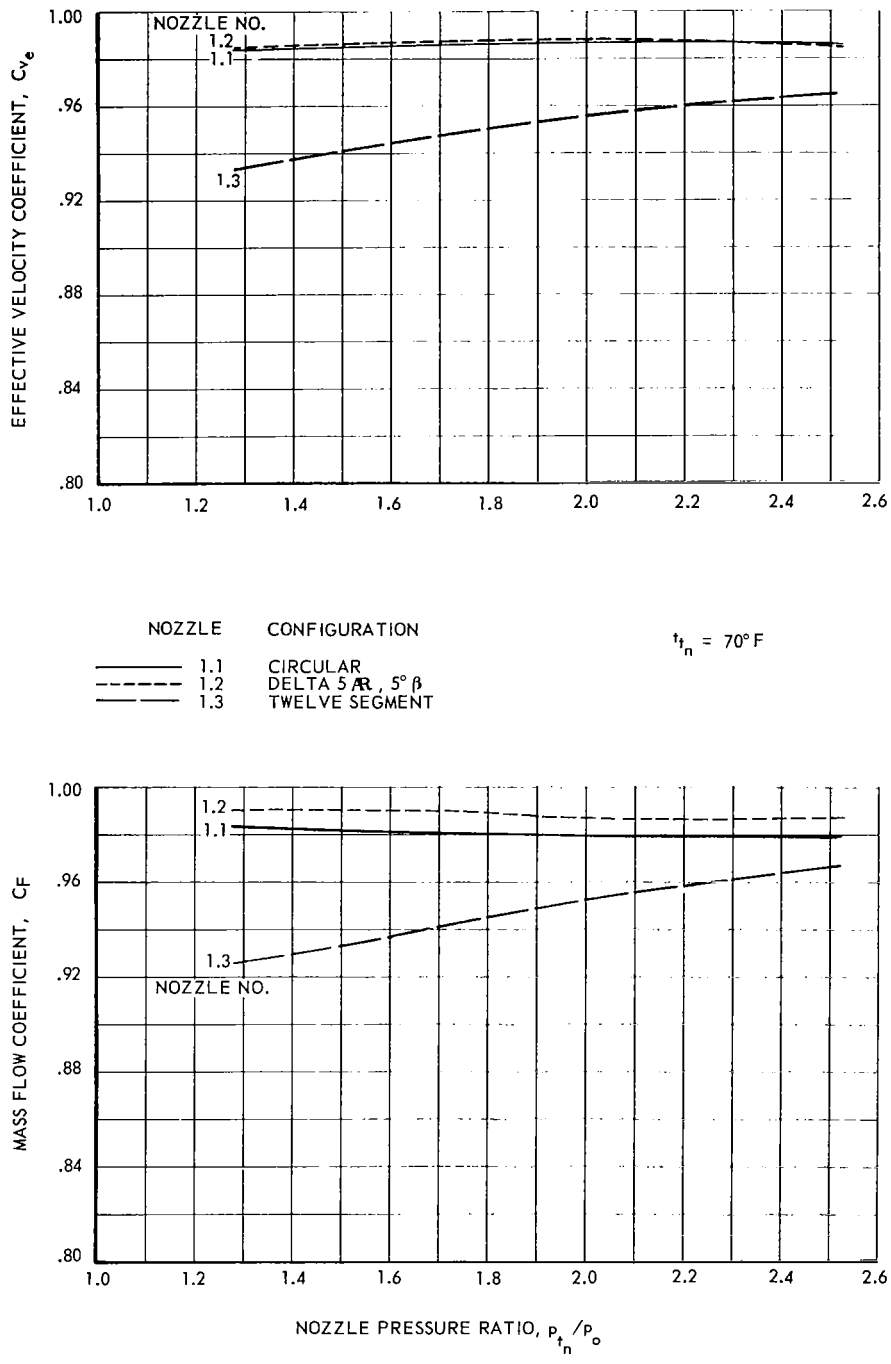

(a) PHASE I NOZZLES

Figure 9 - Variation of effective velocity and mass flow coefficients with nozzle pressure ratio for all basic nozzle configurations

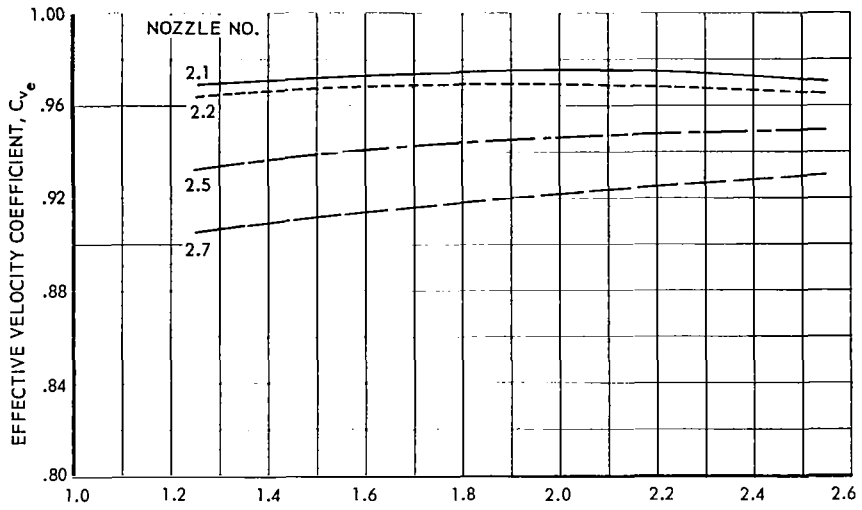

NOZZLE	β
2.1	0°
2.2	5°
2.5	15°
2.7	30°

S/W = 3.0
AR = 5.0
t_{t_n} = 70°F

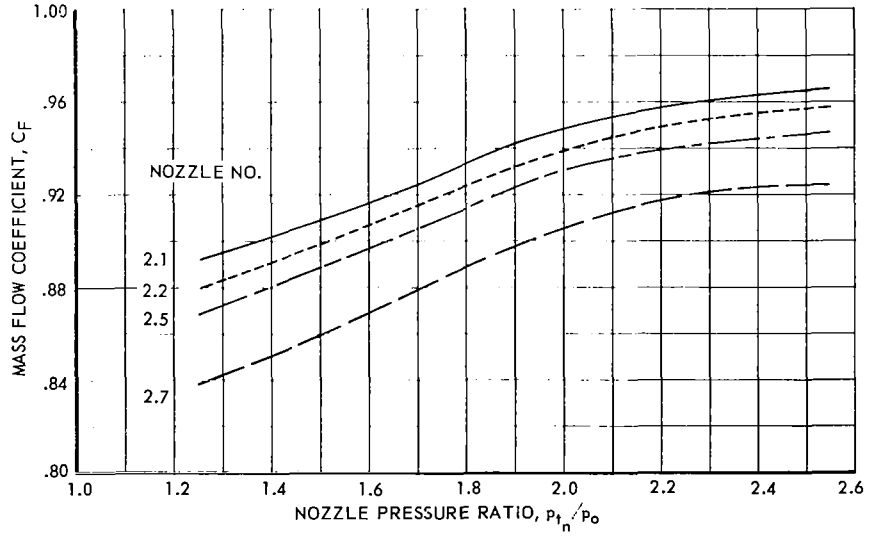

(b) PHASE II NOZZLES - VARIATION OF EXIT WALL ANGLE, β

Figure 9 - Continued

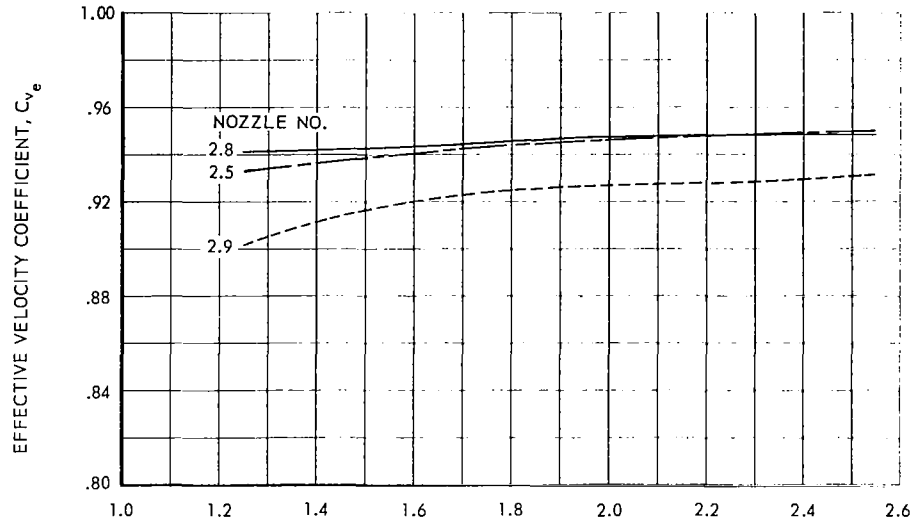

NOZZLE	$\mathcal{AR}$
2.8	3
2.5	5
2.9	10

$\beta = 15°$
$S\sqrt{W} = 3.0$
$t_{t_n} = 70°F$

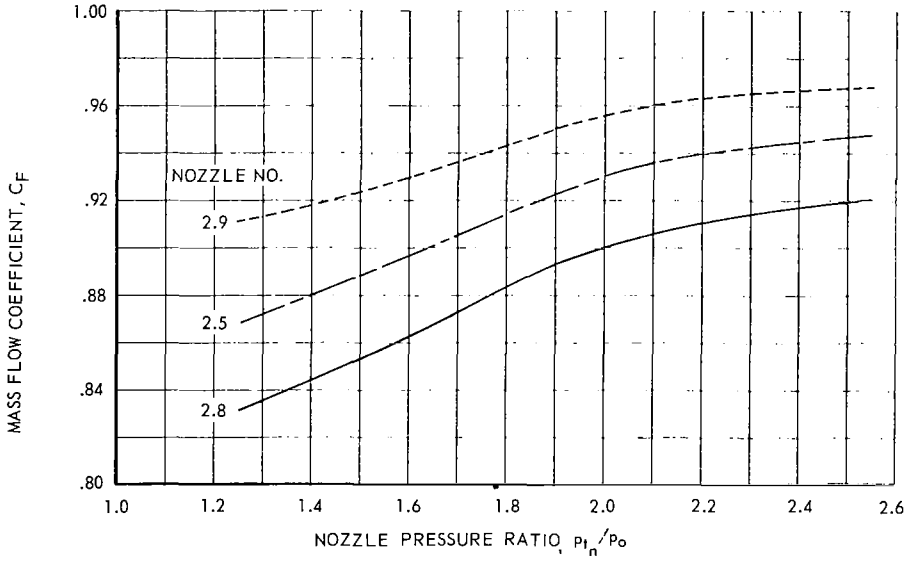

(c) PHASE II NOZZLES - VARIATION OF ASPECT RATIO, $\mathcal{AR}$

Figure 9 - Continued

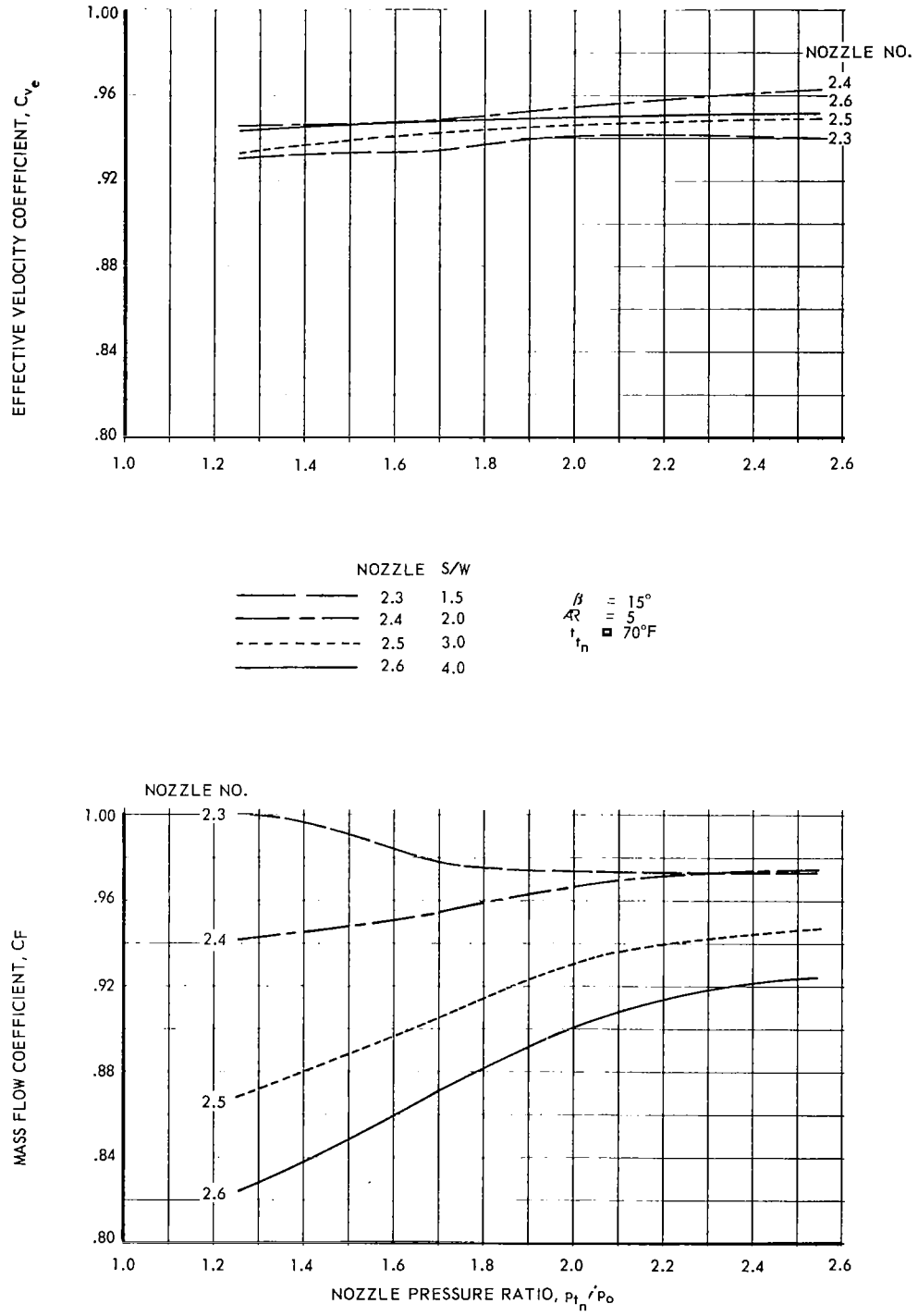

(d) PHASE II NOZZLES - VARIATION OF SPACING RATIO, S/W

Figure 9 - Concluded

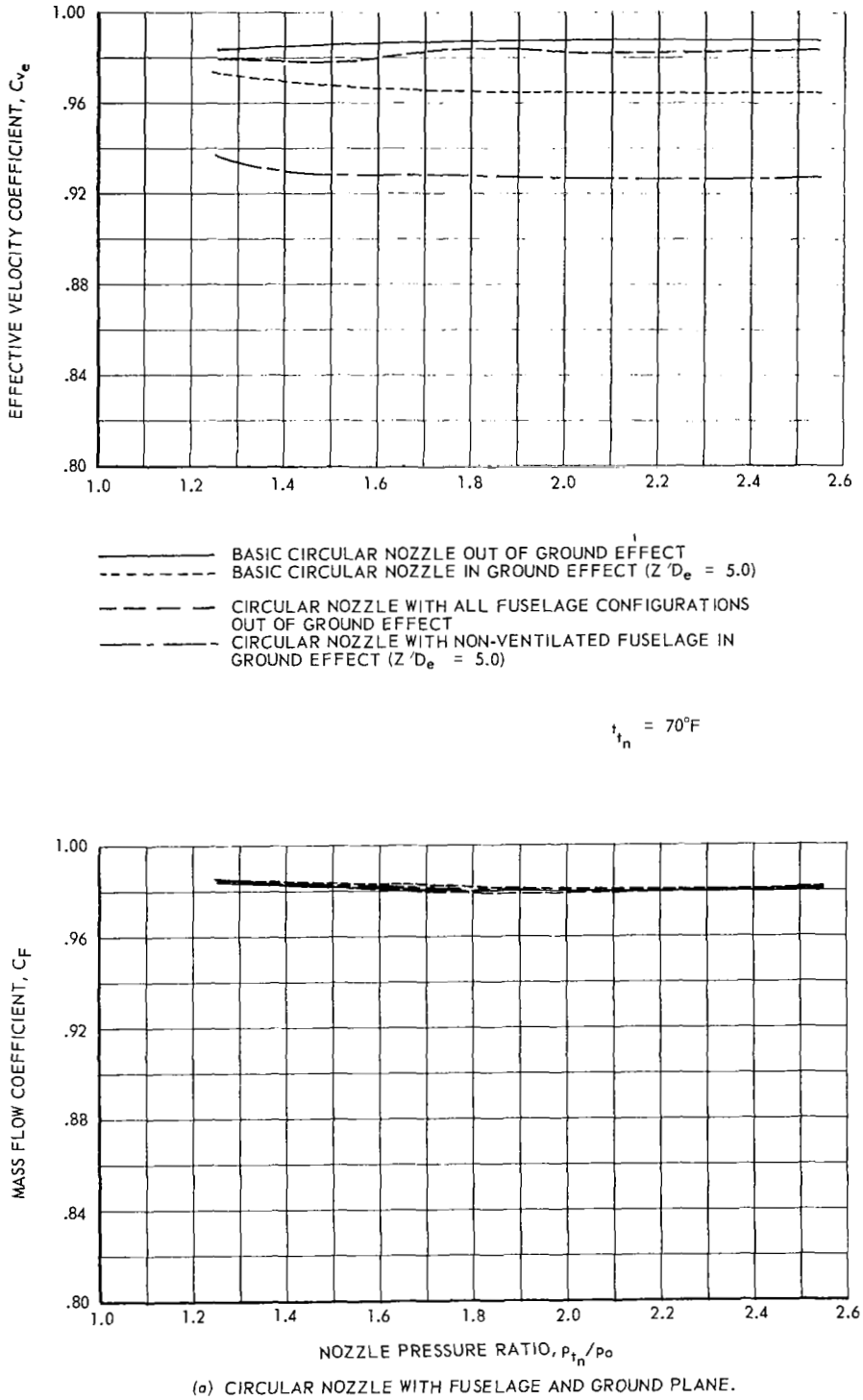

(a) CIRCULAR NOZZLE WITH FUSELAGE AND GROUND PLANE.

Figure 10 - Variation of effective velocity and mass flow coefficient with nozzle pressure ratio for various nozzle and fuselage configurations

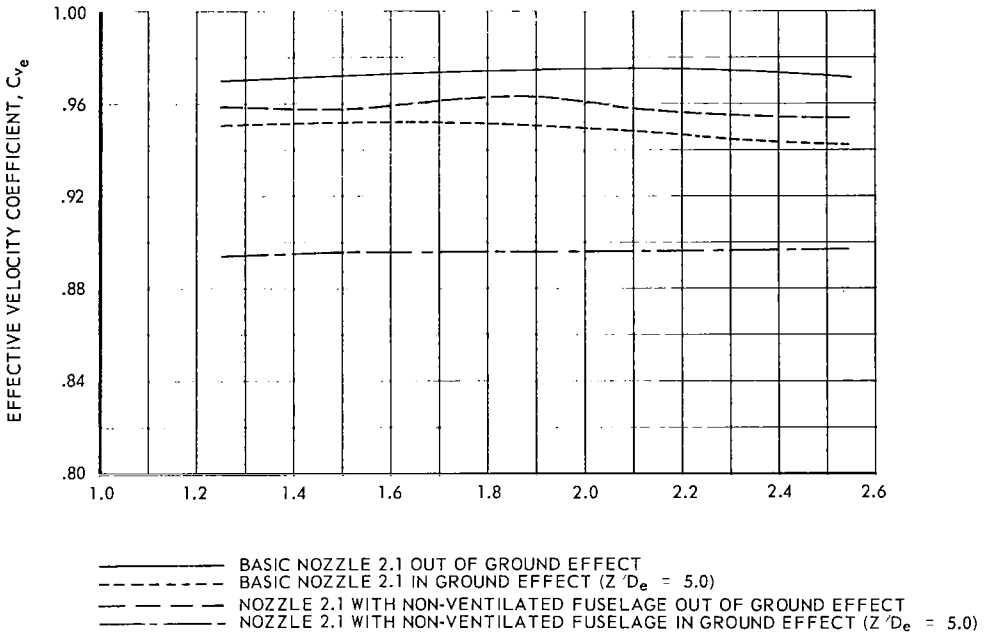

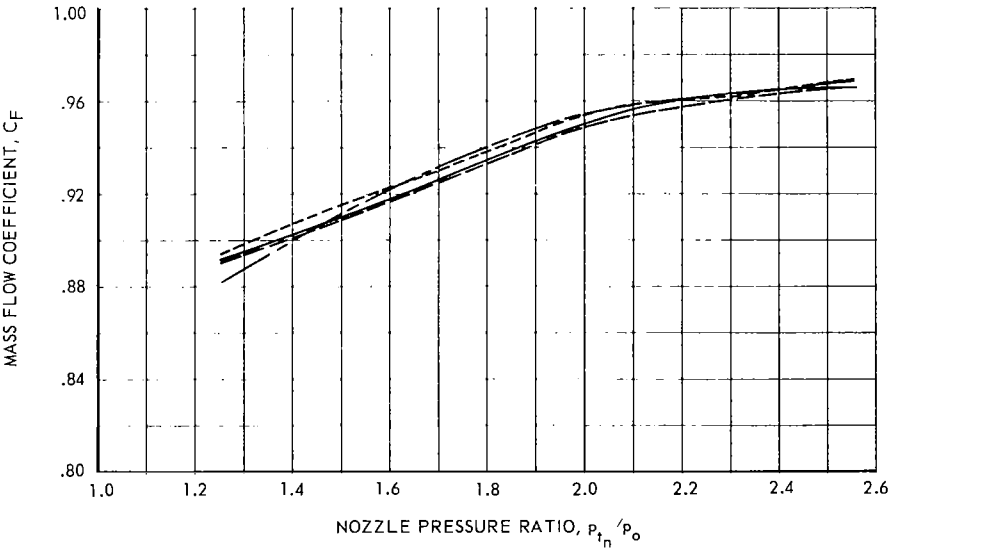

(b) SUPPRESSOR NOZZLE 2.1 WITH FUSELAGE AND GROUND PLANE.

Figure 10 - Continued

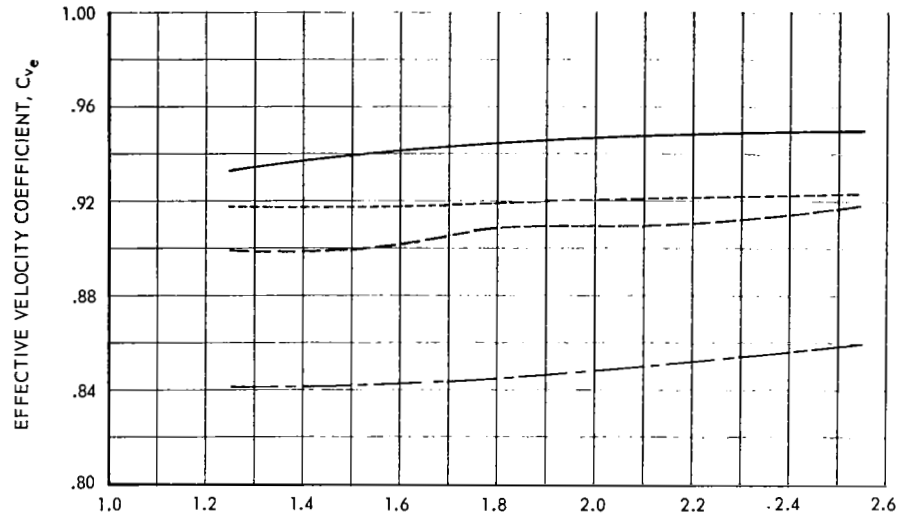

BASIC NOZZLE 2.5 OUT OF GROUND EFFECT
BASIC NOZZLE 2.5 IN GROUND EFFECT (Z/D_e = 5.0)
NOZZLE 2.5 WITH NON-VENTILATED FUSELAGE OUT OF GROUND EFFECT
NOZZLE 2.5 WITH NON-VENTILATED FUSELAGE IN GROUND EFFECT (Z/D_e = 5.0)

t_{t_n} = 70°F

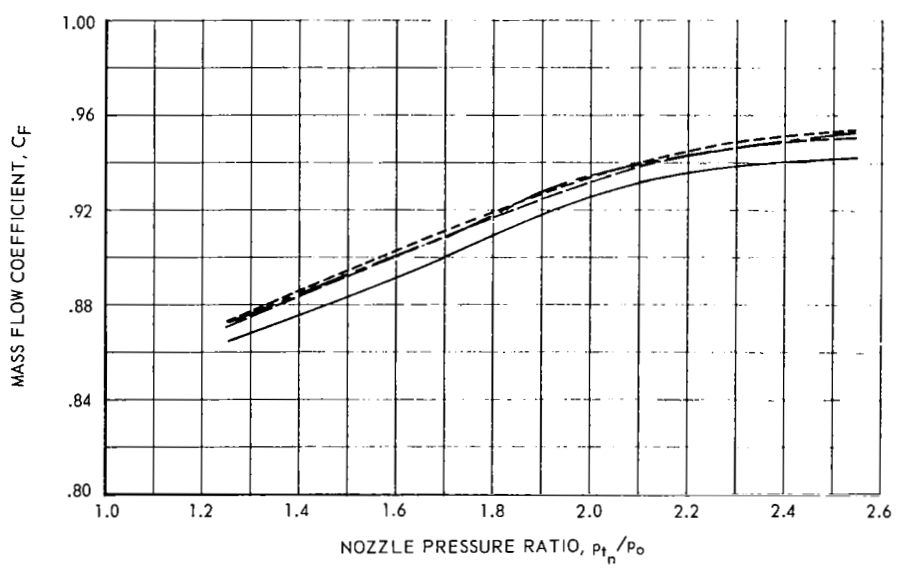

(c) SUPPRESSOR NOZZLE 2.5 WITH FUSELAGE AND GROUND PLANE.

Figure 10 - Concluded

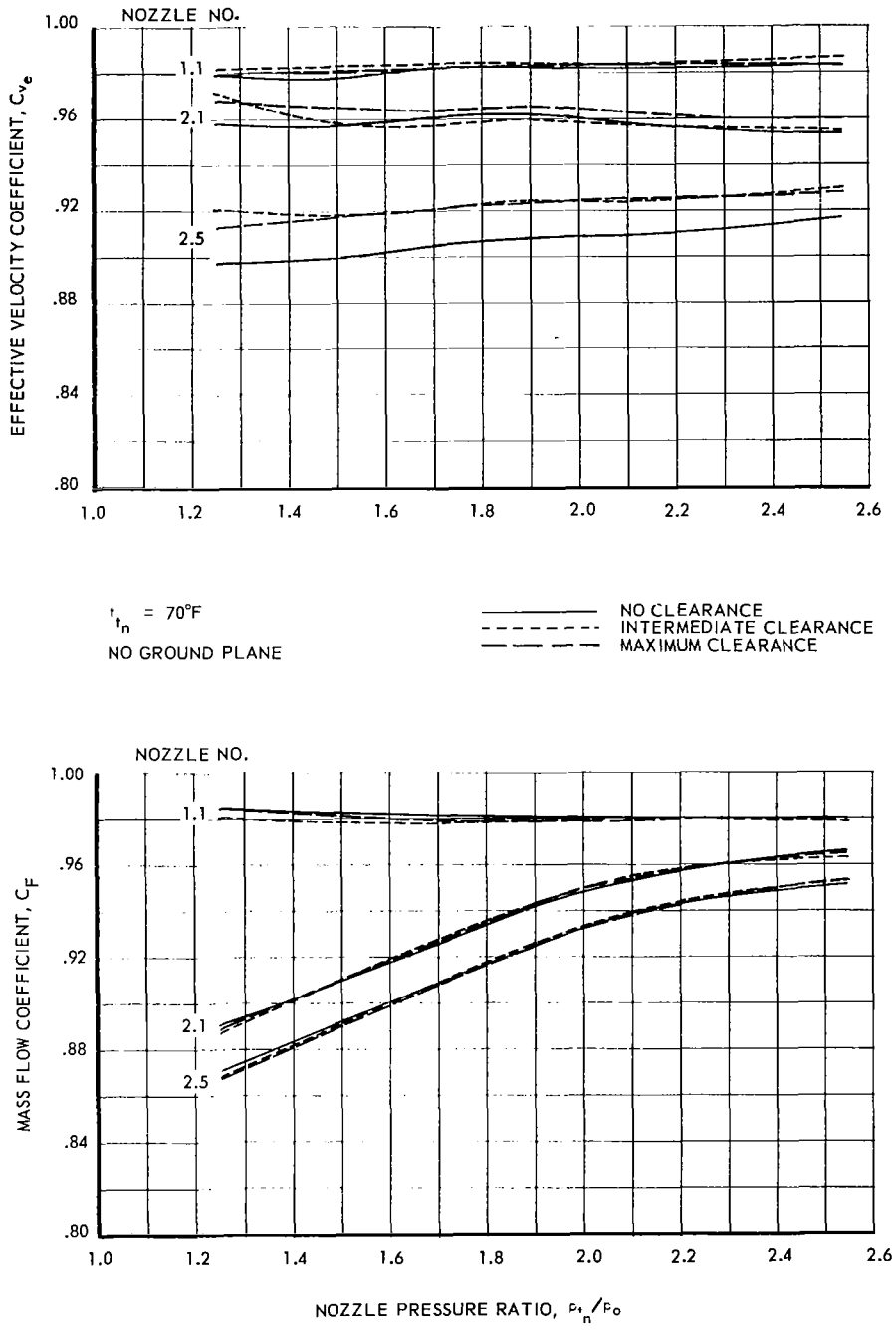

(a) FUSELAGE CAVITY NOT VENTILATED.

Figure 11 - Effect of clearance between fuselage lower surface and nozzle exit on effective velocity and mass flow coefficients for nozzles 1.1, 2.1, and 2.5 out of ground effect

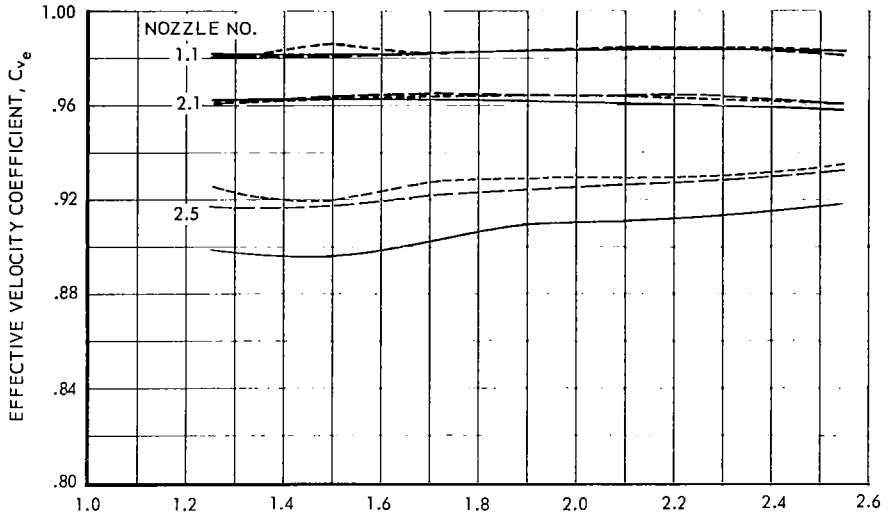

t_{t_n} = 70°F

NO GROUND PLANE

NO CLEARANCE
INTERMEDIATE CLEARANCE
MAXIMUM CLEARANCE

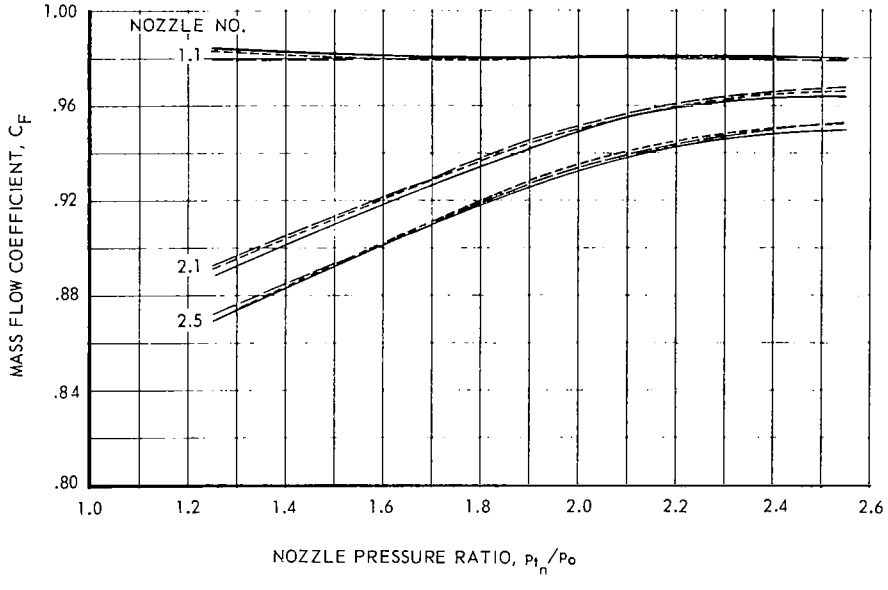

(b) FUSELAGE CAVITY WITH MAXIMUM VENTILATION.

Figure 11 - Concluded

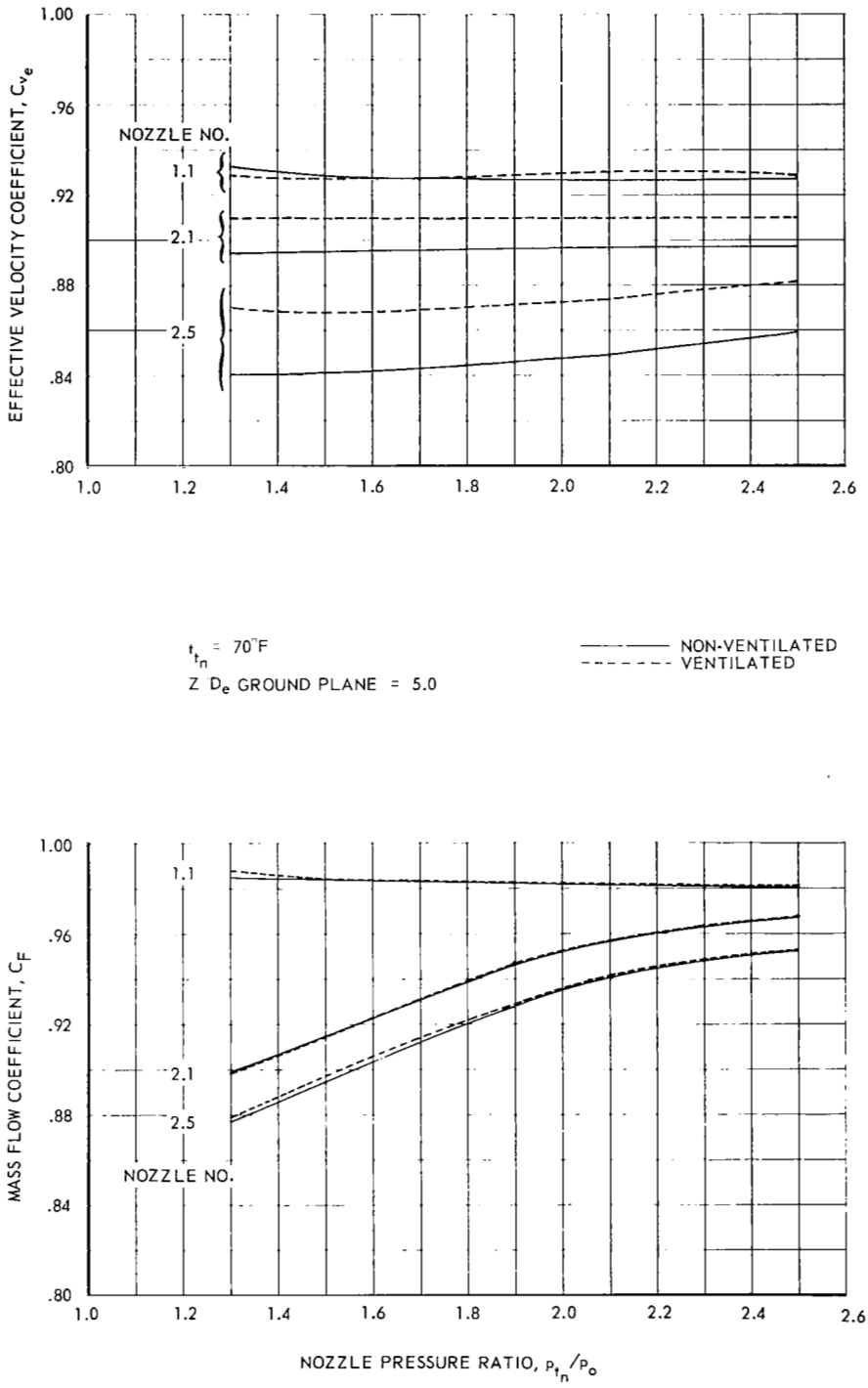

Figure 12 - Effect of fuselage ventilation on effective velocity and mass flow coefficients for nozzles 1.1, 2.1, and 2.5 in ground effect

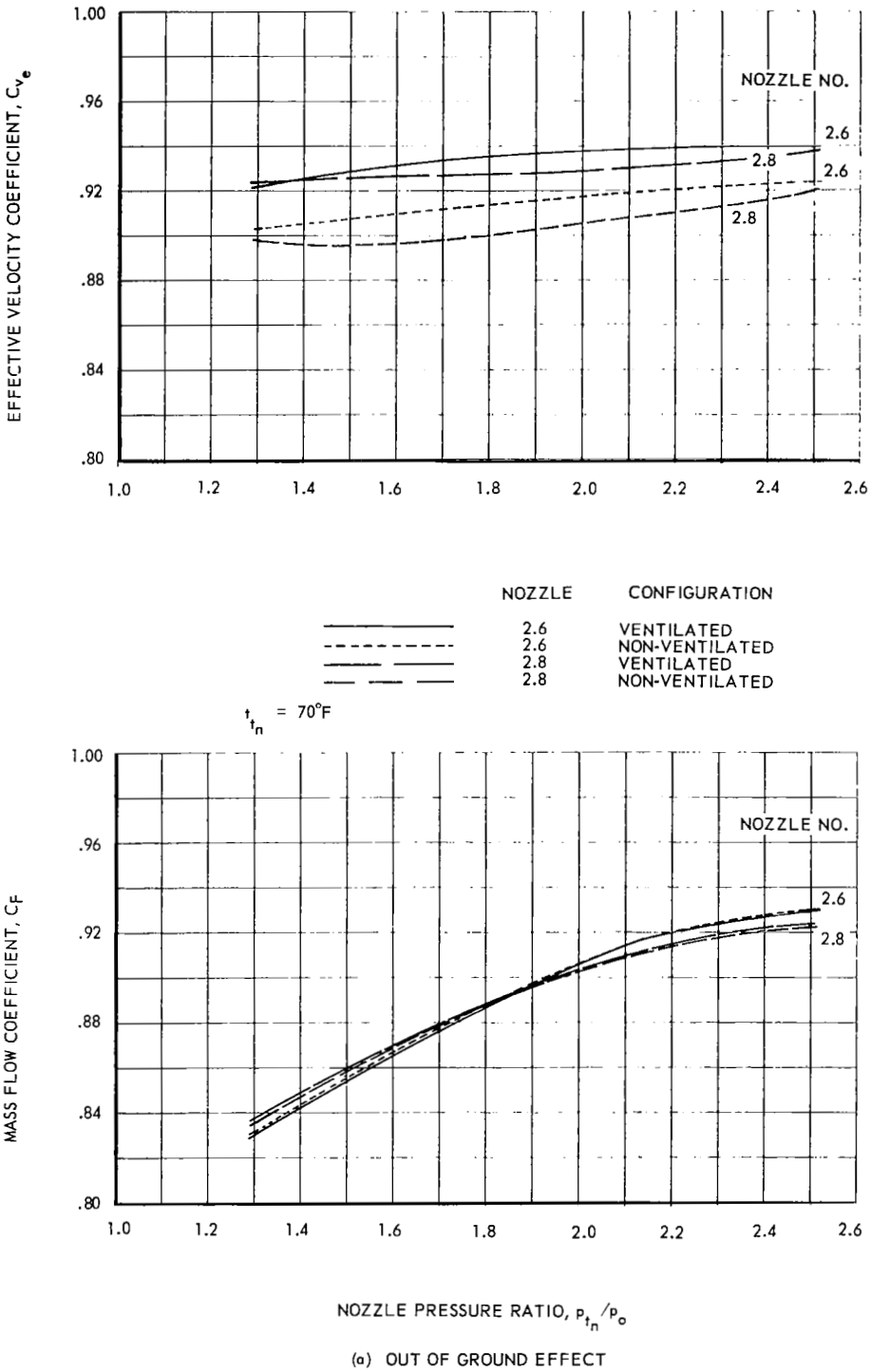

Figure 13 - Effect of fuselage ventilation on effective velocity and mass flow coefficients for nozzles 2.6 and 2.8 in and out of ground effect

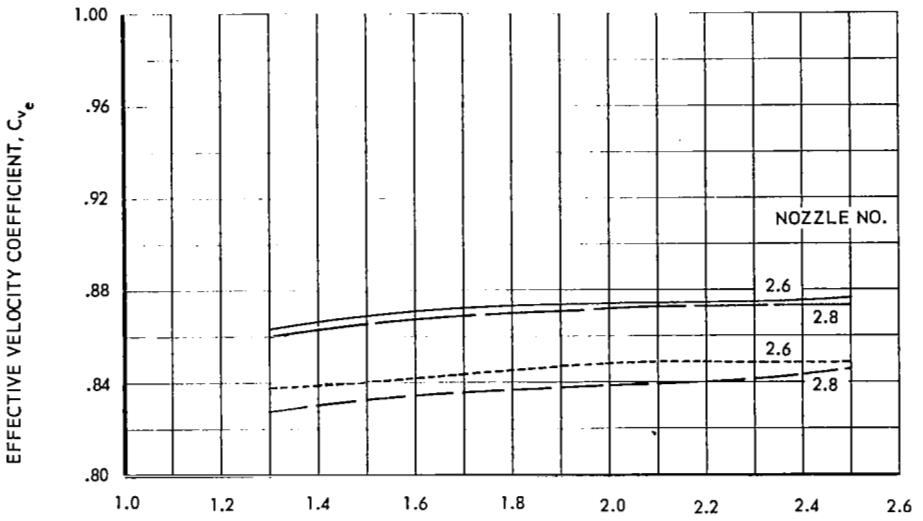

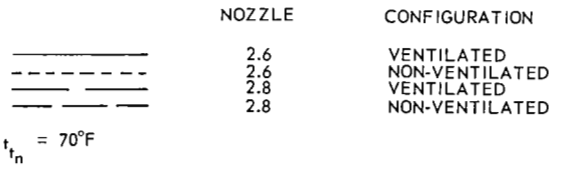

t_{t_n} = 70°F

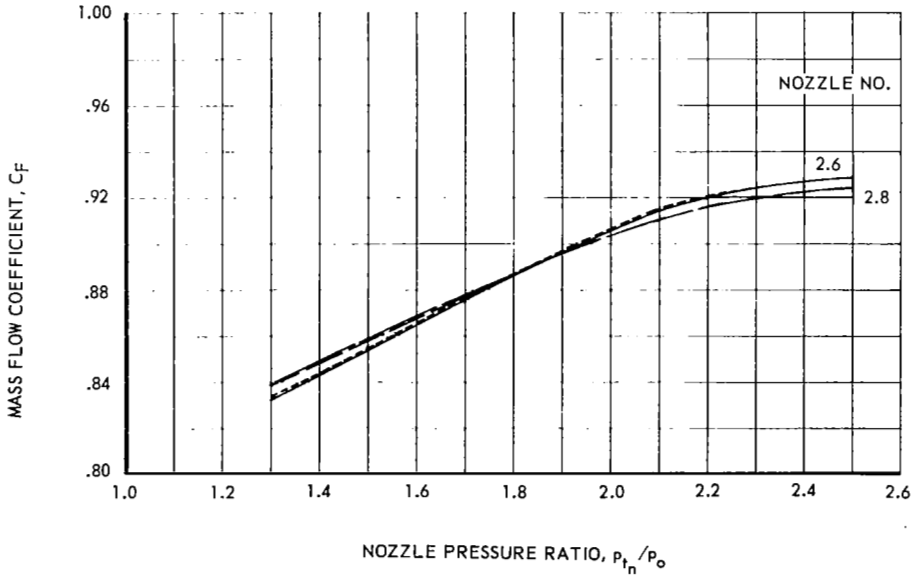

(b) IN GROUND EFFECT (Z/D_e = 5.0)

Figure 13 - Concluded

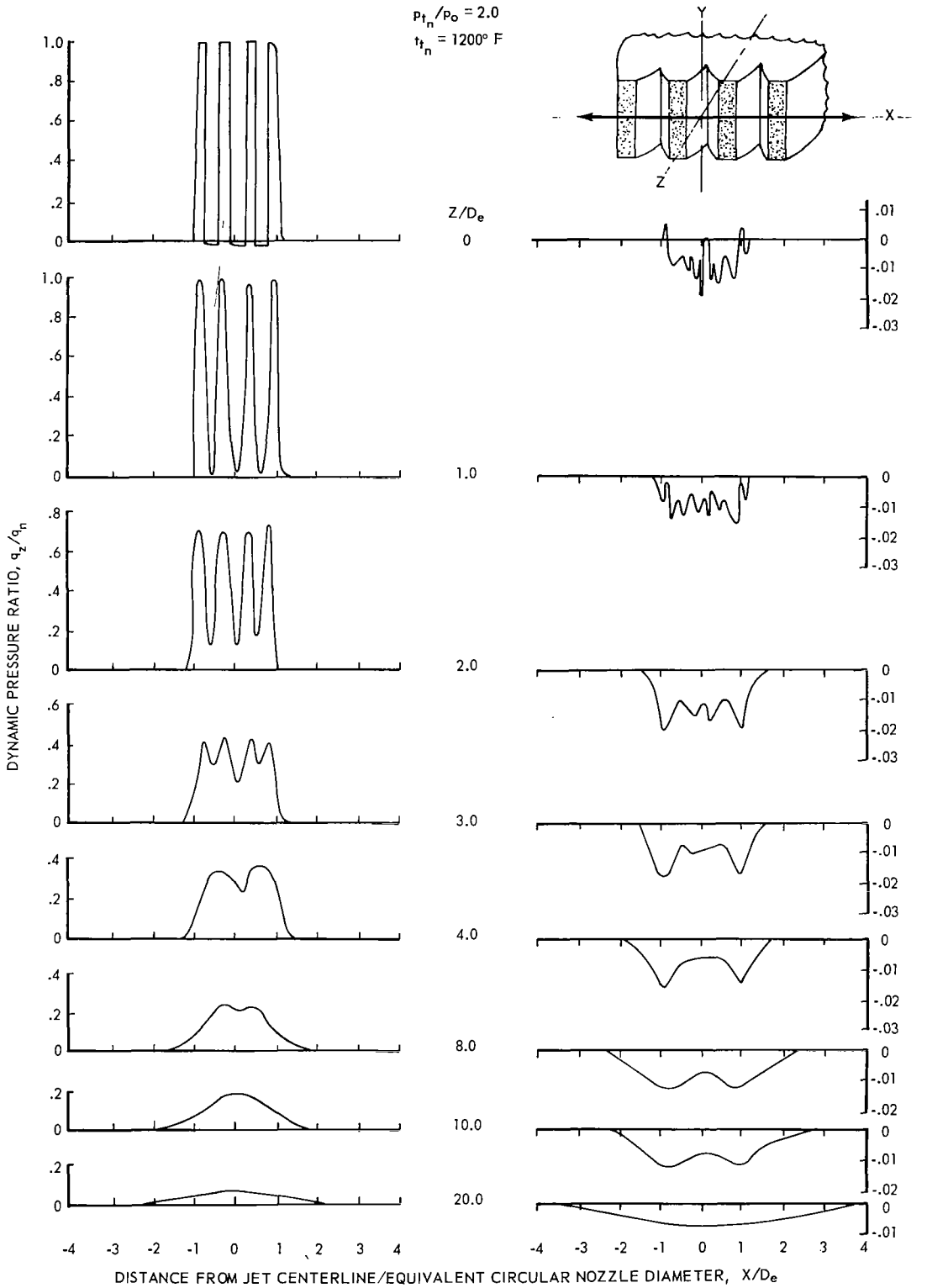

Figure 14 - Dynamic and static pressure surveys for basic suppressor nozzle 2.1 out of ground effect

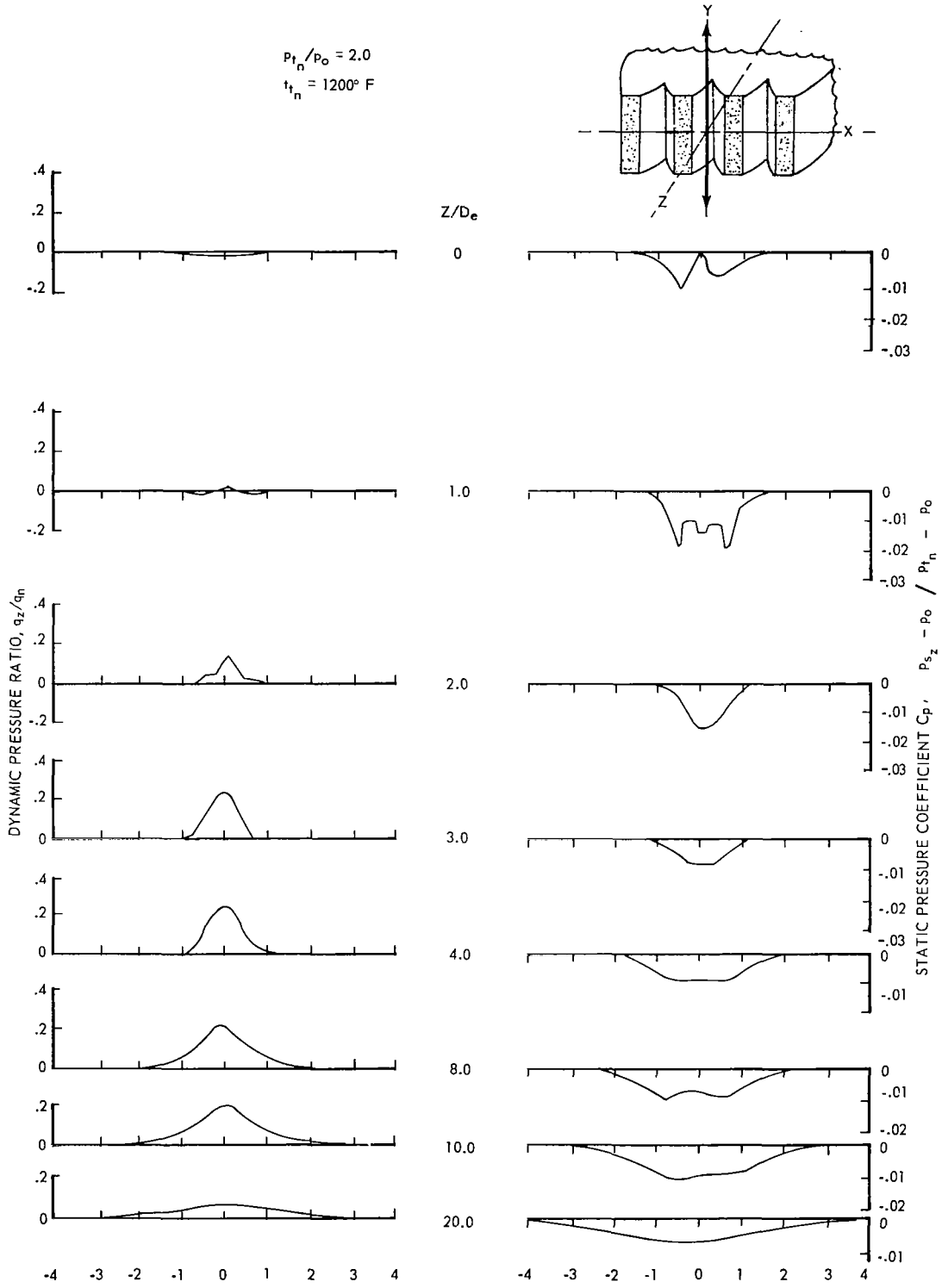

(b) SURVEYS ALONG Y AXIS

Figure 14 - Continued

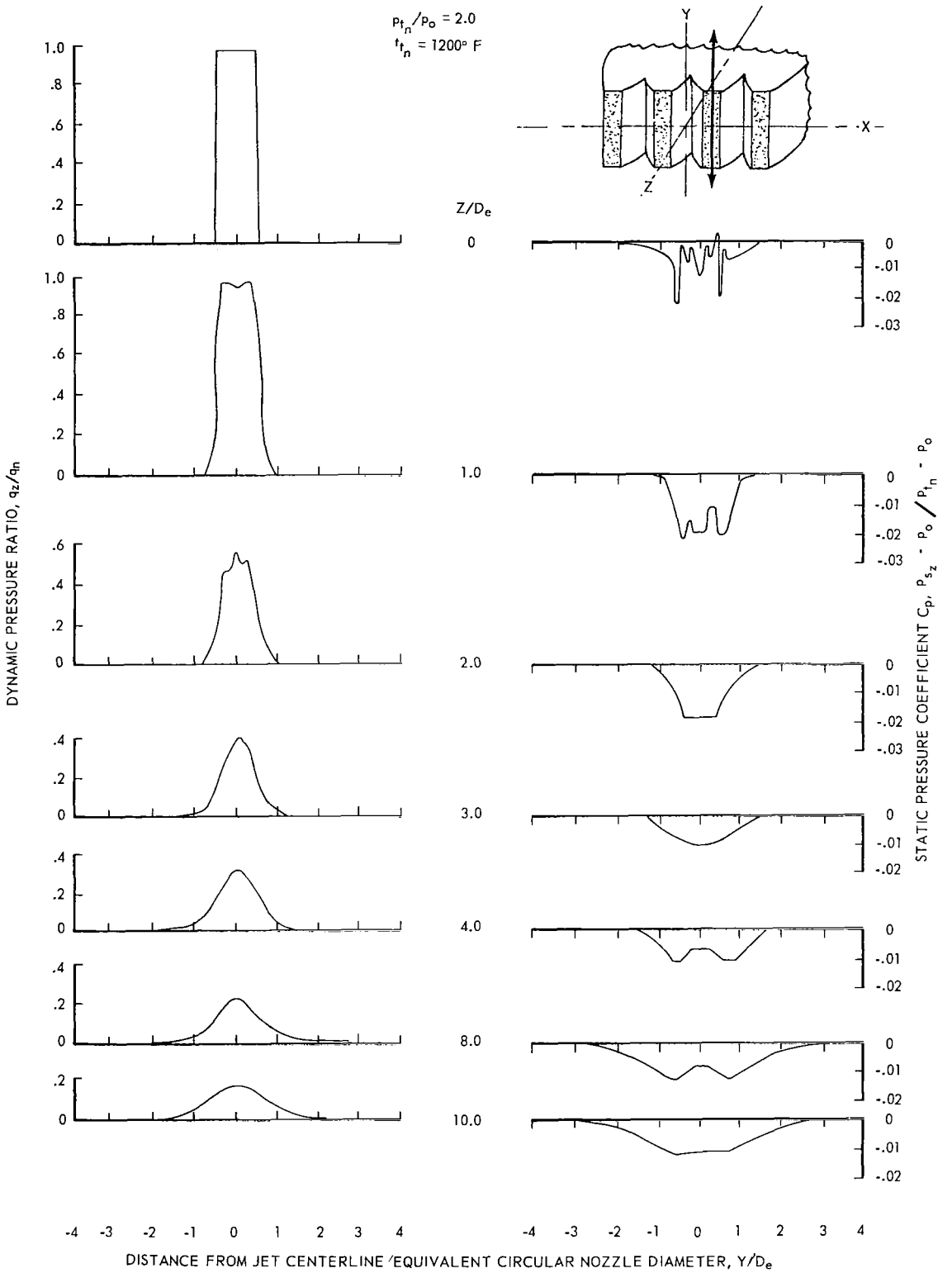

(c) SURVEY AT DISTANCE OF 0.90 INCHES FROM NOZZLE CENTERLINE.

Figure 14 - Continued

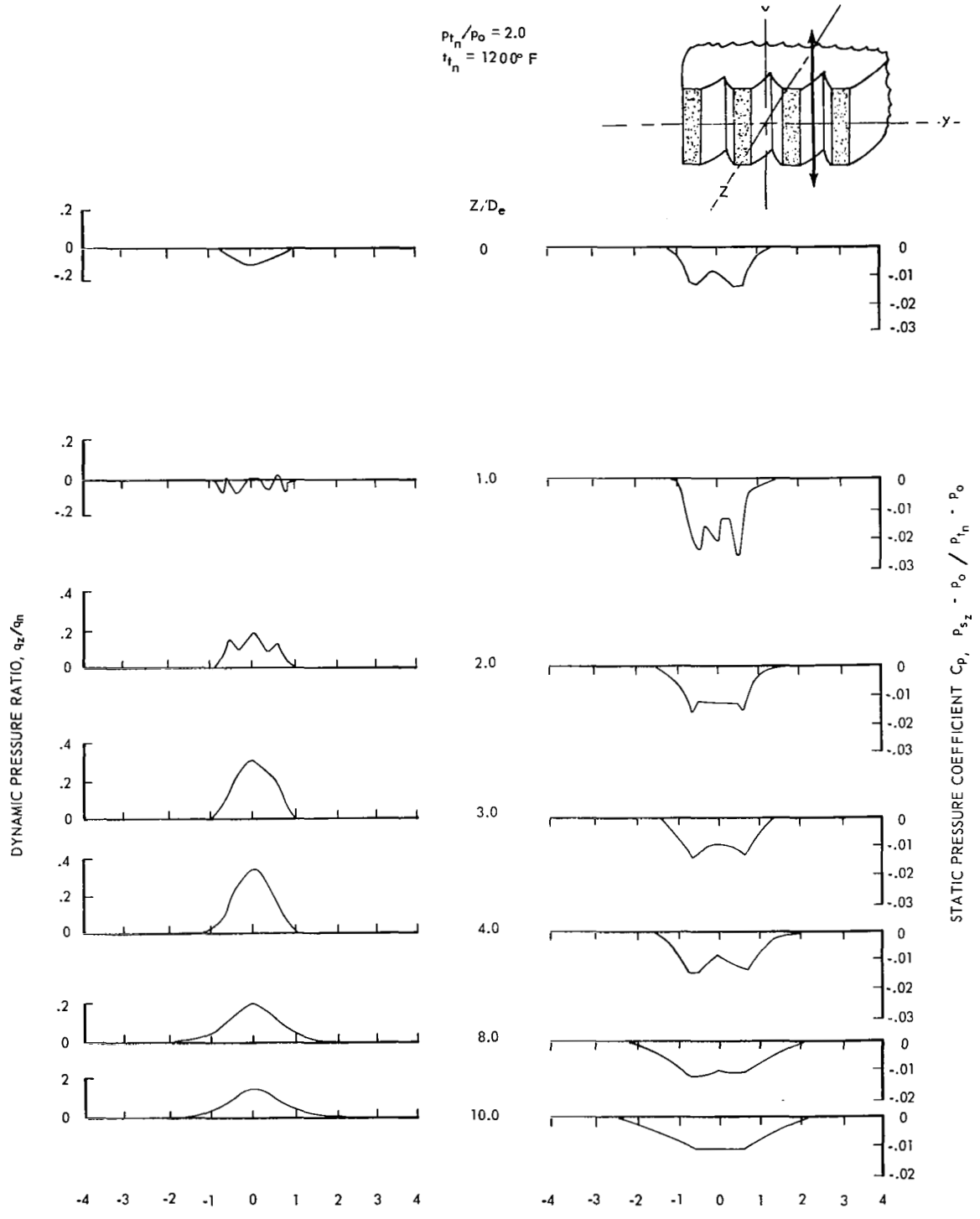

(d) SURVEYS AT DISTANCE OF 1.80 INCHES FROM NOZZLE CENTERLINE

Figure 14 - Continued

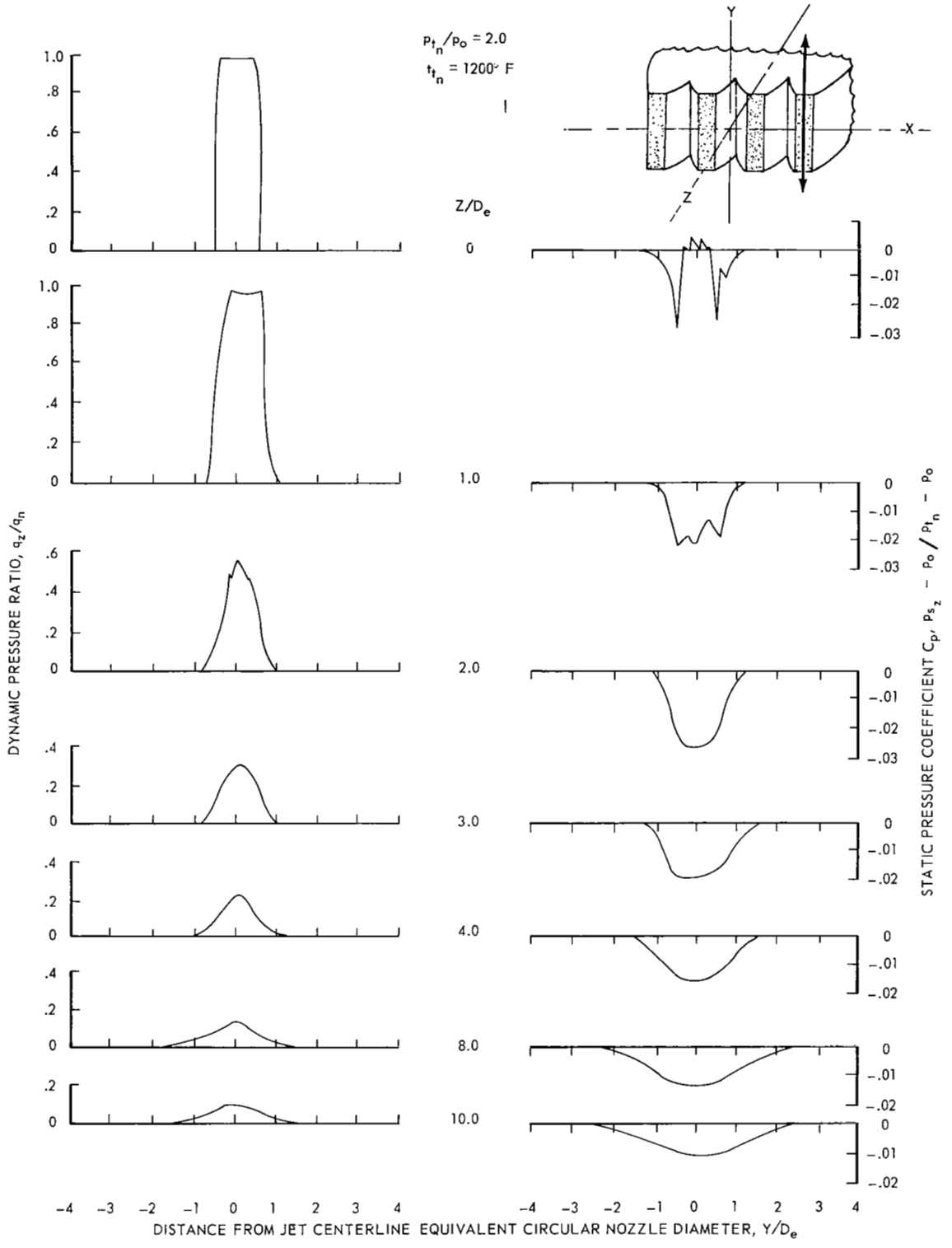

(e) SURVEY AT DISTANCE OF 2.70 INCHES FROM NOZZLE CENTERLINE

Figure 14 - Concluded

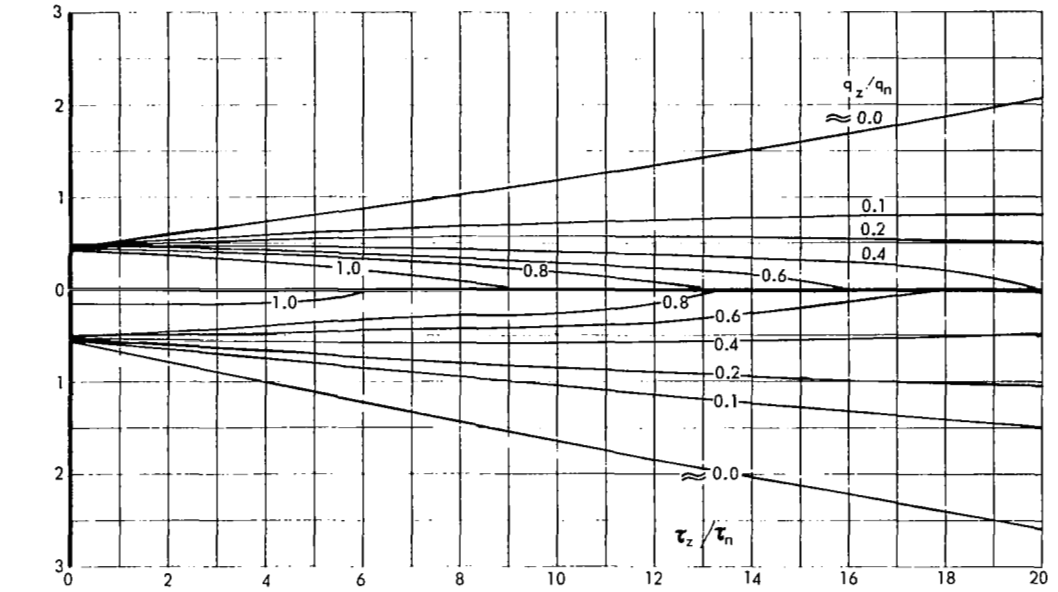

(a) CIRCULAR NOZZLE 1.1 (Y = 0)

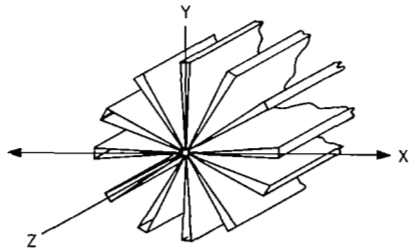

P_{t_n}/P_o = 2.0

t_{t_n} = 1200° F

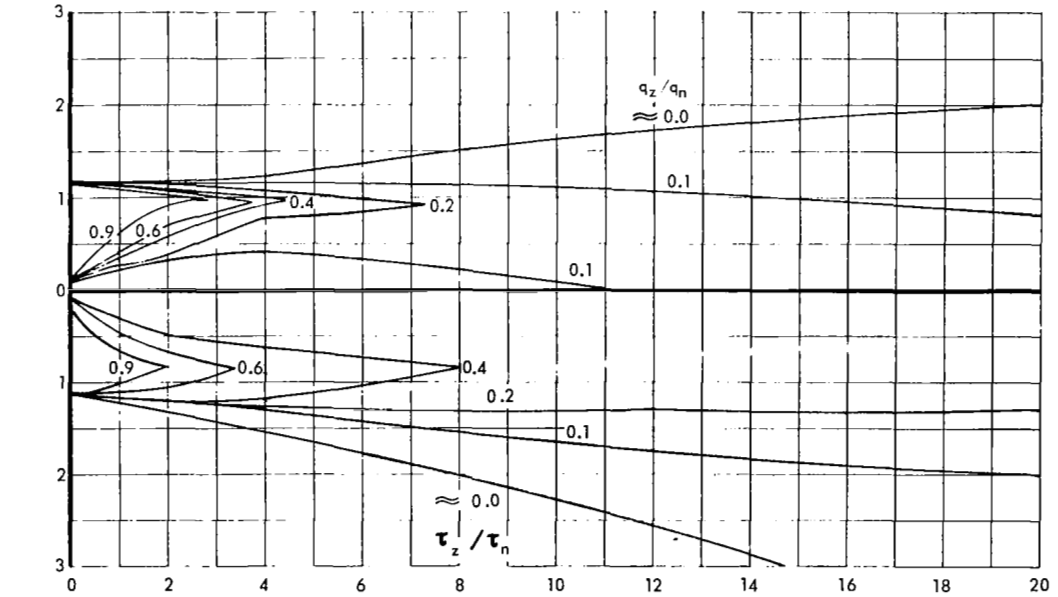

DISTANCE FROM JET CENTERLINE /EQUIVALENT CIRCULAR NOZZLE DIAMETER, X/D_e

AXIAL DISTANCE FROM NOZZLE EXIT/EQUIVALENT CIRCULAR NOZZLE DIAMETER, Z/D_e

(b) TWELVE-SEGMENT NOZZLE 1.3 (Y = 0)

Figure 15 - Jet wake dynamic pressure and differential temperature surveys of several basic nozzles out of ground effect

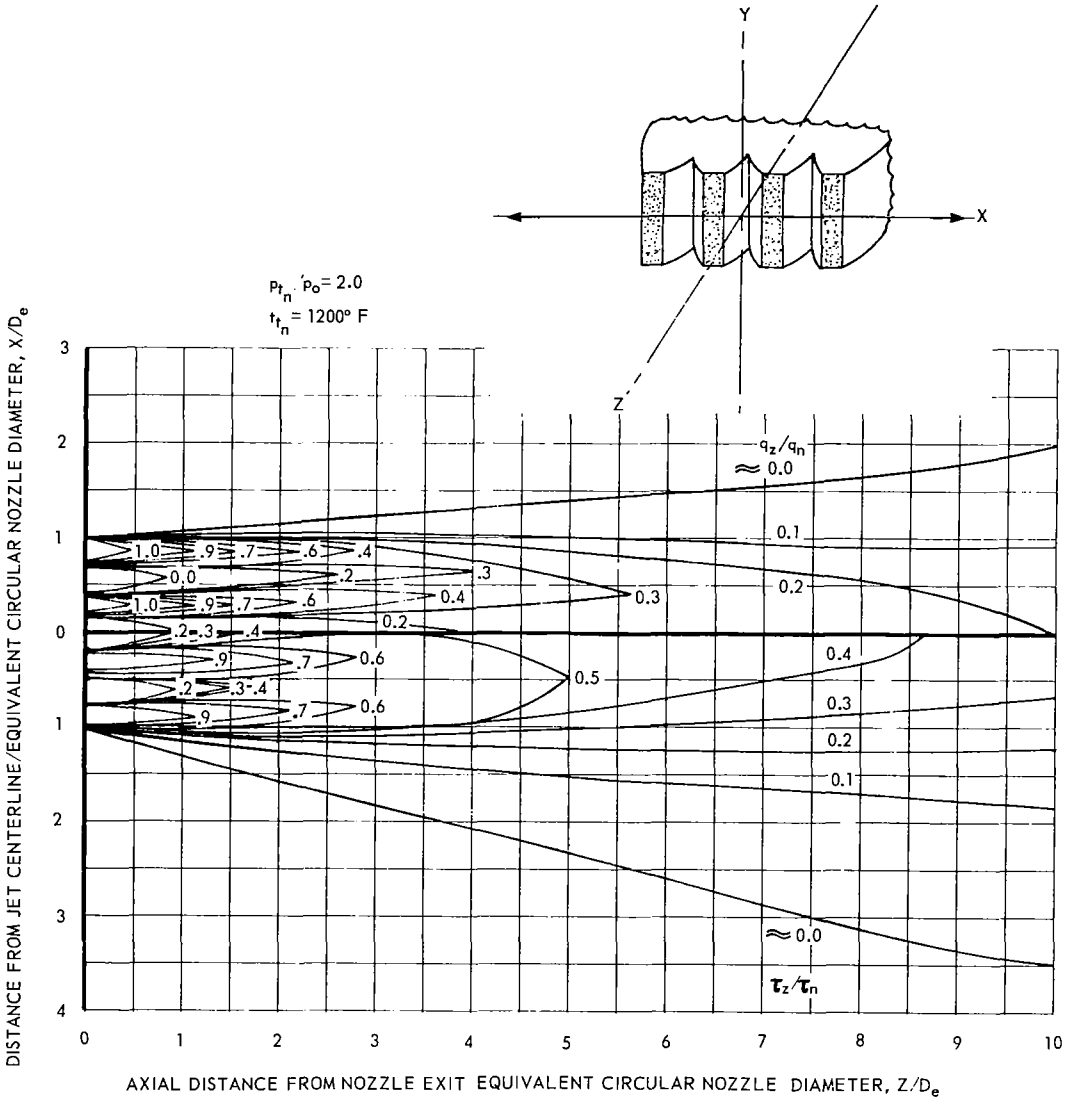

(c) SUPPRESSOR NOZZLE 2.1 (Y ▫ 0)

Figure 15 - Continued

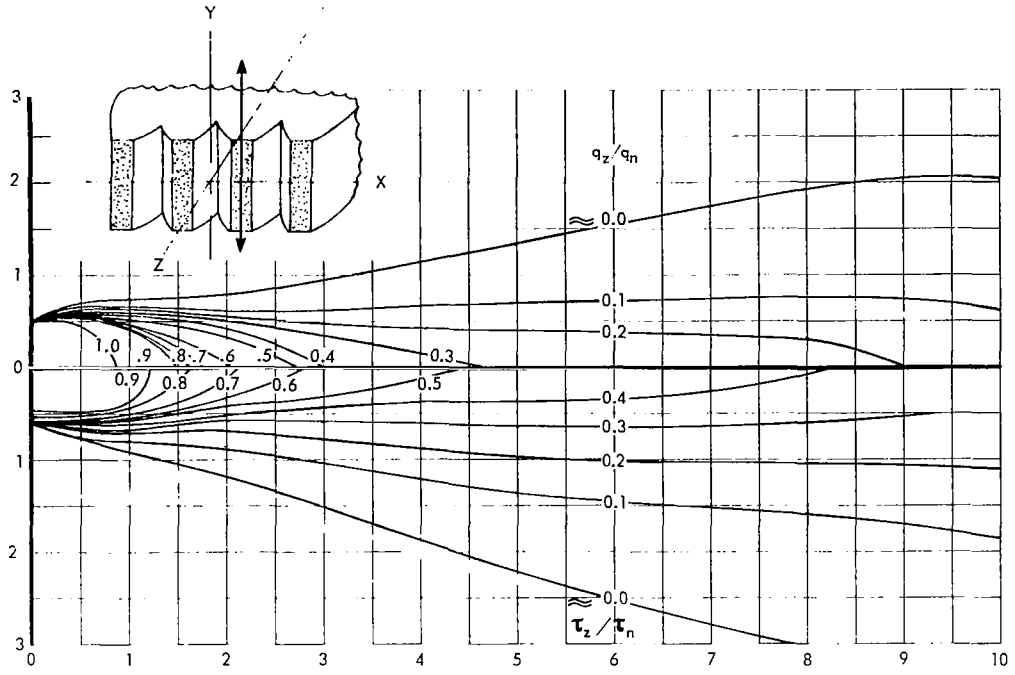

(d) SUPPRESSOR NOZZLE 2.1 (X = 0.90 INCHES).

P_{t_n}/P_o = 2.0

t_{t_n} = 1200° F

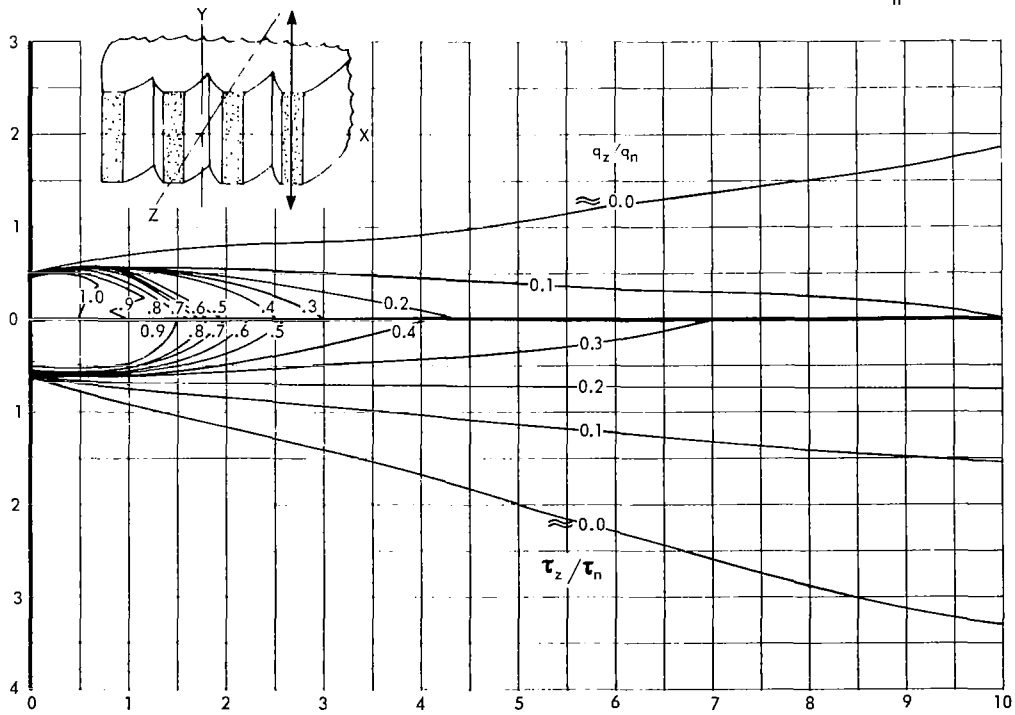

DISTANCE FROM JET CENTERLINE EQUIVALENT CIRCULAR NOZZLE DIAMETER, Y D_e

AXIAL DISTANCE FROM NOZZLE EXIT / EQUIVALENT CIRCULAR NOZZLE DIAMETER, Z D_e

(e) SUPPRESSOR NOZZLE 2.1 (X = 2.70 INCHES).

Figure 15 - Continued

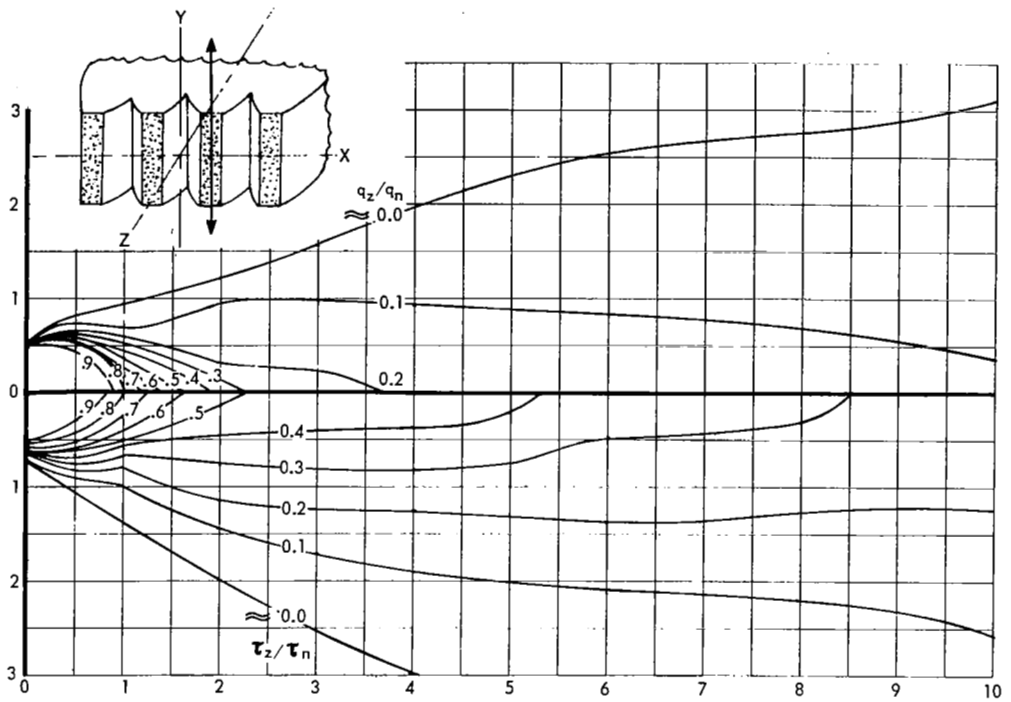

(f) SUPPRESSOR NOZZLE 2.7 (X = 0.90 INCHES)

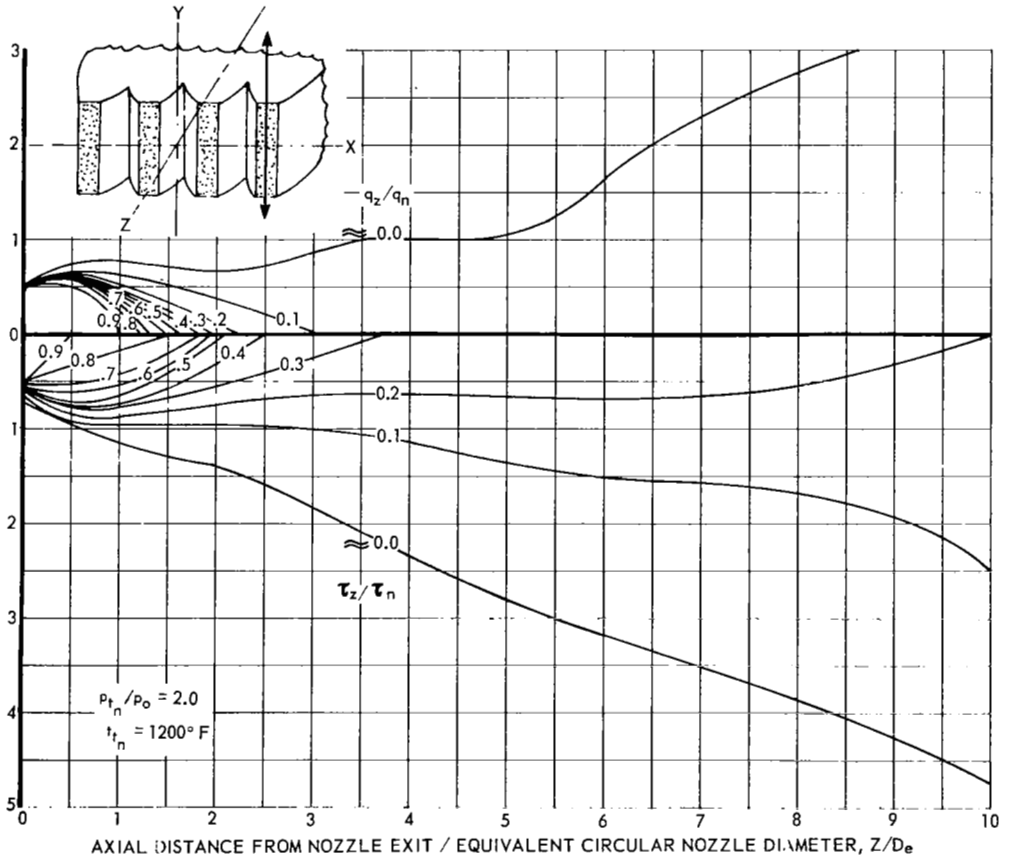

DISTANCE FROM JET CENTERLINE/EQUIVALENT CIRCULAR NOZZLE DIAMETER Y/D_e

AXIAL DISTANCE FROM NOZZLE EXIT / EQUIVALENT CIRCULAR NOZZLE DIAMETER, Z/D_e

(g) SUPPRESSOR NOZZLE 2.7 (X = 2.70 INCHES)

Figure 15 - Concluded

NOZZLE	CONFIGURATION			
		AR	S/W	β
△	2.1	5	3.0	0°
◇	2.2	5	3.0	5°
⊙	2.3	5	1.5	15°
×	2.4	5	2.0	15°

NOZZLE	CONFIGURATION			
		AR	S/W	β
⬡	2.5	5	3.0	15°
⬠	2.6	5	4.0	15°
⬭	2.7	5	3.0	30°
△	2.8	3	3.0	15°

NOZZLE	CONFIGURATION			
		AR	S/W	β
▷	2.9	10	3.0	15°
⊙	1.1	CIRCULAR		
⬚	1.2	DELTA 5 AR ,5° β		
◇	1.3	TWELVE SEGMENT		

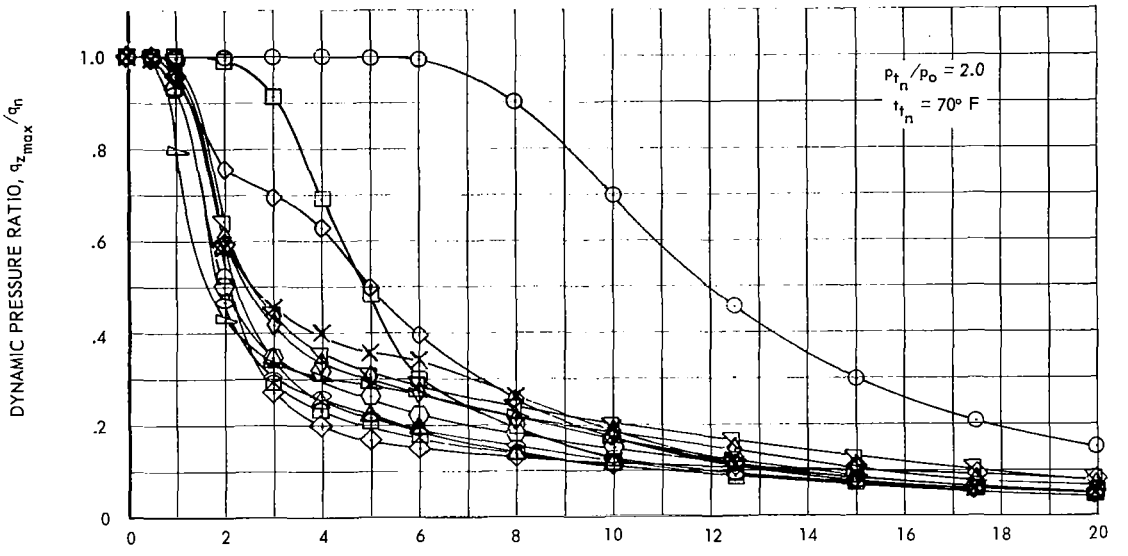

(a) NOZZLE DISCHARGE TEMPERATURE = 70°F

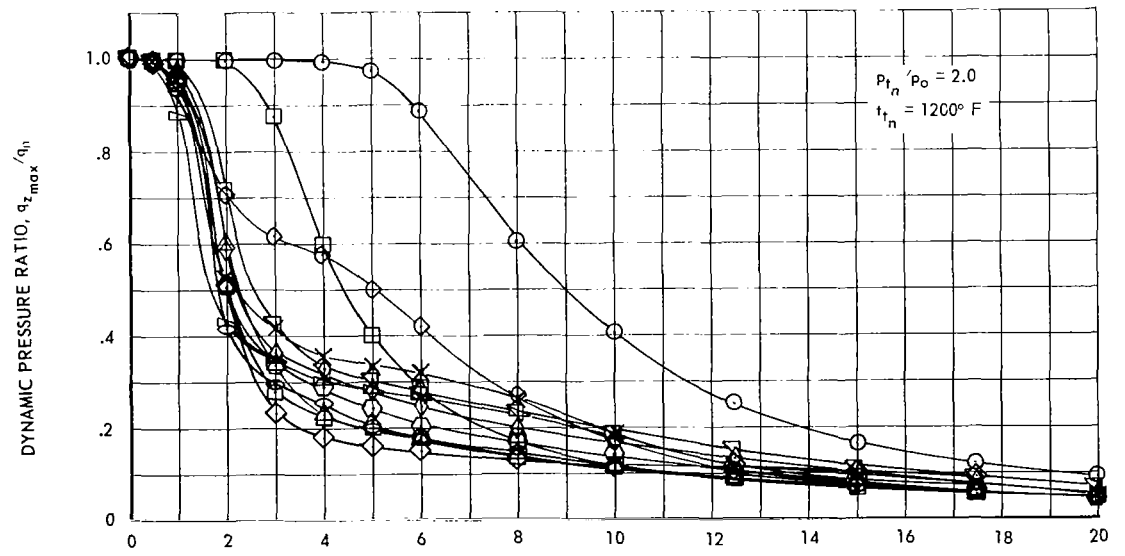

(b) NOZZLE DISCHARGE TEMPERATURE = 1200° F

Figure 16 - Jet wake dynamic pressure degradation versus distance from nozzle exit for all basic nozzle out of ground effect

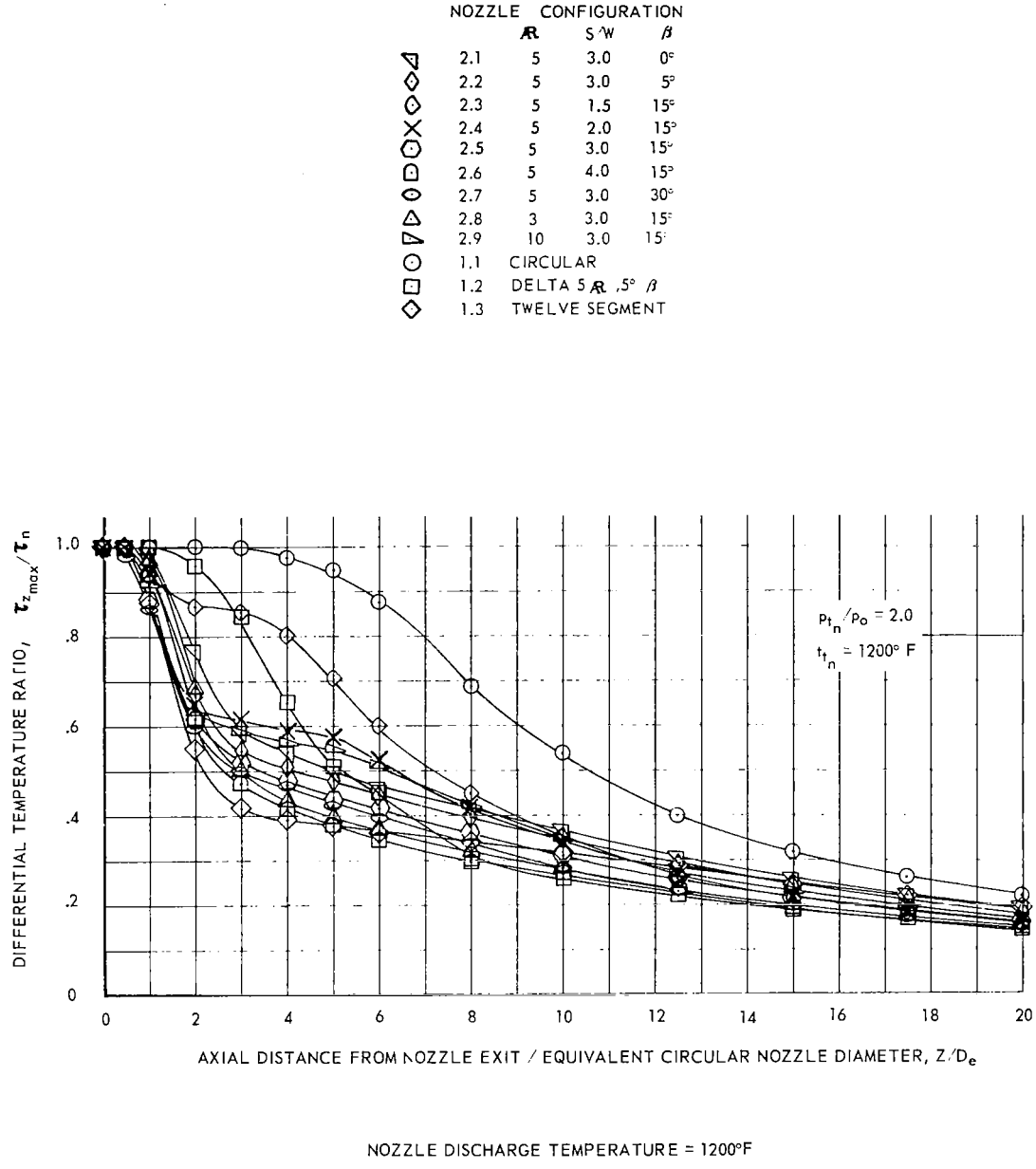

Figure 17 - Jet wake differential temperature degradation versus distance from nozzle exit for all basic nozzles out of ground effect

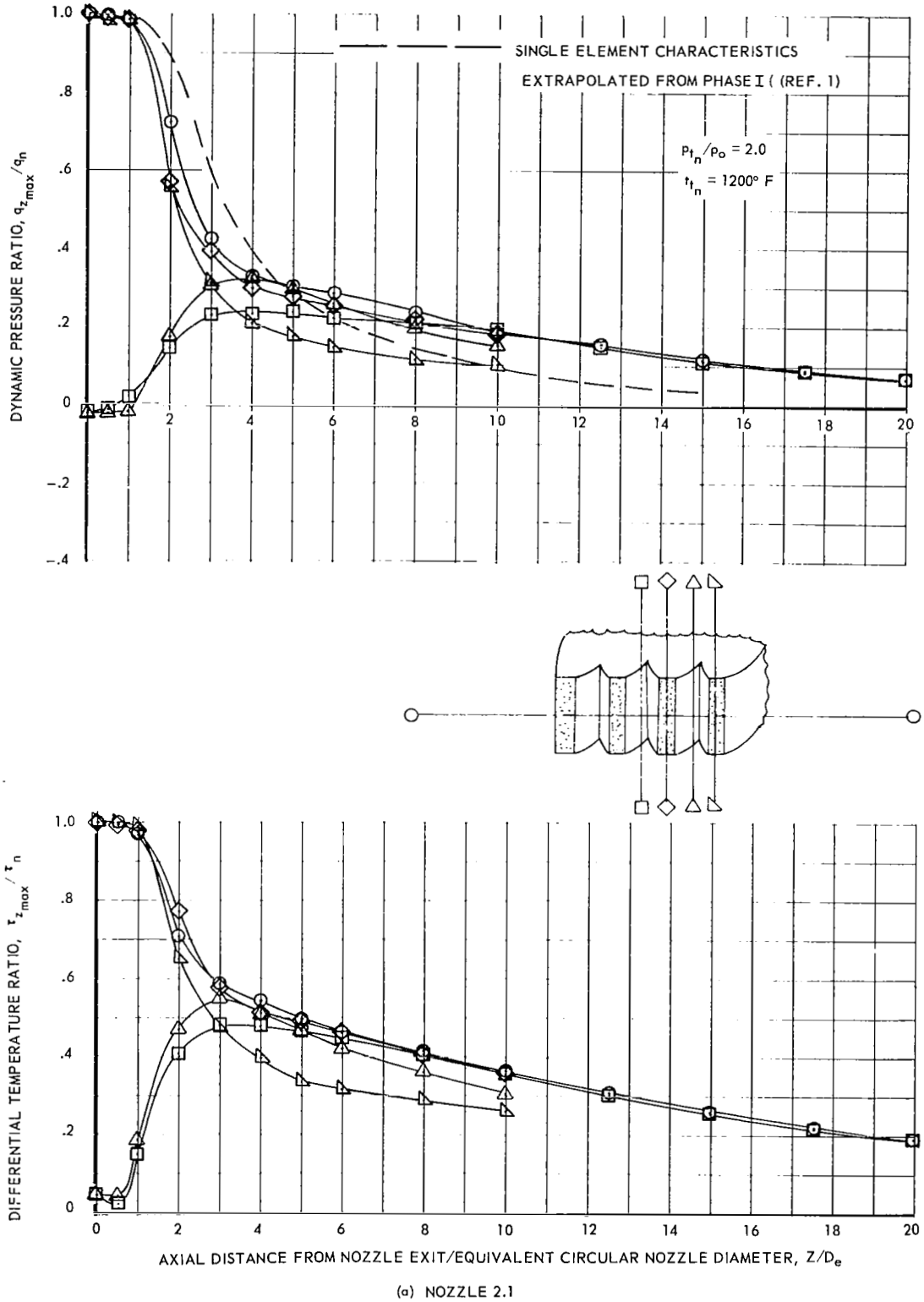

(a) NOZZLE 2.1

Figure 18 - Jet wake degradation characteristics for several basic nozzle configurations and survey planes

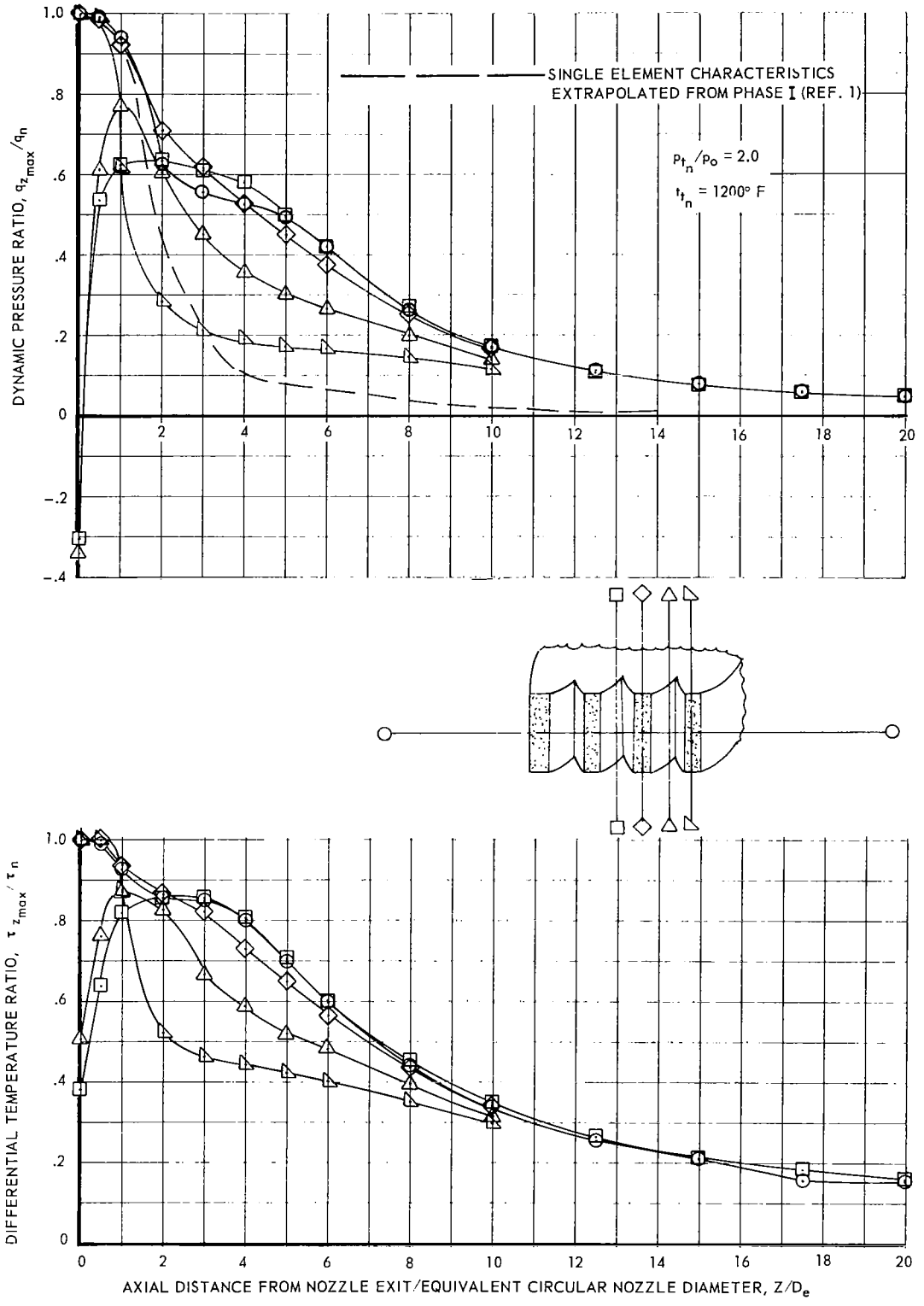

(b) NOZZLE 2.3

Figure 18 - Continued

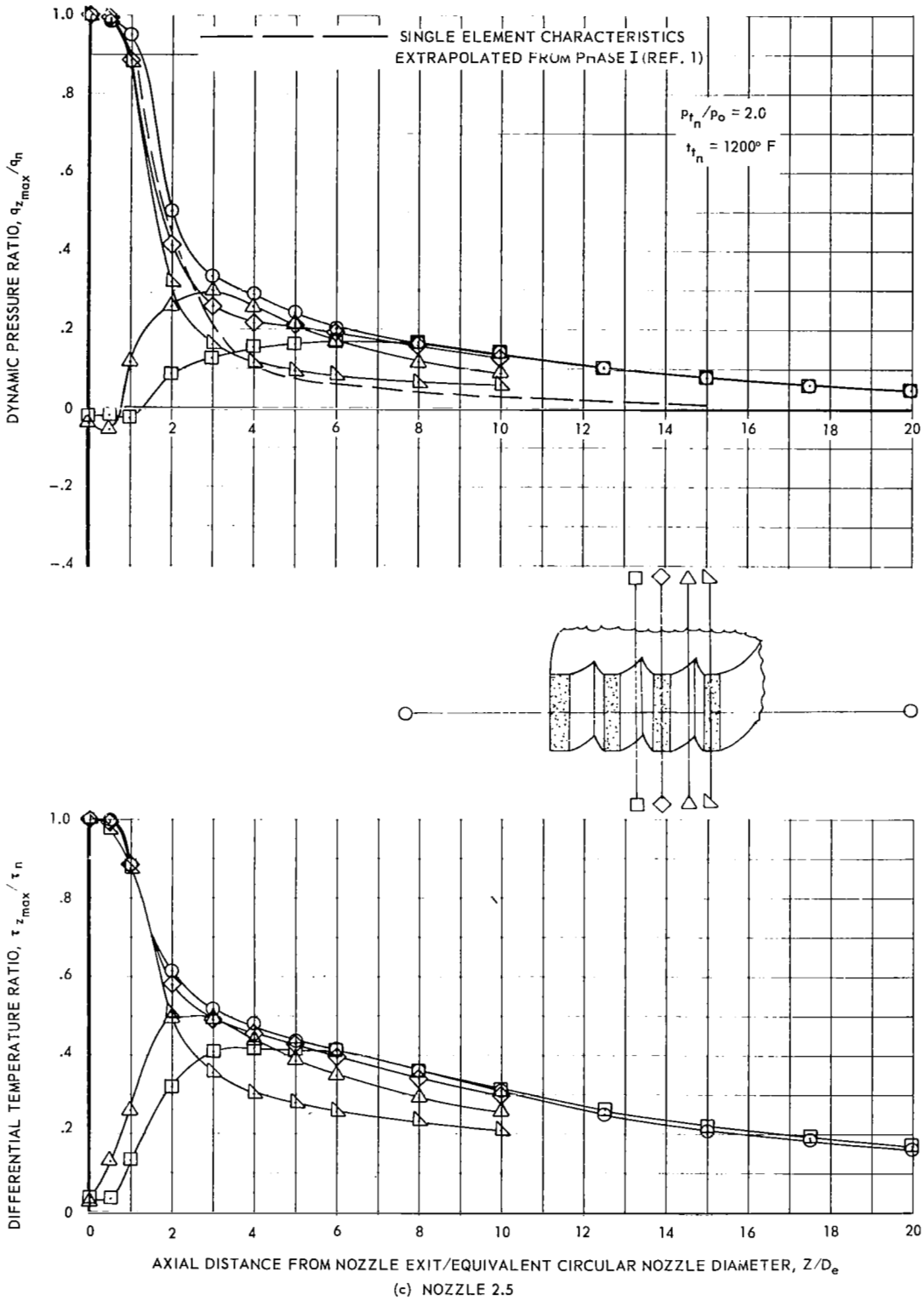

(c) NOZZLE 2.5

Figure 18 - Continued

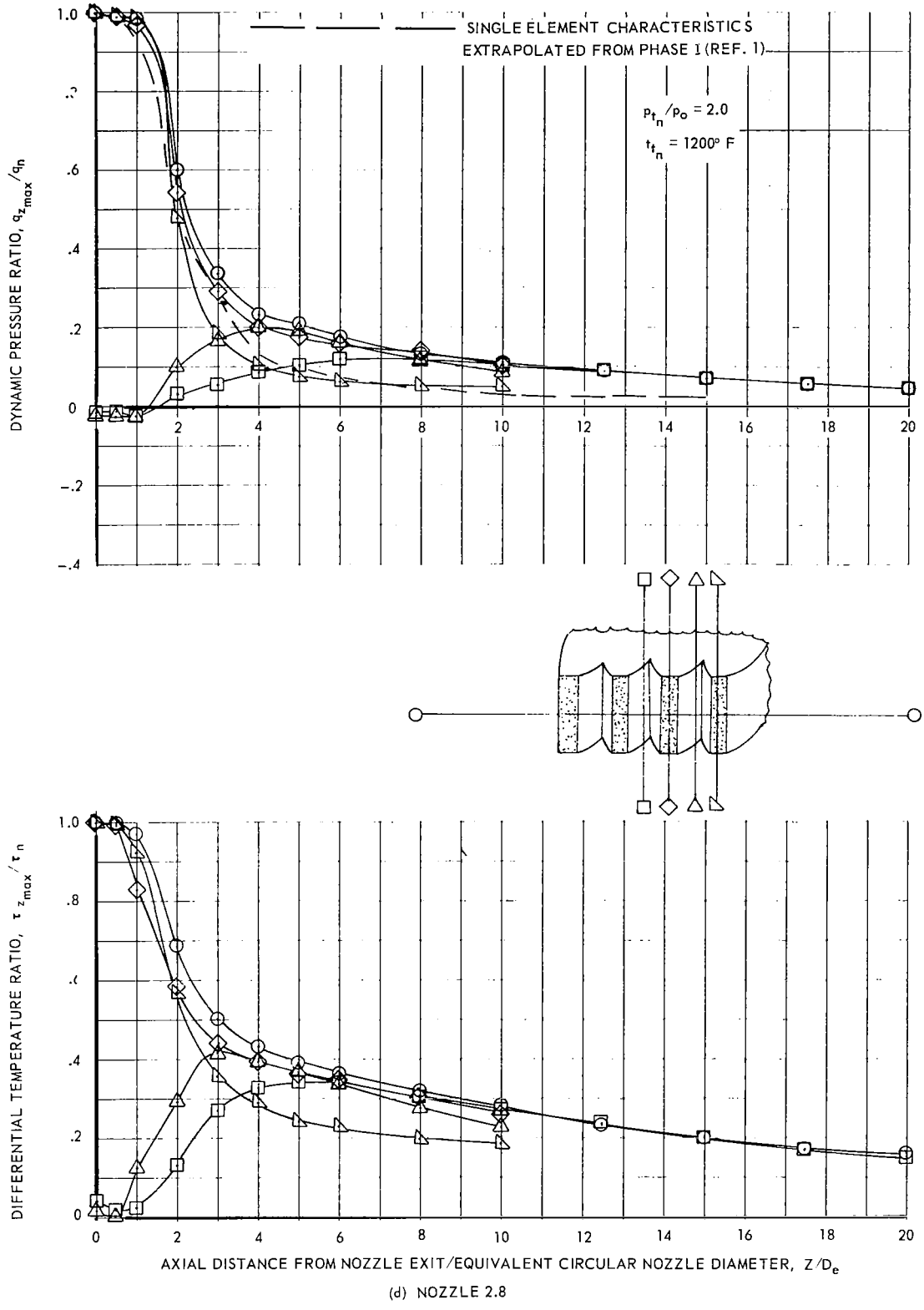

(d) NOZZLE 2.8

Figure 18 - Continued

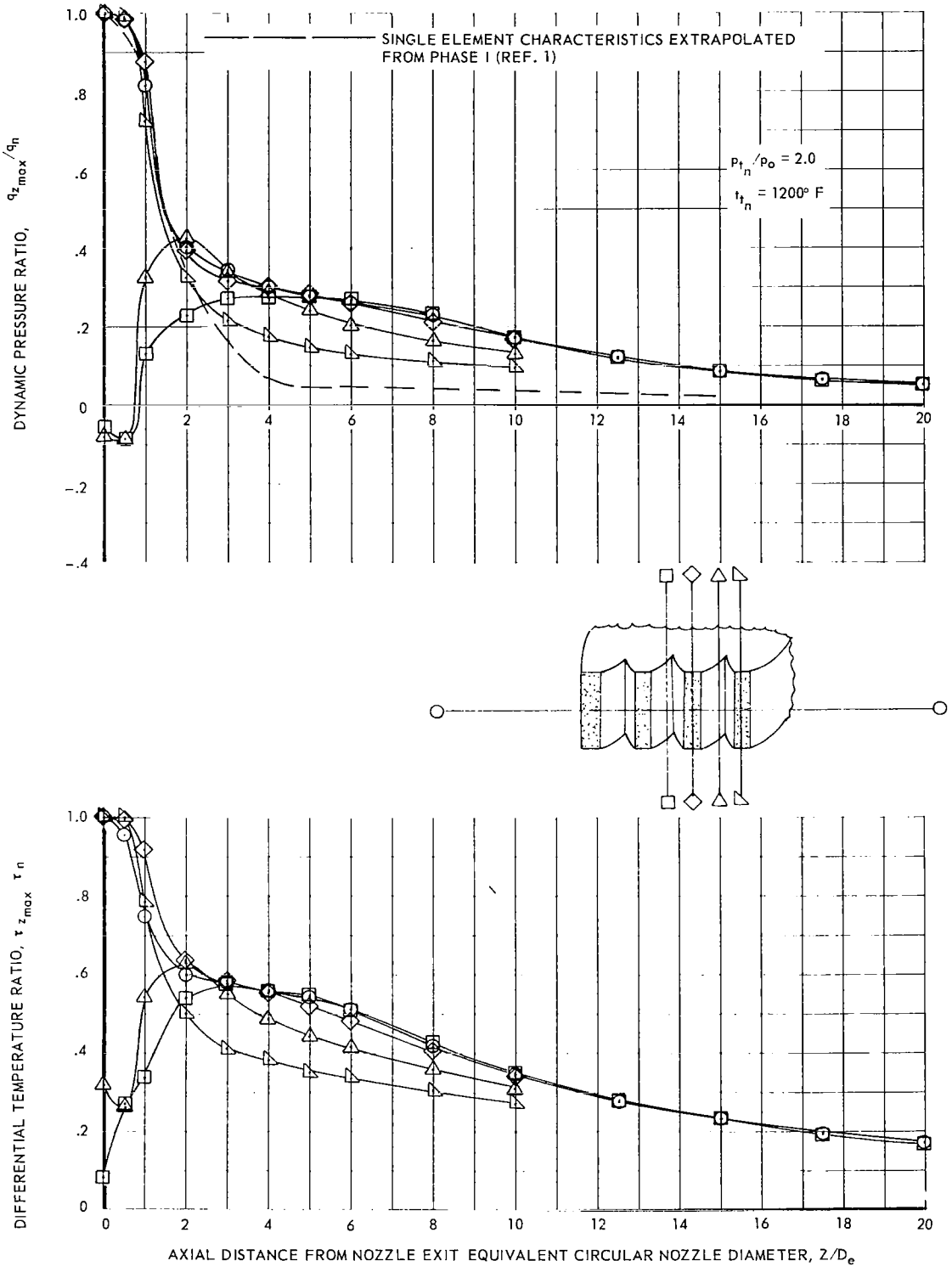

(e) NOZZLE 2.9

Figure 18 - Concluded

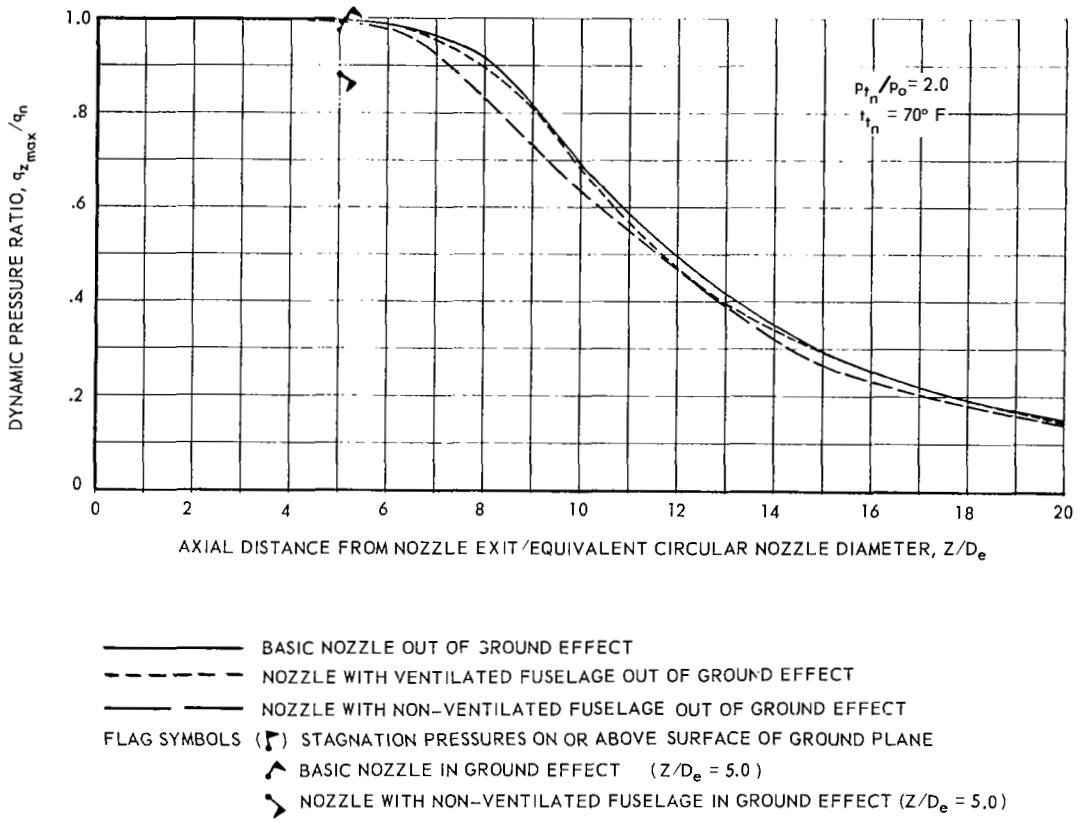

(a) CIRCULAR NOZZLE 1.1 WITH DISCHARGE TEMPERATURE = 70° F

Figure 19 - Effect of fuselage and ground plane on jet wake degradation characteristics

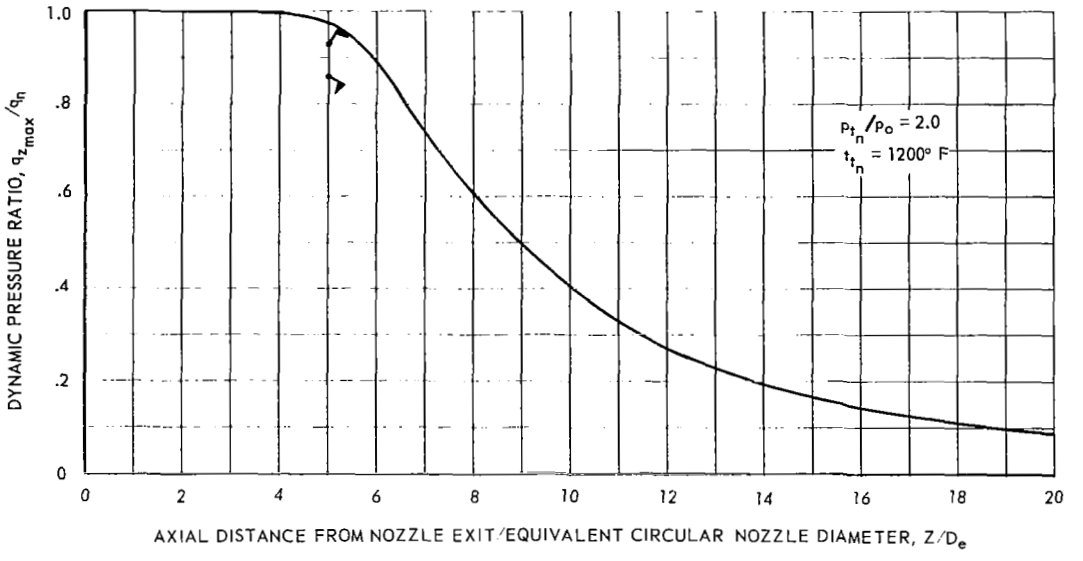

BASIC NOZZLE, OUT OF GROUND EFFECT

FLAG SYMBOLS ( ) STAGNATION PRESSURES OR DIFFERENTIAL TEMPERATURES ON OR ABOVE SURFACE OF GROUND PLANE

BASIC NOZZLE IN GROUND EFFECT ($Z/D_e = 5.0$)

NOZZLE WITH NON-VENTILATED FUSELAGE IN GROUND EFFECT ($Z/D_e = 5.0$)

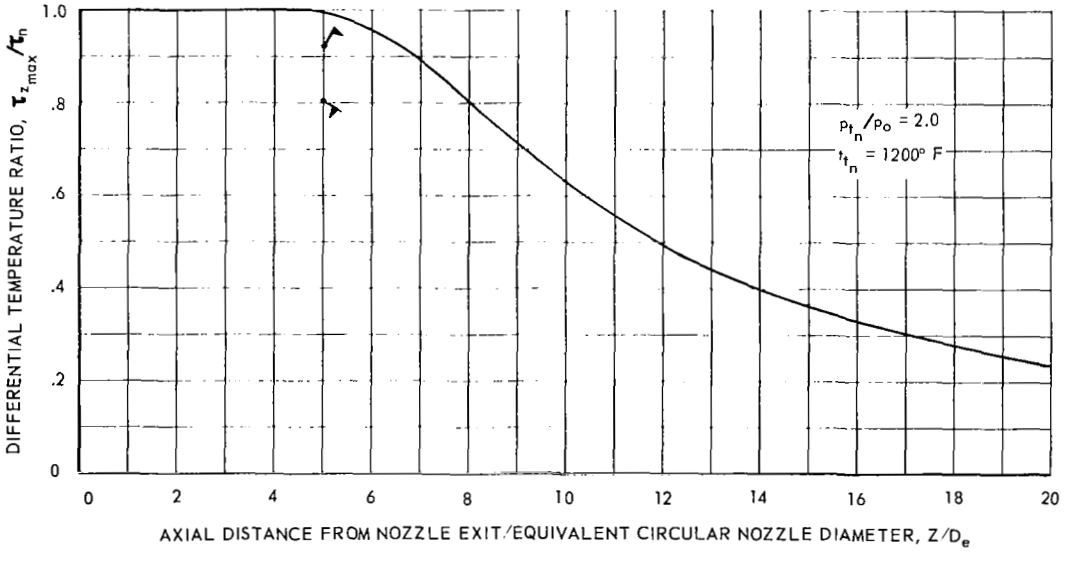

(b) CIRCULAR NOZZLE 1.1 WITH DISCHARGE TEMPERATURE ■ 1200° F

Figure 19 - Continued

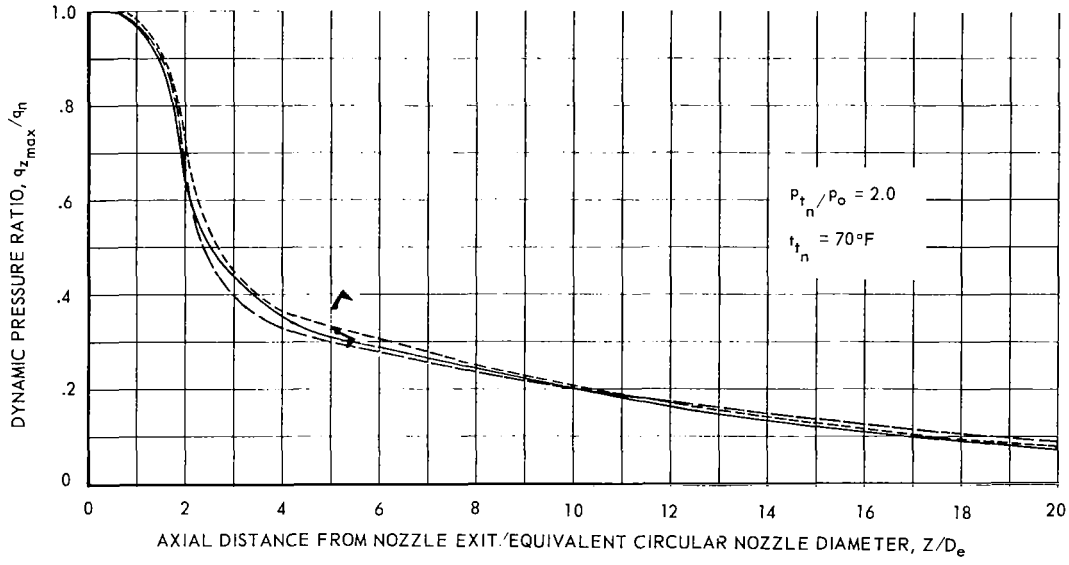

BASIC NOZZLE OUT OF GROUND EFFECT

NOZZLE WITH VENTILATED FUSELAGE OUT OF GROUND EFFECT

NOZZLE WITH NON-VENTILATED FUSELAGE OUT OF GROUND EFFECT

FLAG SYMBOLS ( ) STAGNATION PRESSURES ON OR ABOVE SURFACE OF GROUND PLANE

BASIC NOZZLE IN GROUND EFFECT (Z/D_e = 5.0)

NOZZLE WITH NON-VENTILATED FUSELAGE IN GROUND EFFECT (Z/D_e = 5.0)

(c) SUPPRESSOR NOZZLE 2.1 WITH DISCHARGE TEMPERATURE ◻ 70° F

Figure 19 - Continued

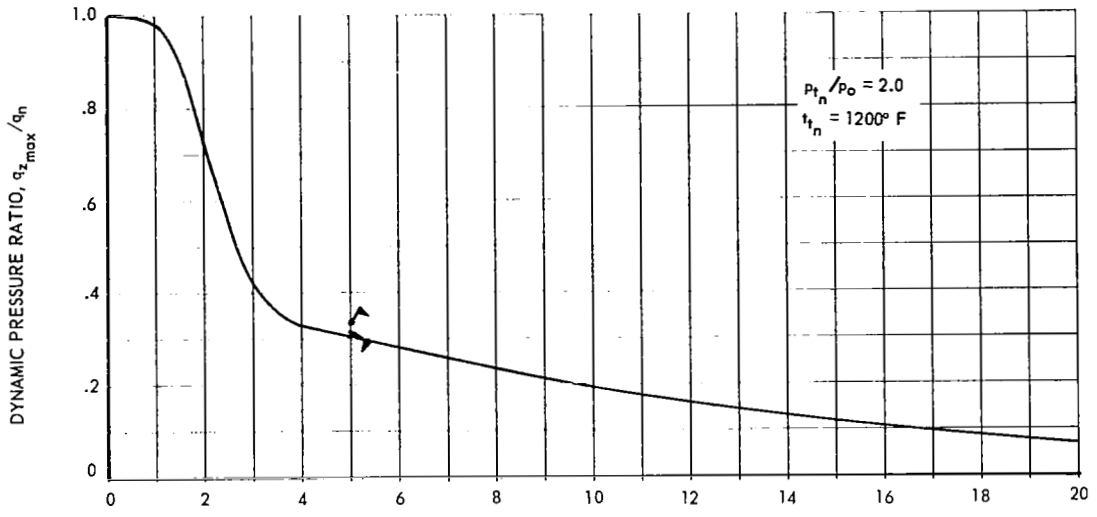

BASIC NOZZLE, OUT OF GROUND EFFECT

FLAG SYMBOLS
- STAGNATION PRESSURES OR DIFFERENTIAL TEMPERATURES ON OR ABOVE SURFACE OF GROUND PLANE
- BASIC NOZZLE IN GROUND EFFECT (Z/D_e = 5.0)
- NOZZLE WITH NON-VENTILATED FUSELAGE IN GROUND EFFECT (Z/D_e = 5.0)

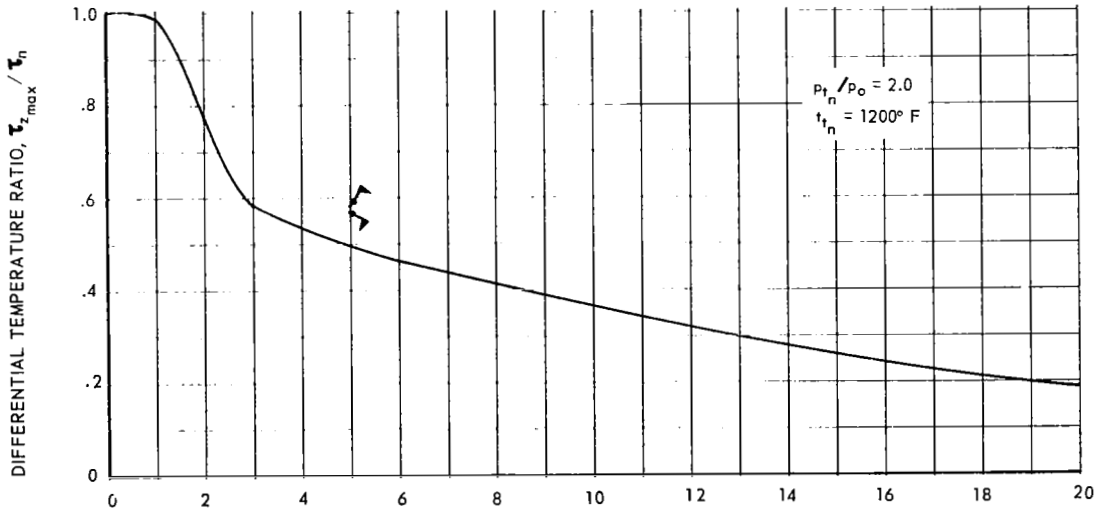

(d) SUPPRESSOR NOZZLE 2.1 WITH DISCHARGE TEMPERATURE = 1200° F

Figure 19 - Continued

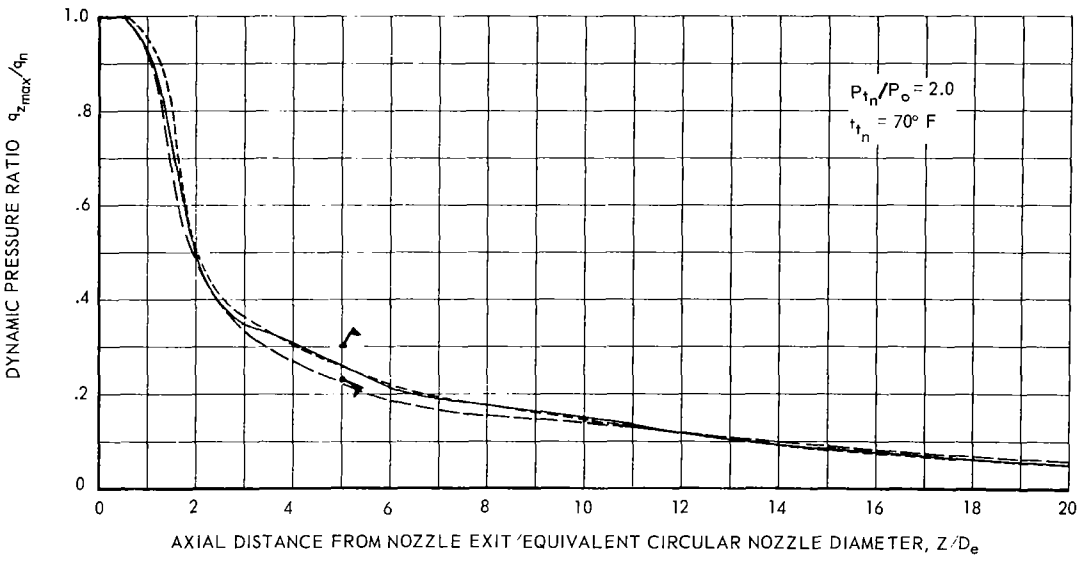

BASIC NOZZLE OUT OF GROUND EFFECT

NOZZLE WITH VENTILATED FUSELAGE OUT OF GROUND EFFECT

NOZZLE WITH NON-VENTILATED FUSELAGE OUT OF GROUND EFFECT

FLAG SYMBOLS (⚑) STAGNATION PRESSURES OR DIFFERENTIAL TEMPERATURES ON OR ABOVE SURFACE OF GROUND PLANE

BASIC NOZZLE IN GROUND EFFECT (Z/D_e = 5.0)

NOZZLE WITH NON-VENTILATED FUSELAGE IN GROUND EFFECT (Z/D_e = 5.0)

(e) SUPPRESSOR NOZZLE 2.5 WITH DISCHARGE TEMPERATURE = 70° F

Figure 19 - Continued

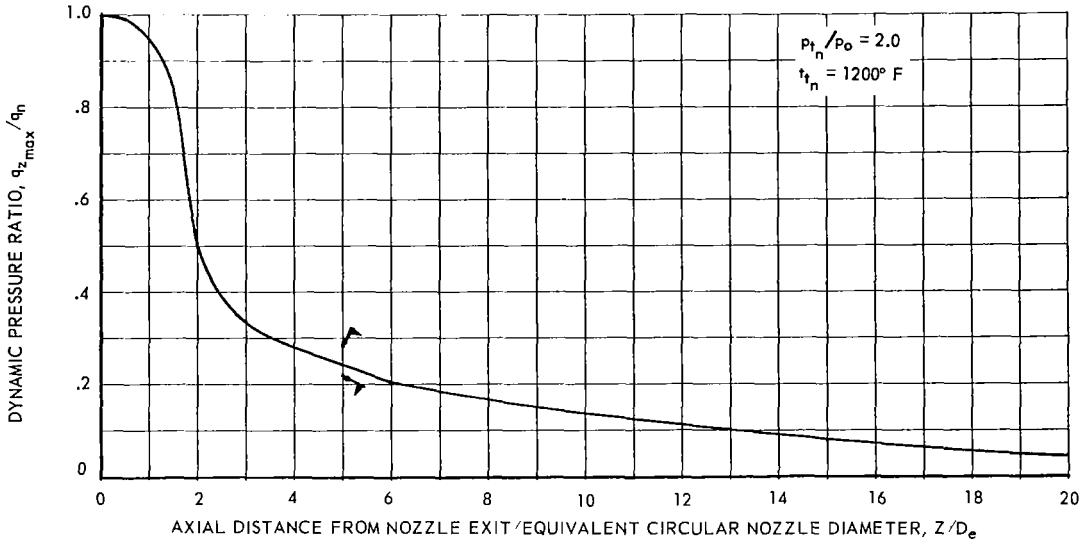

BASIC NOZZLE, OUT OF GROUND EFFECT

FLAG SYMBOLS
- STAGNATION PRESSURES OR DIFFERENTIAL TEMPERATURES ON OR ABOVE SURFACE OF GROUND PLANE
- BASIC NOZZLE IN GROUND EFFECT (Z/D_e = 5.0)
- NOZZLE WITH NON-VENTILATED FUSELAGE IN GROUND EFFECT (Z/D_e = 5.0)

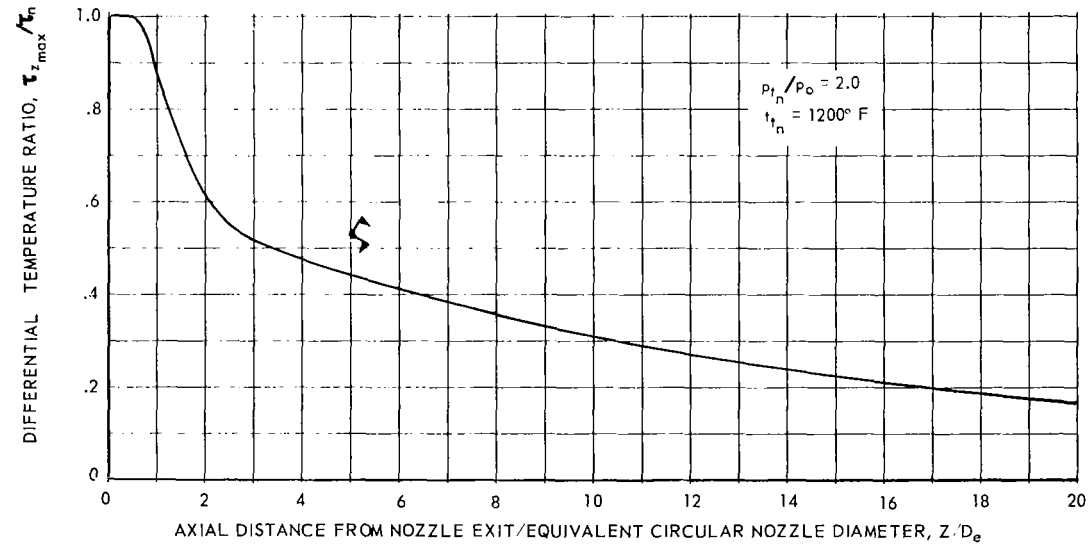

(f) SUPPRESSOR NOZZLE 2.5 WITH DISCHARGE TEMPERATURE = 1200° F

Figure 19 - Concluded

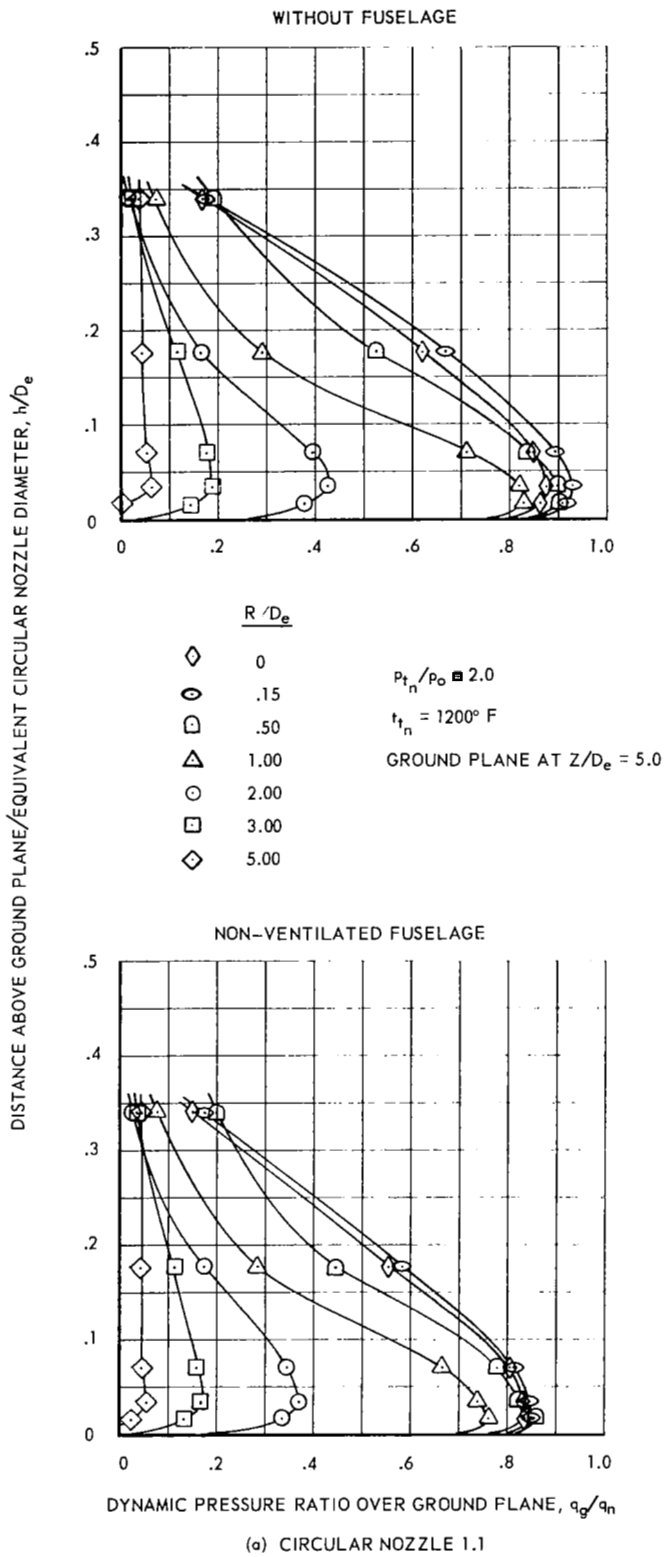

(a) CIRCULAR NOZZLE 1.1

Figure 20 - Dynamic pressure distribution in the jet efflux adjacent to the ground plane

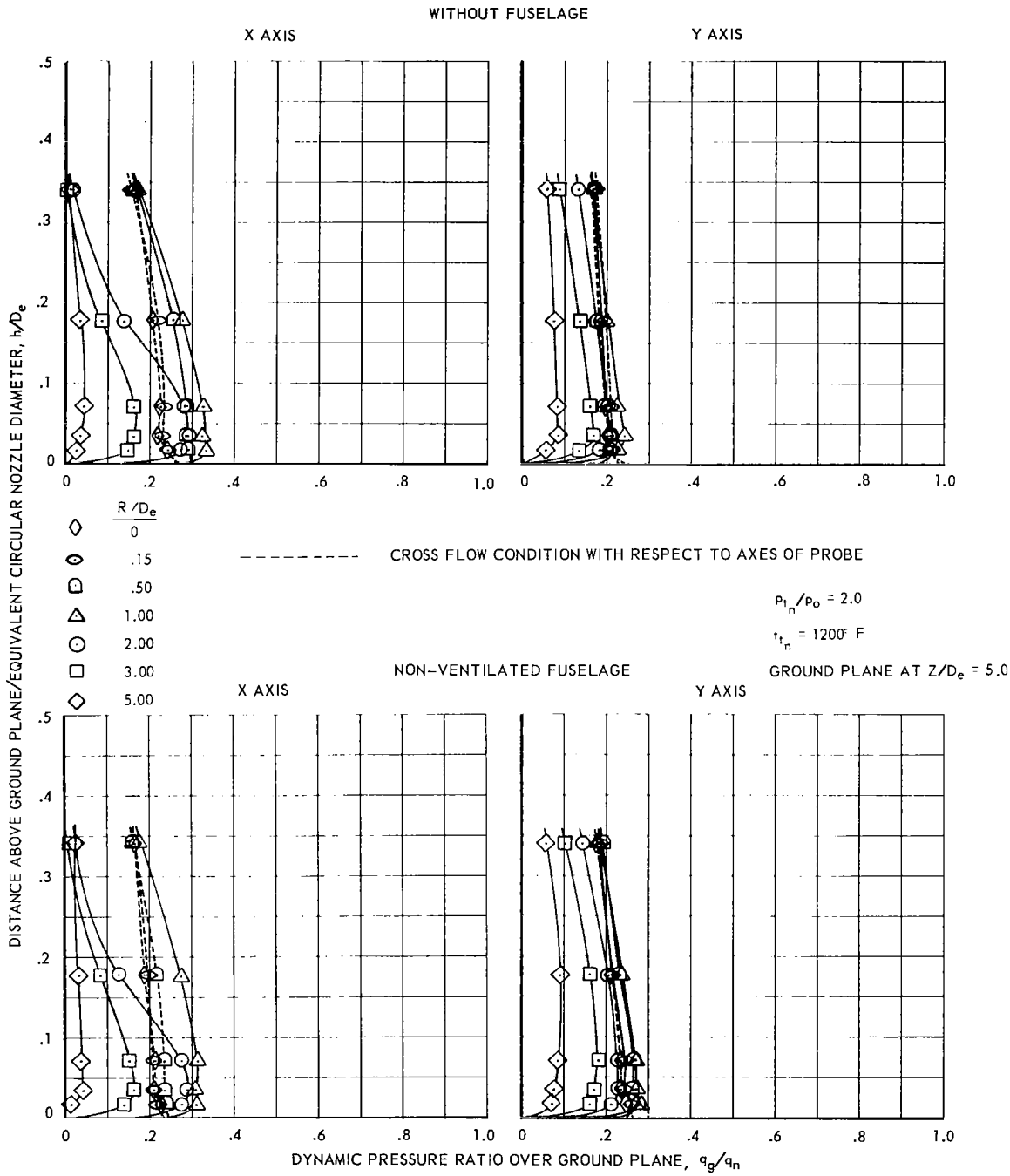

(b) SUPPRESSOR NOZZLE 2.1

Figure 20 - Continued

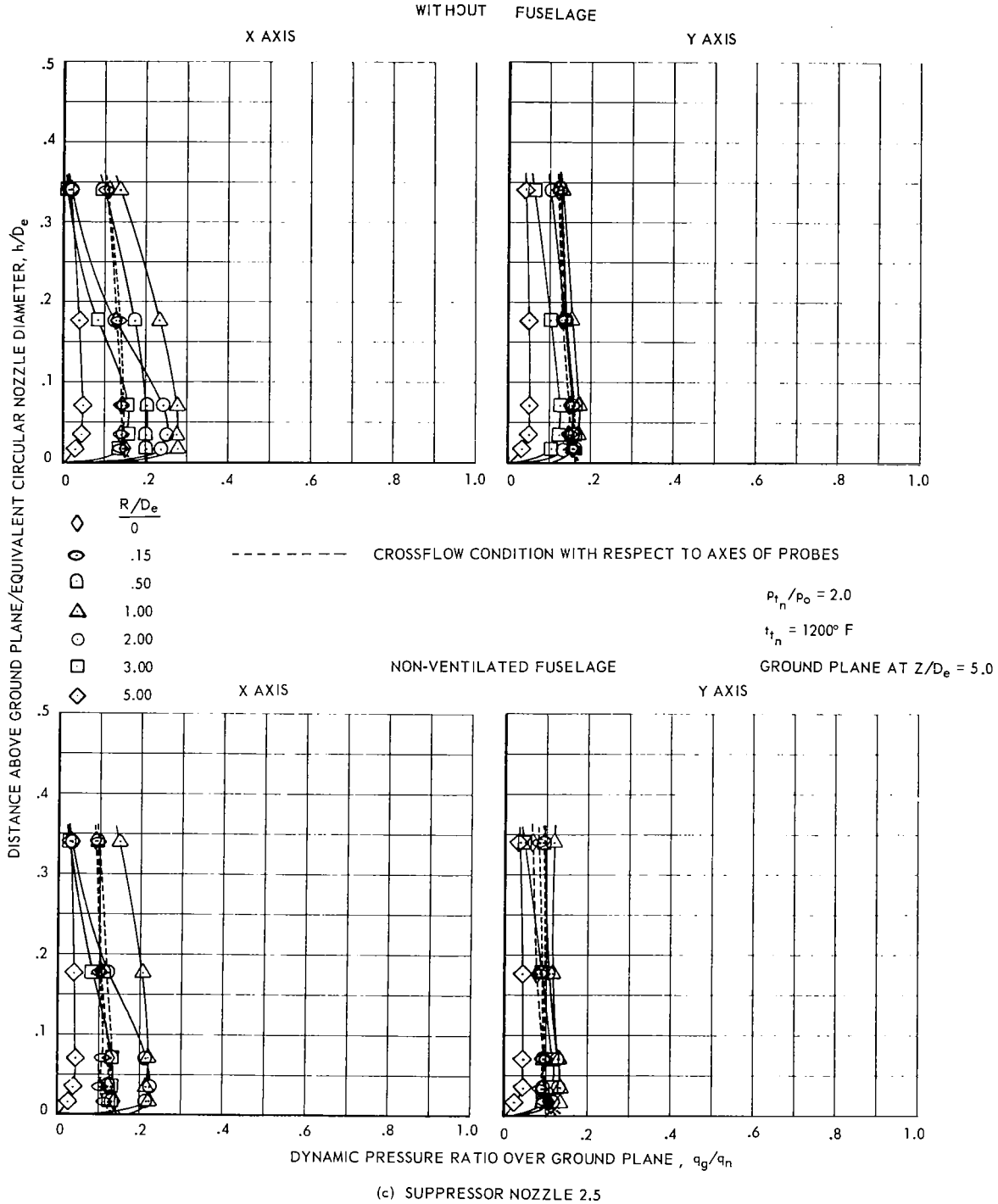

(c) SUPPRESSOR NOZZLE 2.5

Figure 20 - Concluded

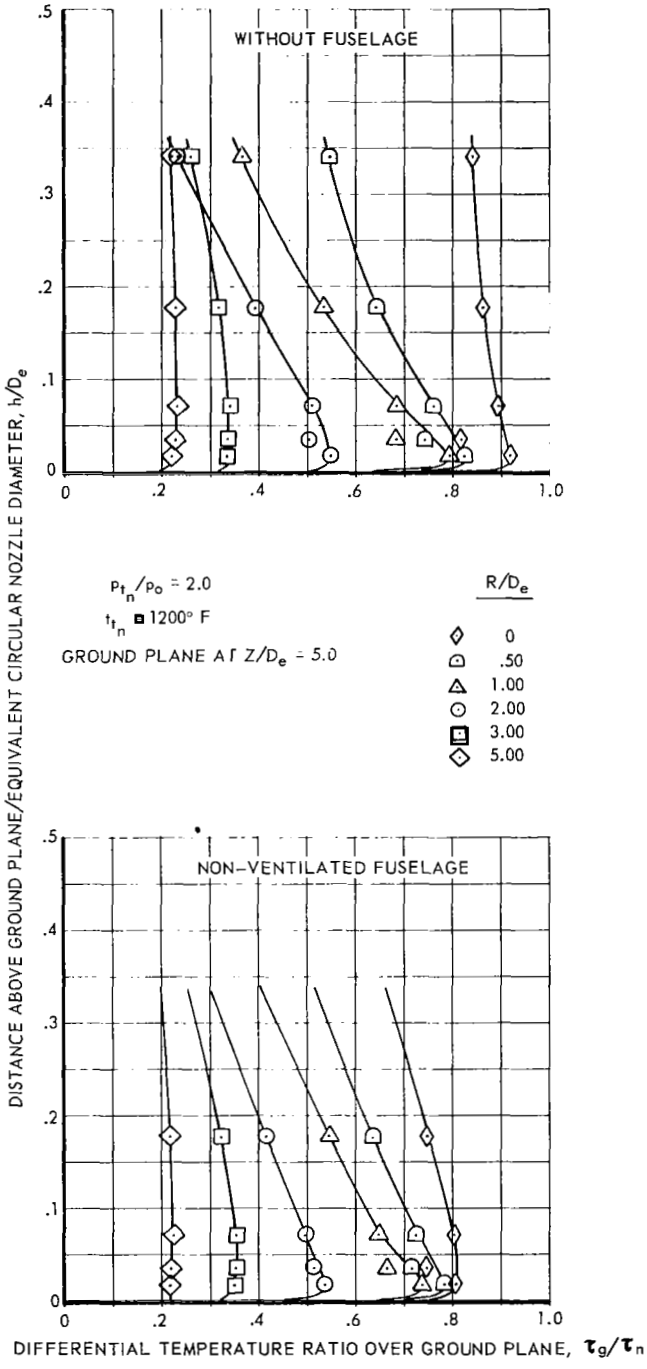

(a) CIRCULAR NOZZLE 1.1

Figure 21 - Differential temperature distribution adjacent to ground plane

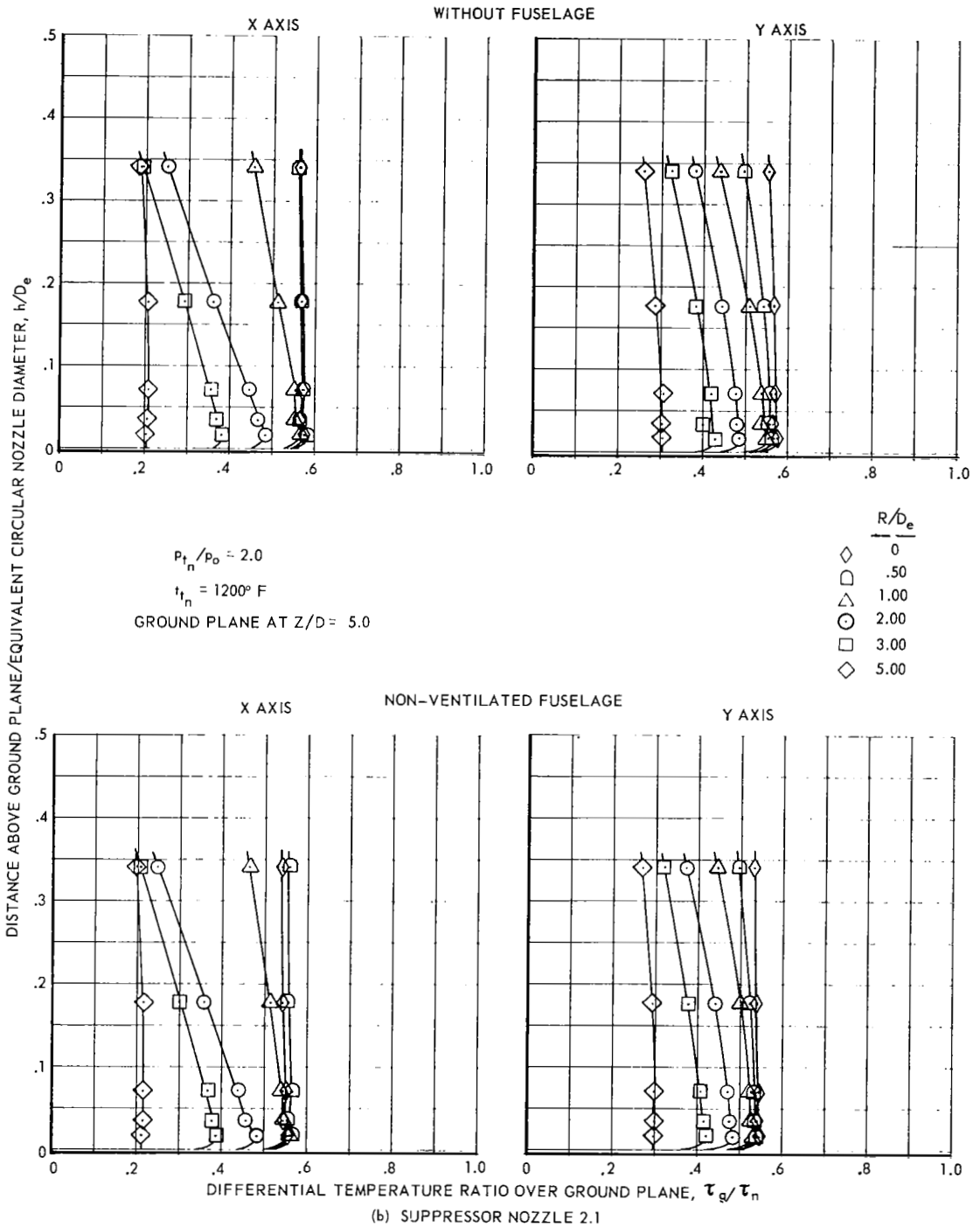

(b) SUPPRESSOR NOZZLE 2.1

Figure 21 - Continued

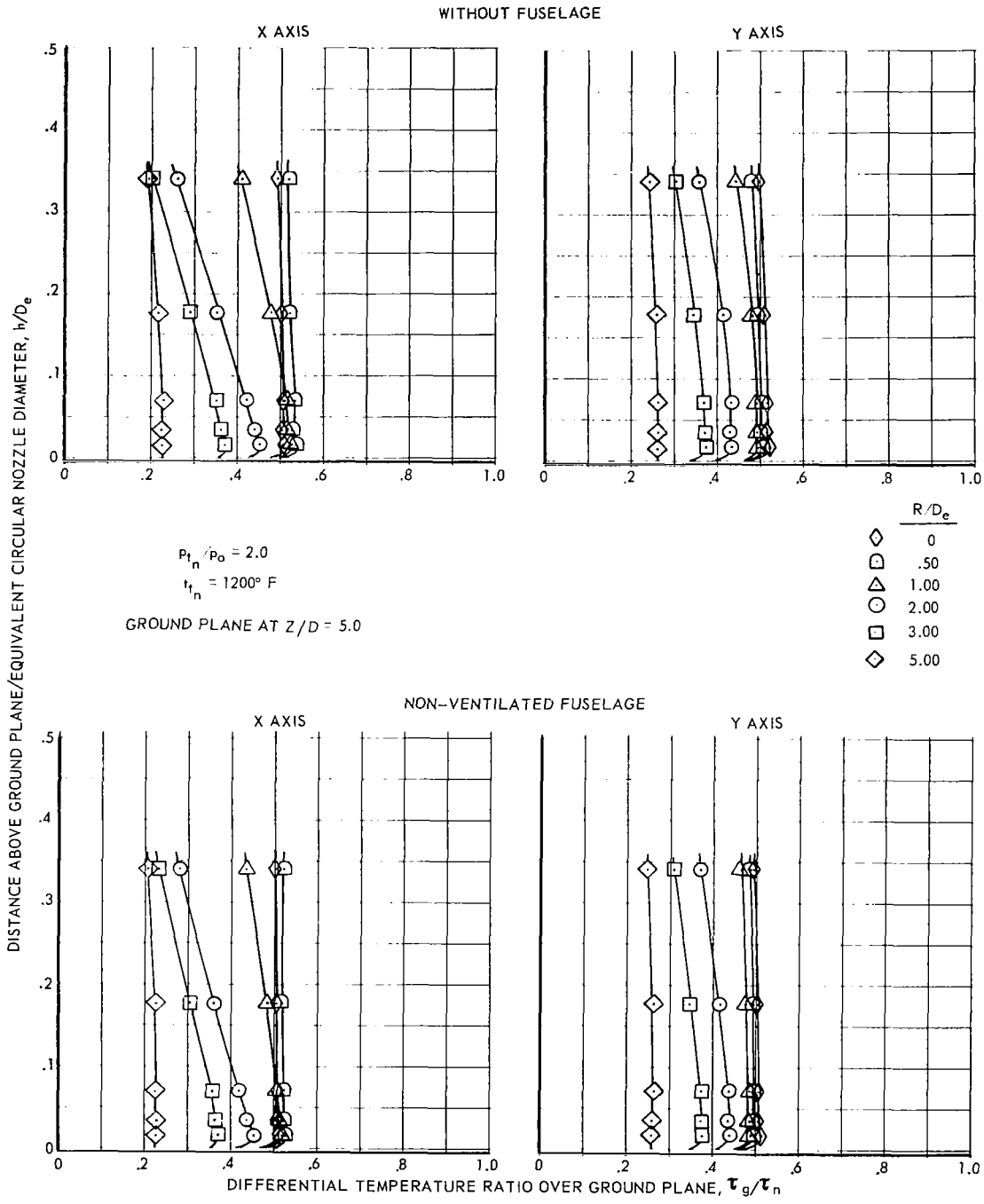

(c) SUPPRESSOR NOZZLE 2.5

Figure 21 - Concluded

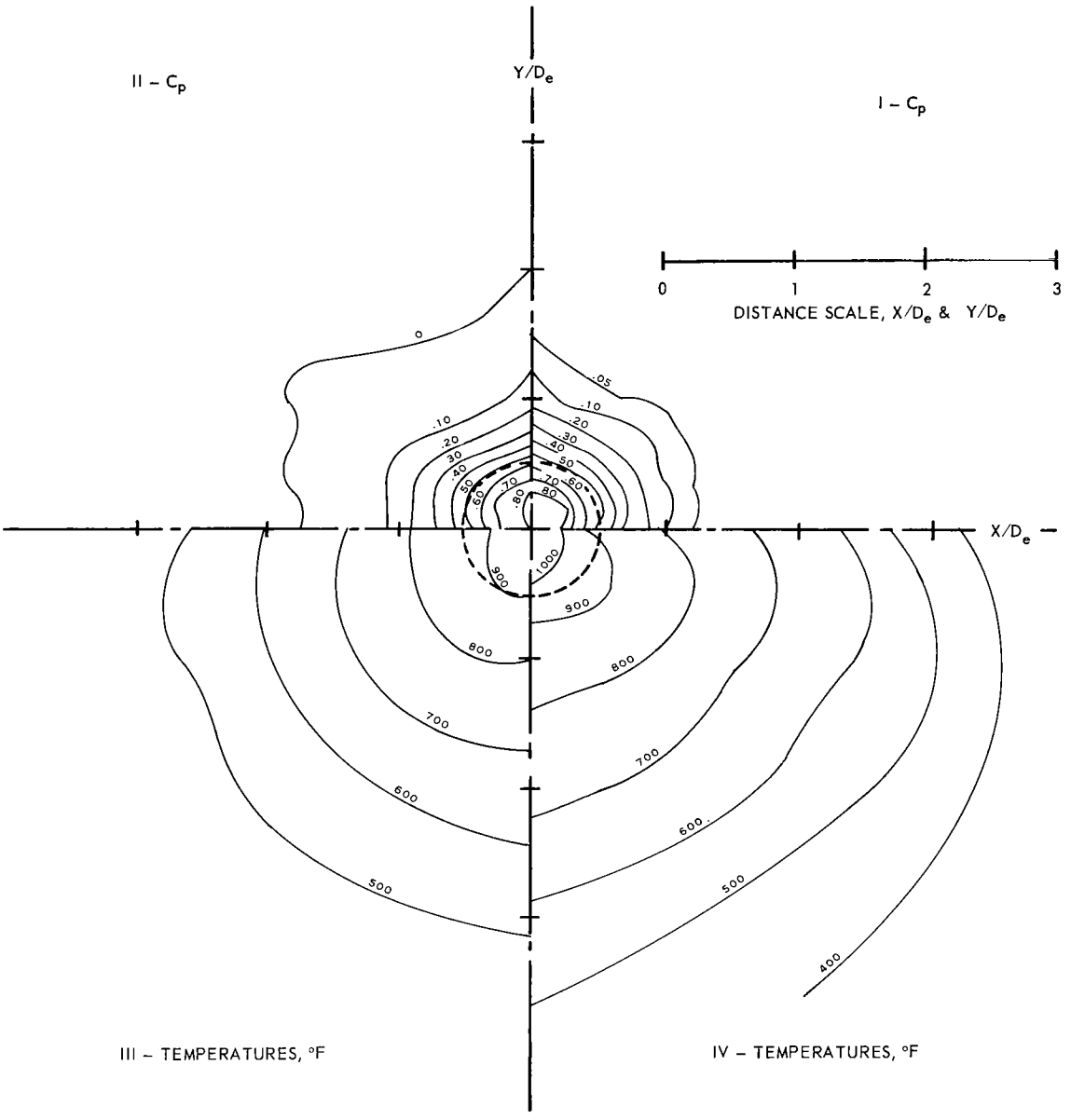

QUADRANT	CONFIGURATION
I AND IV	NOZZLE 1.1 WITHOUT FUSELAGE
II AND III	NOZZLE 1.1 WITH NON-VENTILATED FUSELAGE

P_{t_n}/P_o = 2.0
t_{t_n} = 1200°F
Z/D_e GROUND PLANE = 5.0

(a) CIRCULAR NOZZLE 1.1

Figure 22 - Distribution of surface static pressures and exhaust gas temperatures adjacent to ground plane for various nozzle and fuselage configurations

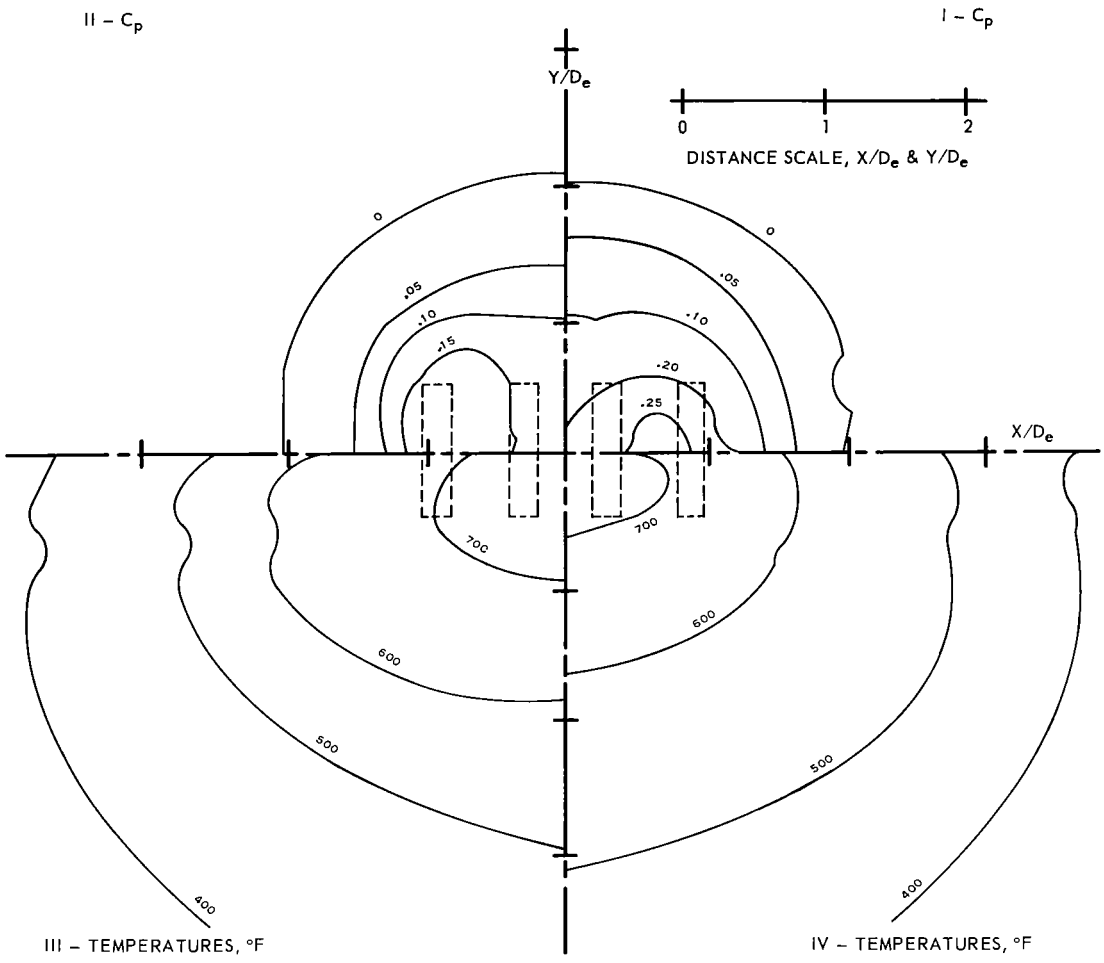

QUADRANT	CONFIGURATION
I AND IV	NOZZLE 2.1 WITH NON-VENTILATED FUSELAGE
II AND III	NOZZLE 2.5 WITH NON-VENTILATED FUSELAGE

P_{t_n}/P_o = 2.0

t_{t_n} = 1200°F

Z/D_e GROUND PLANE = 5.0

(b) SUPPRESSOR NOZZLES 2.1 AND 2.5

Figure 22 - Concluded

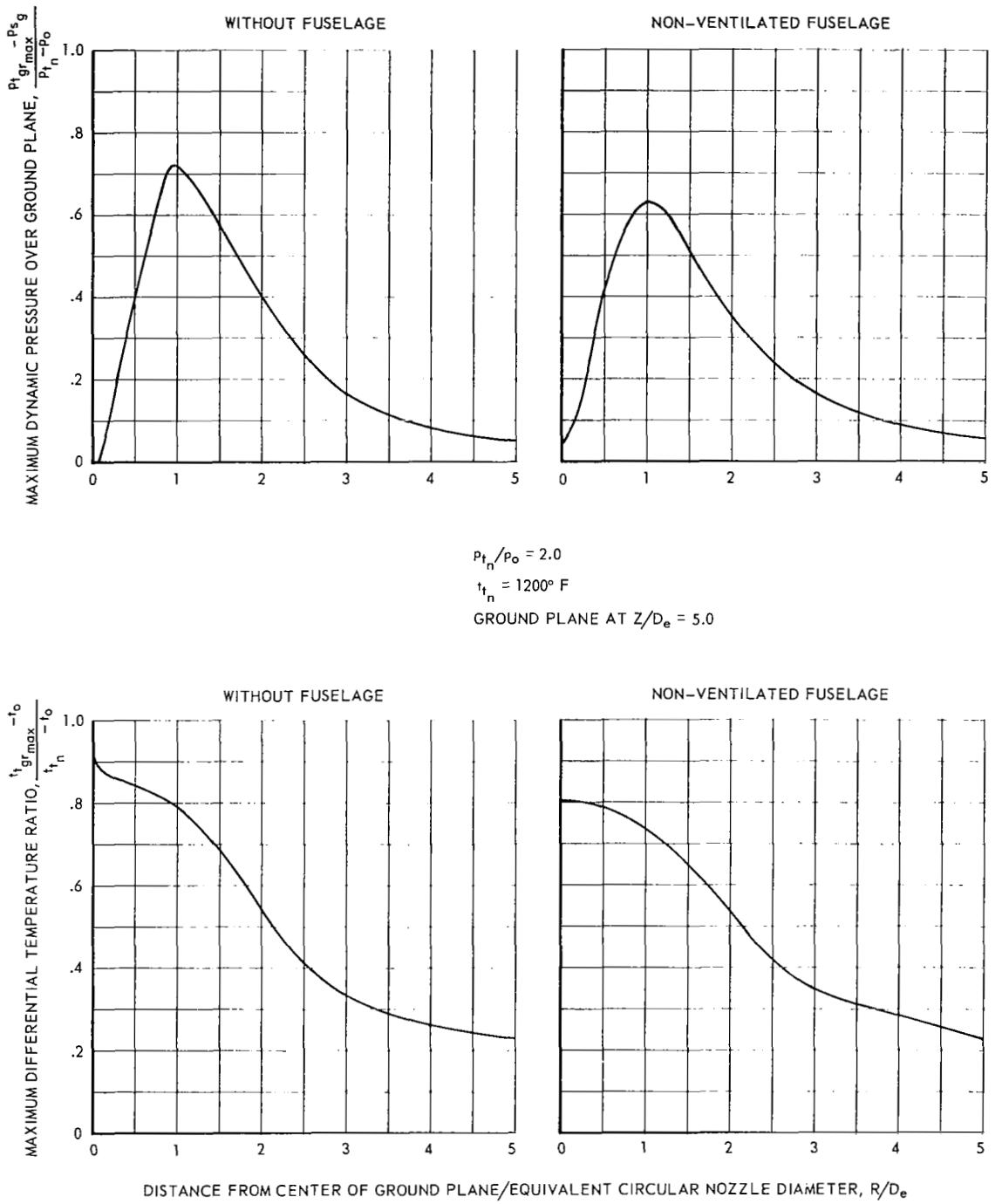

(a) CIRCULAR NOZZLE 1.1

Figure 23 - Radial distribution of maximum dynamic pressures and differential temperatures in the efflux over the ground plane for various nozzle and fuselage configurations

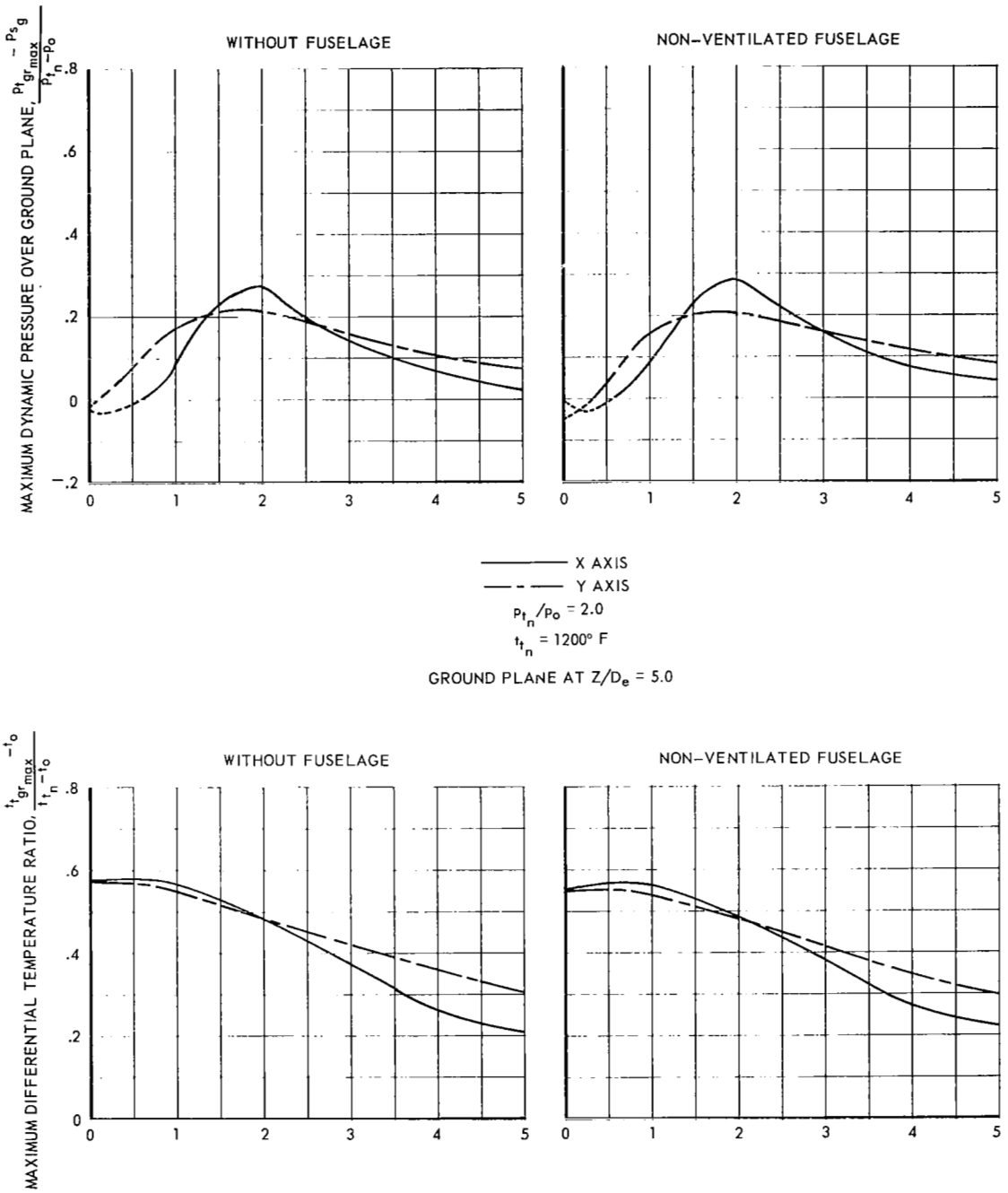

(b) SUPPRESSOR NOZZLE 2.1

Figure 23 - Continued

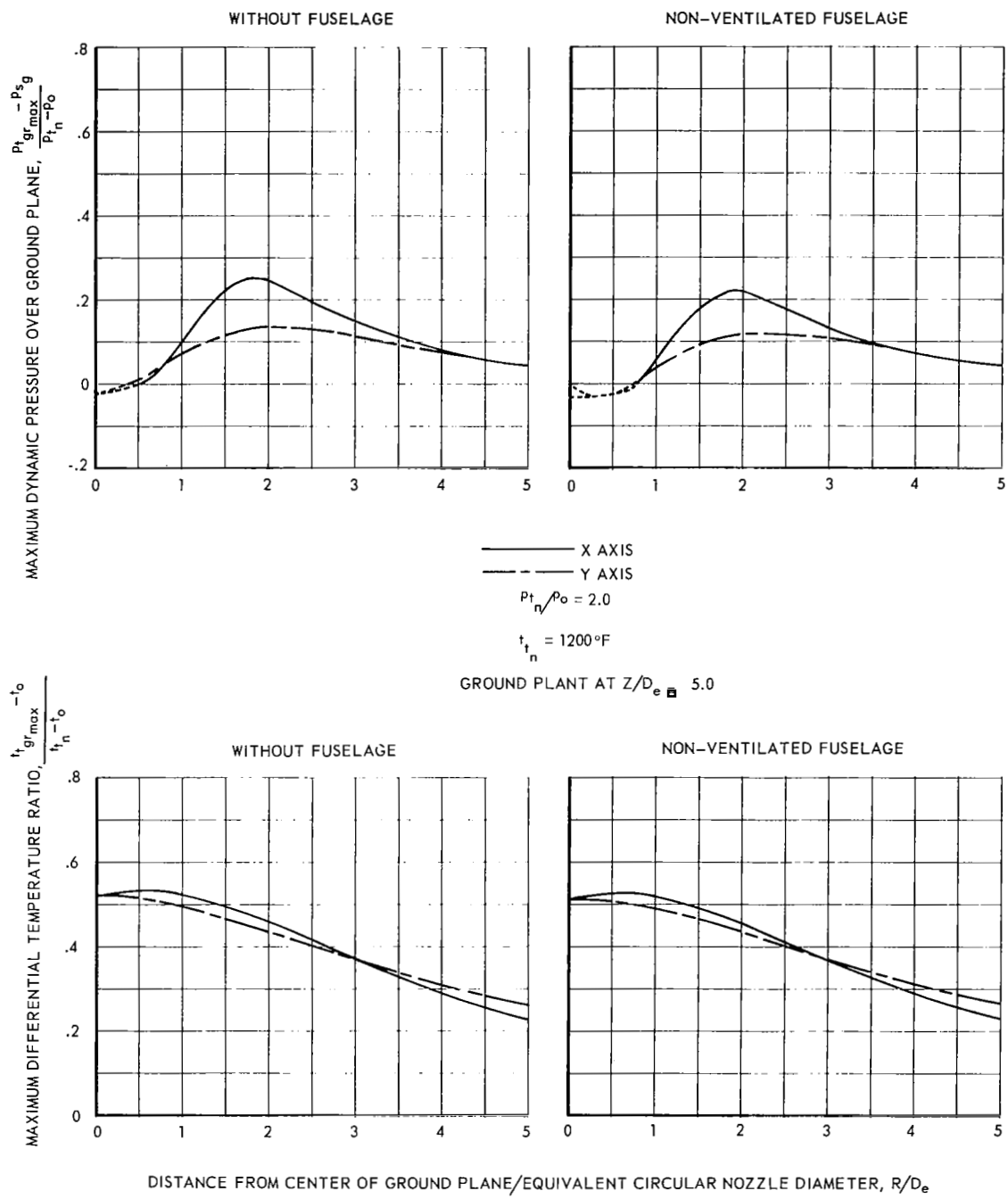

(c) SUPPRESSOR NOZZLE 2.5

Figure 23 - Concluded

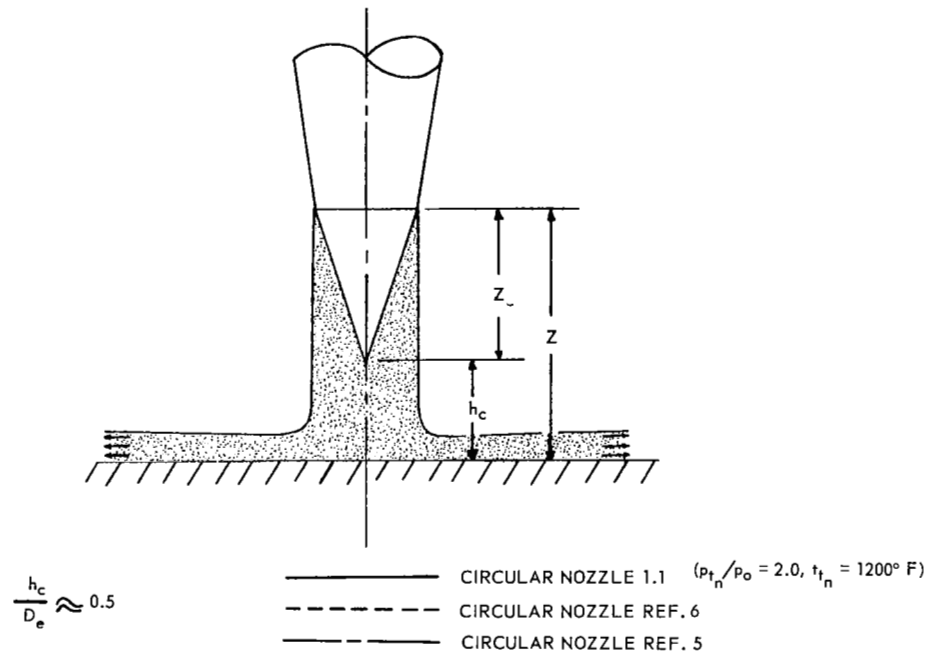

Figure 24 - Radial variation of local dynamic pressure over ground plane for various investigations

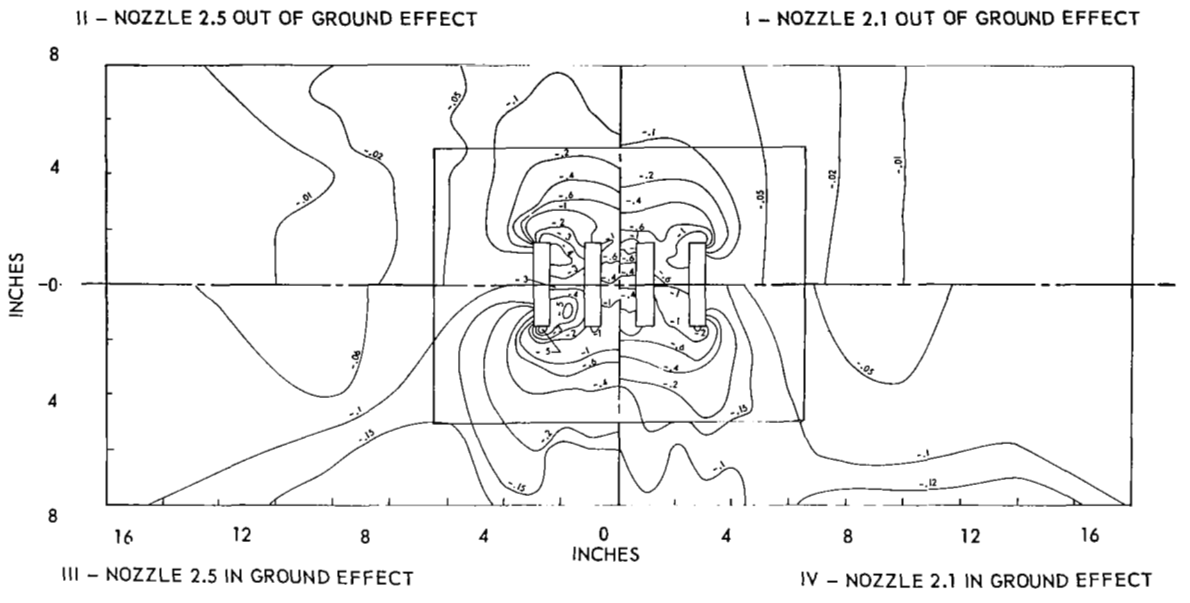

VALUE OF C_p SHOWN ARE ACTUAL VALUES X 100

(a) STATIC PRESSURE DISTRIBUTION ON THE LOWER FUSELAGE SURFACE, C_p

$P_{t_n}/P_o = 2.0$

$t_{t_n} = 1200\ ^\circ F$

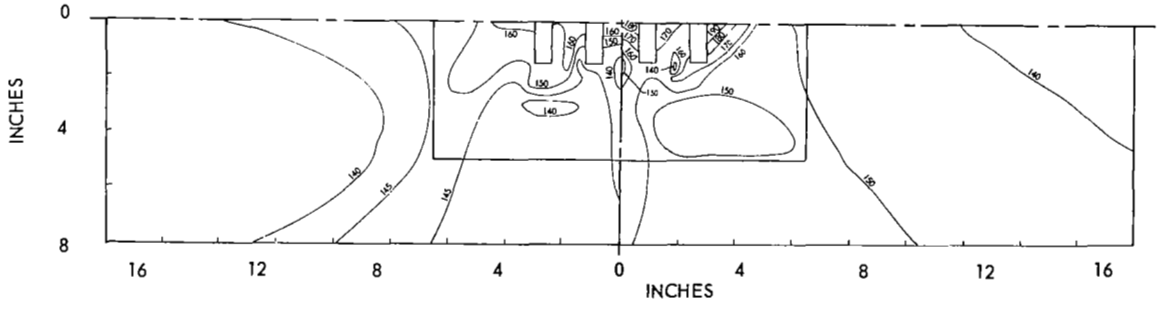

(b) TEMPERATURE DISTRIBUTION ADJACENT TO THE LOWER FUSELAGE SURFACE, °F

Figure 25 - Static pressure and temperature distributions on lower surface of non-ventilated fuselage for various nozzle configurations

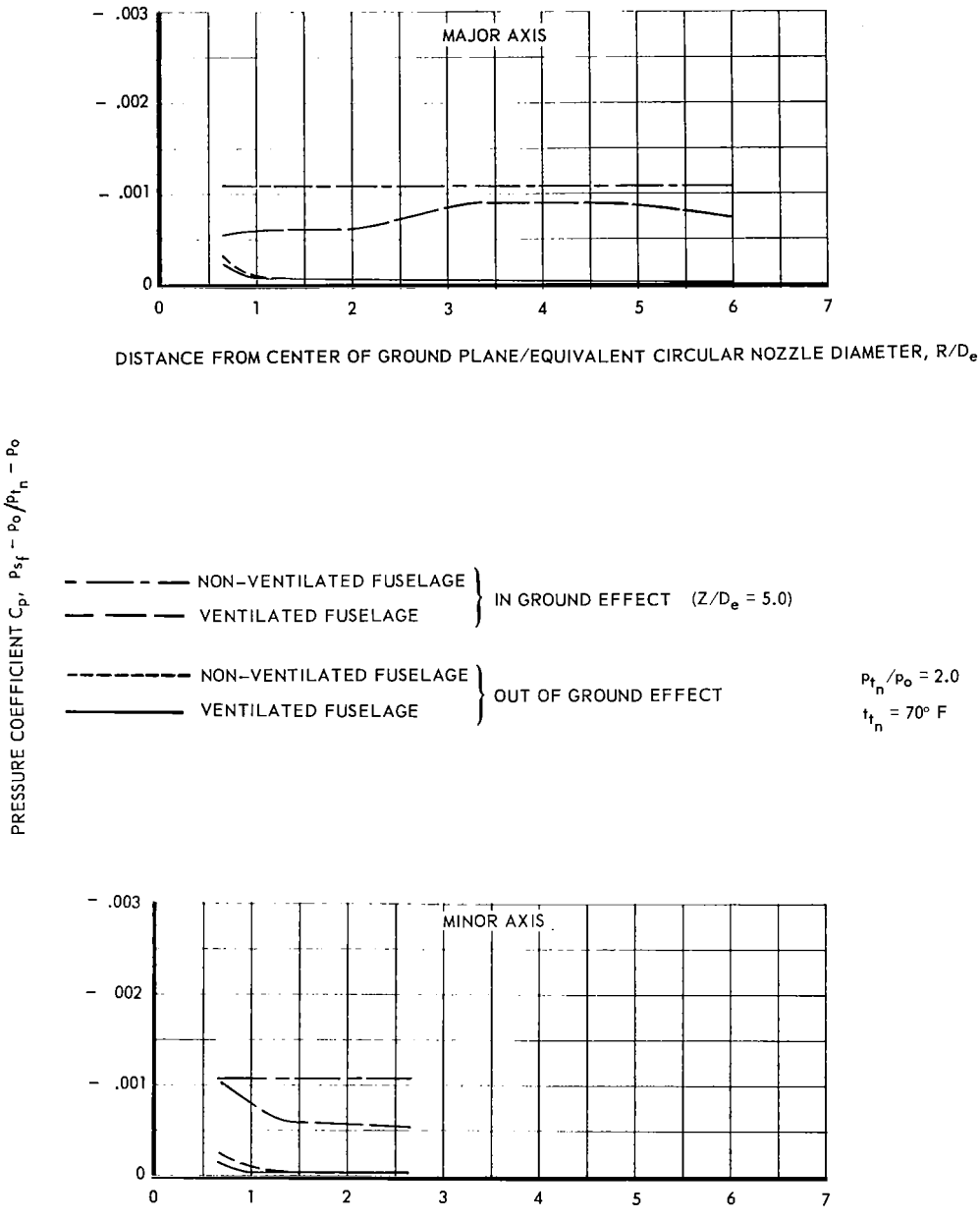

(a) CIRCULAR NOZZLE 1.1

Figure 26 - Radial distribution of pressures induced on the lower surface of the fuselage by the jet

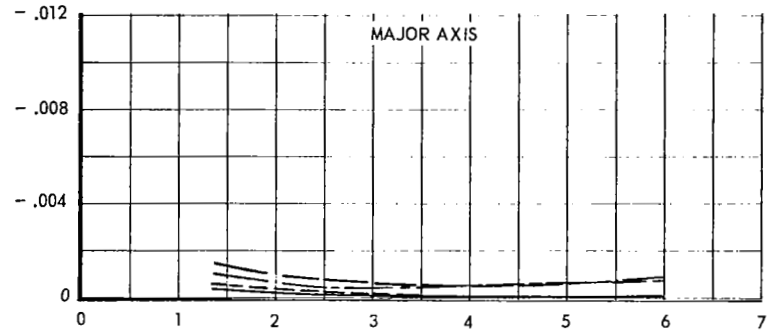

DISTANCE FROM CENTER OF GROUND PLANE/EQUIVALENT CIRCULAR NOZZLE DIAMETER, R/D_e

PRESSURE COEFFICIENT C_p, $P_{s_f} - P_o/P_{t_n} - P_o$

NON-VENTILATED FUSELAGE
VENTILATED FUSELAGE
} IN GROUND EFFECT ($Z/D_e = 5.0$)

NON-VENTILATED FUSELAGE
VENTILATED FUSELAGE
} OUT OF GROUND EFFECT

$P_{t_n}/P_o = 2.0$

$t_{t_n} = 70°$ F

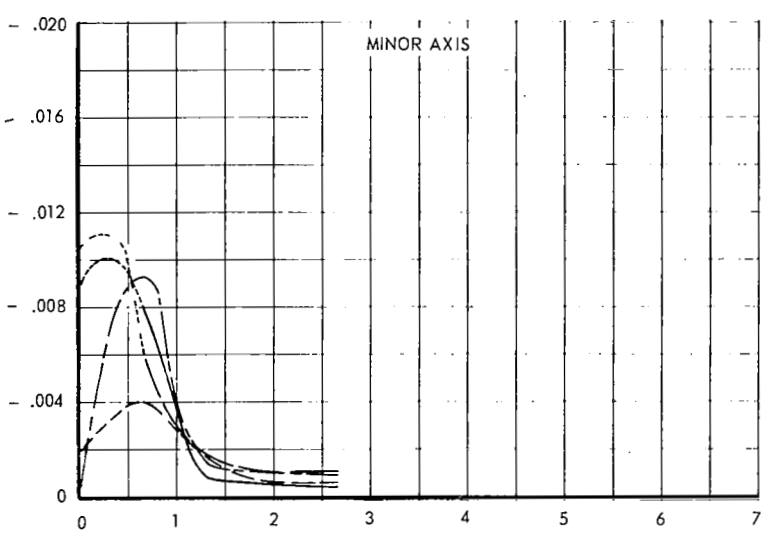

DISTANCE FROM CENTER OF GROUND PLANE/EQUIVALENT CIRCULAR NOZZLE DIAMETER, R/D_e

(b) SUPPRESSOR NOZZLE 2.1

Figure 26 - Continued

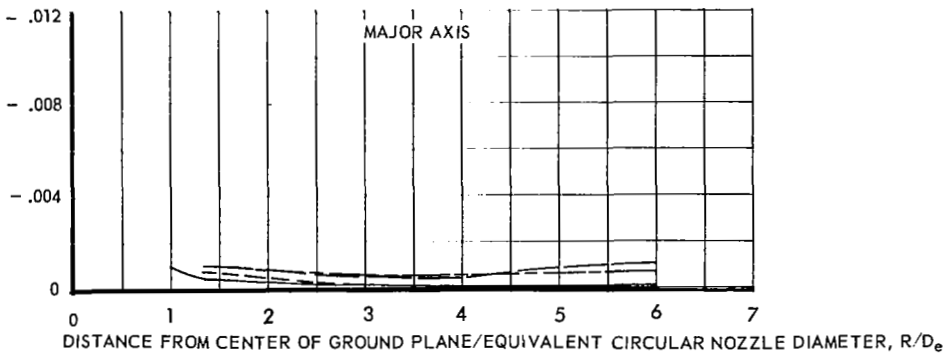

PRESSURE COEFFICIENT C_p, $P_{s_f} - P_o / P_{t_n} - P_o$

NON-VENTILATED FUSELAGE
VENTILATED FUSELAGE
} IN GROUND EFFECT ($Z/D_e = 5.0$)

NON-VENTILATED FUSELAGE
VENTILATED FUSELAGE
} OUT OF GROUND EFFECT

$P_{t_n}/P_o = 2.0$
$t_{t_n} = 70°$ F

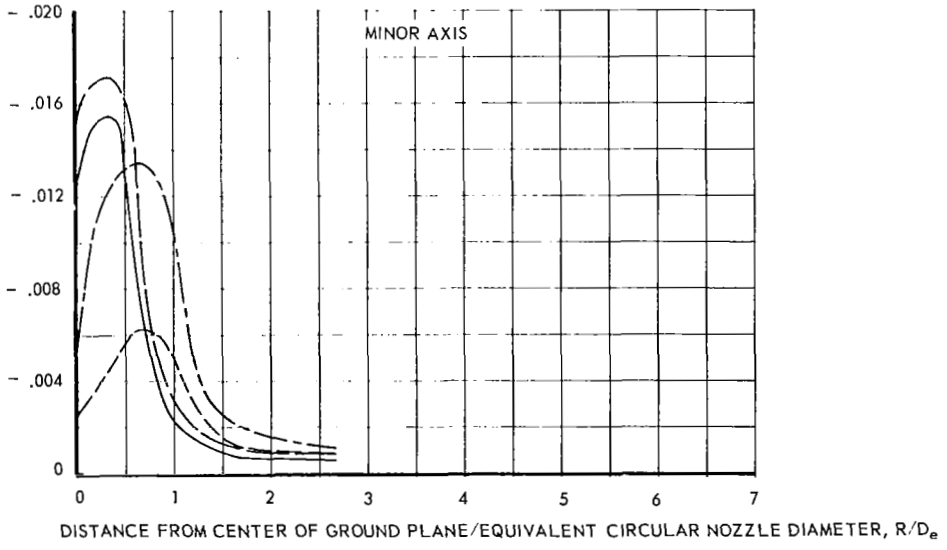

(c) SUPPRESSOR NOZZLE 2.5

Figure 26 - Concluded

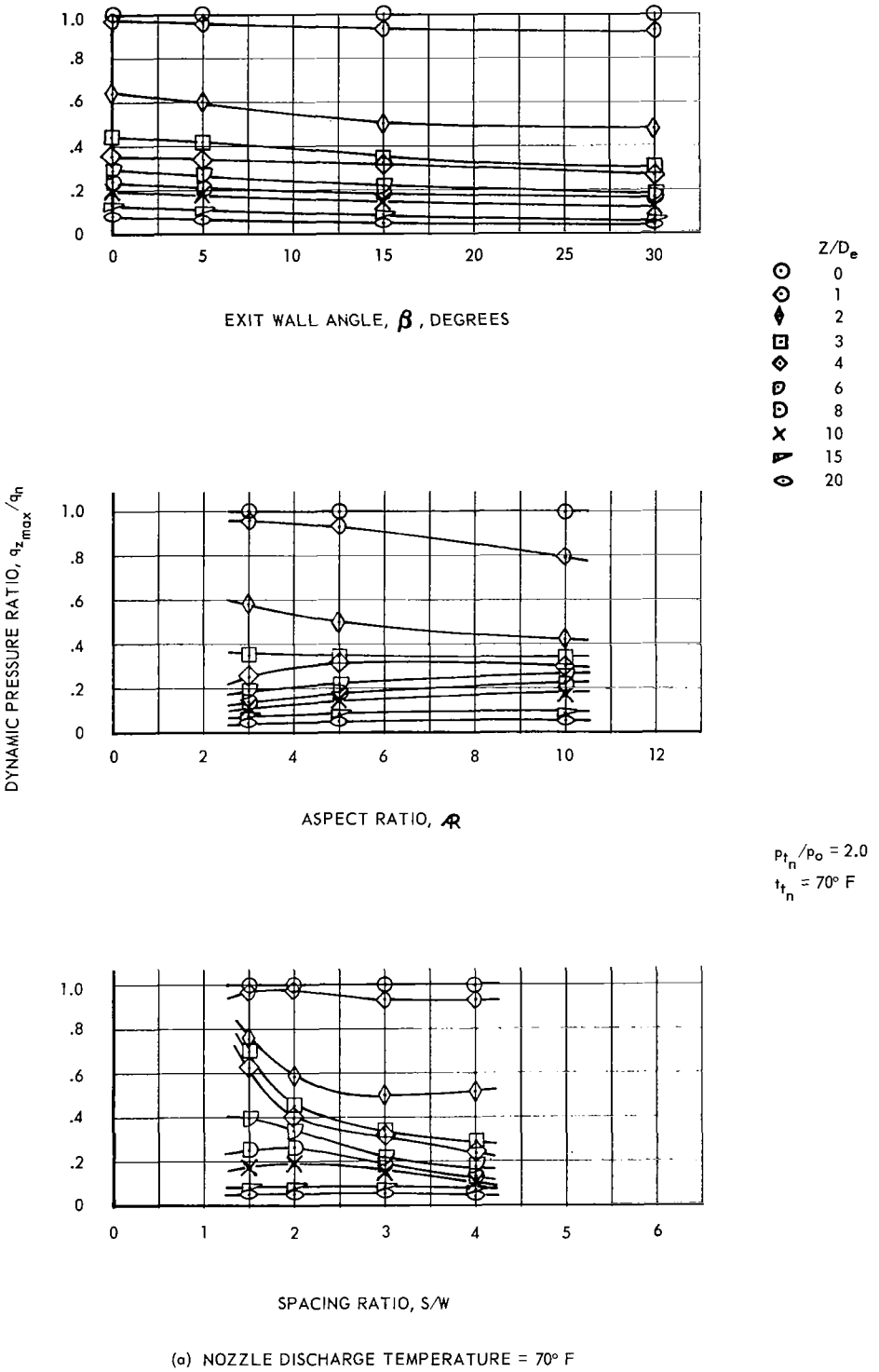

(a) NOZZLE DISCHARGE TEMPERATURE = 70° F

Figure 27 - Dynamic pressure degradation versus exit wall angle, aspect ratio, and spacing ratio for all basic suppressor nozzles out of ground effect

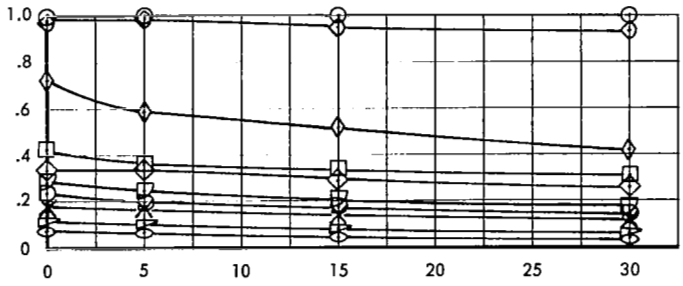

EXIT WALL ANGLE, β , DEGREES

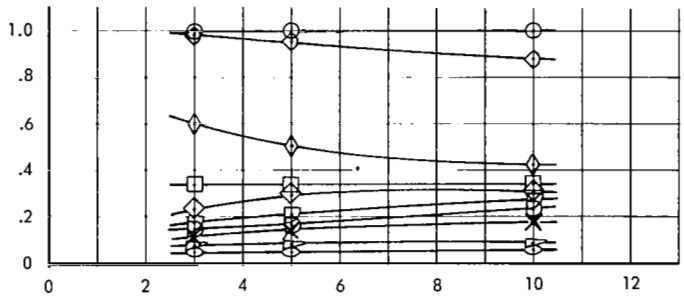

ASPECT RATIO, AR

$P_{t_n}/P_o = 2.0$

$t_{t_n} = 1200°$ F

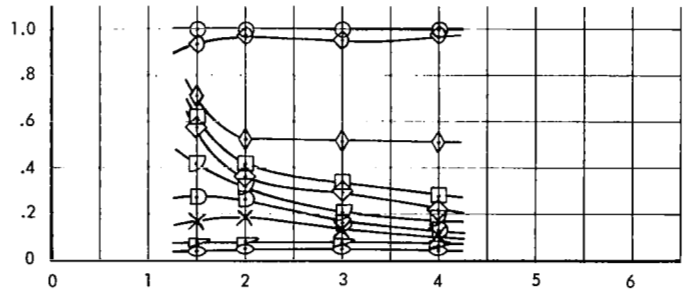

SPACING RATIO, S/W

(b) NOZZLE DISCHARGE TEMPERATURE = 1200° F

Figure 27 - Concluded

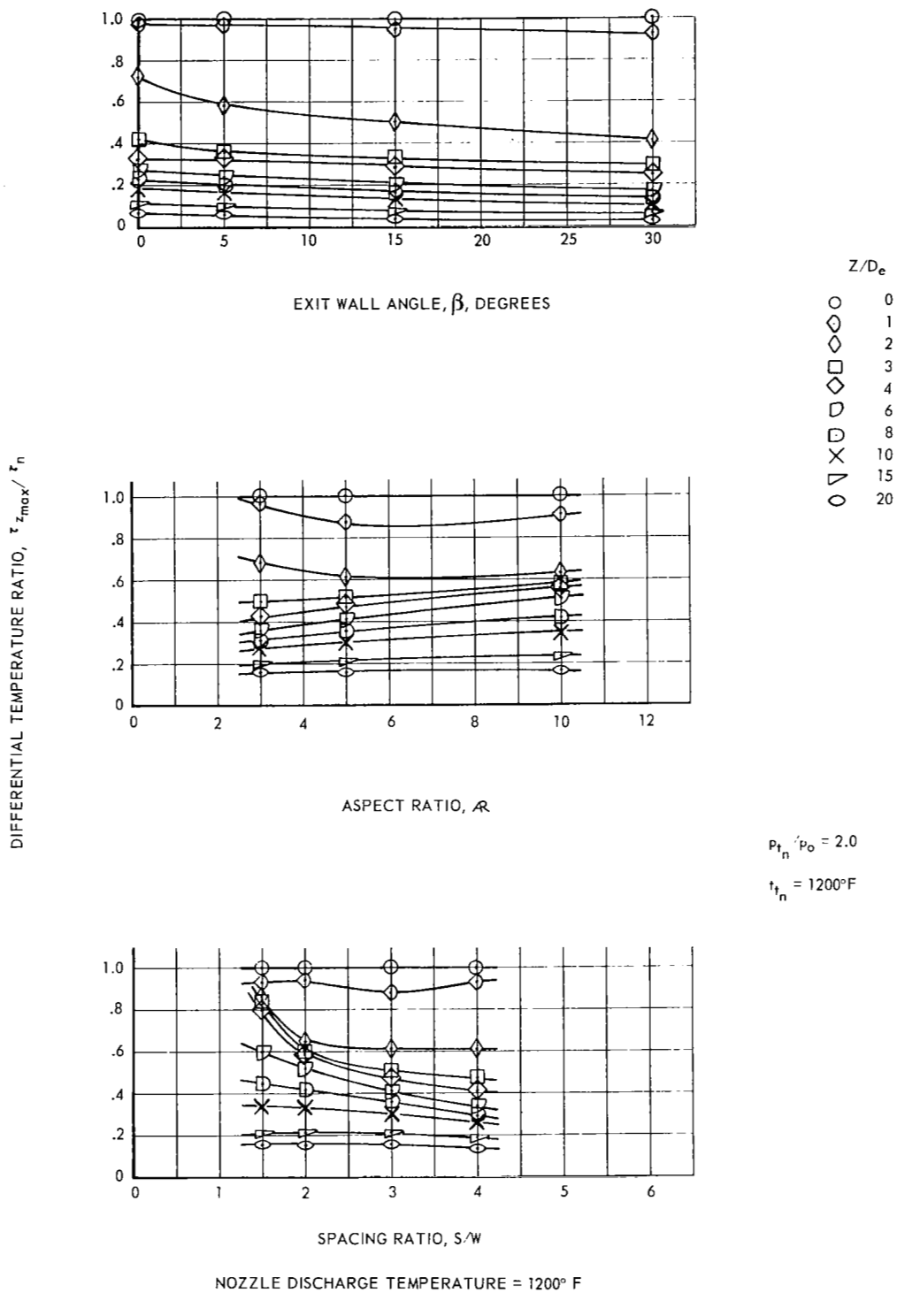

Figure 28 - Differential temperature degradation versus exit wall angle, aspect ratio, and spacing ratio for all basic suppressor nozzles out of ground effect

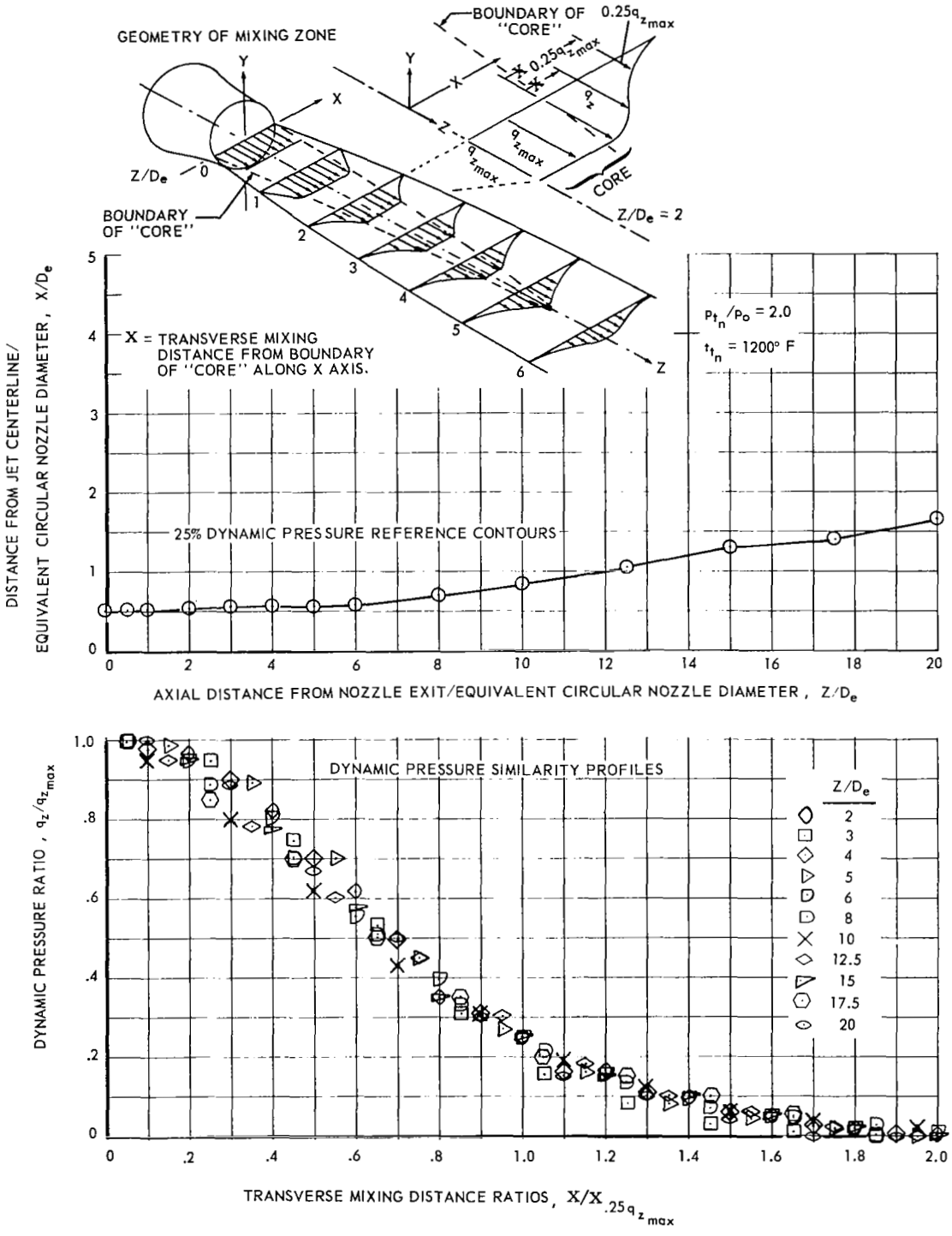

(a) CIRCULAR NOZZLE 1.1 – DYNAMIC PRESSURE RATIO

Figure 29 - Jet wake dynamic pressure and differential temperature reference contours and similarity profiles of several basic nozzles out of ground effect

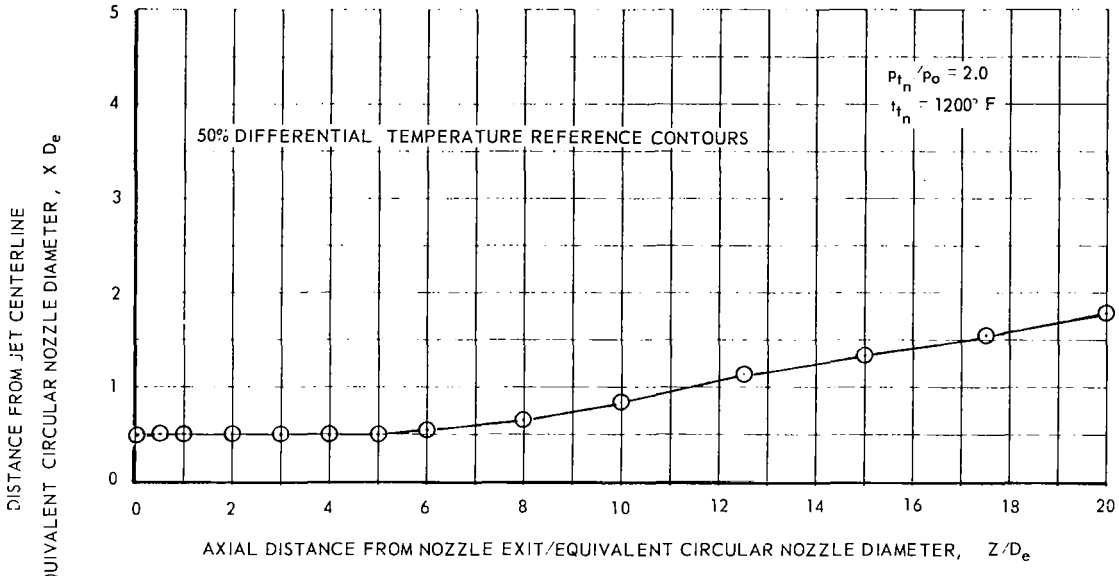

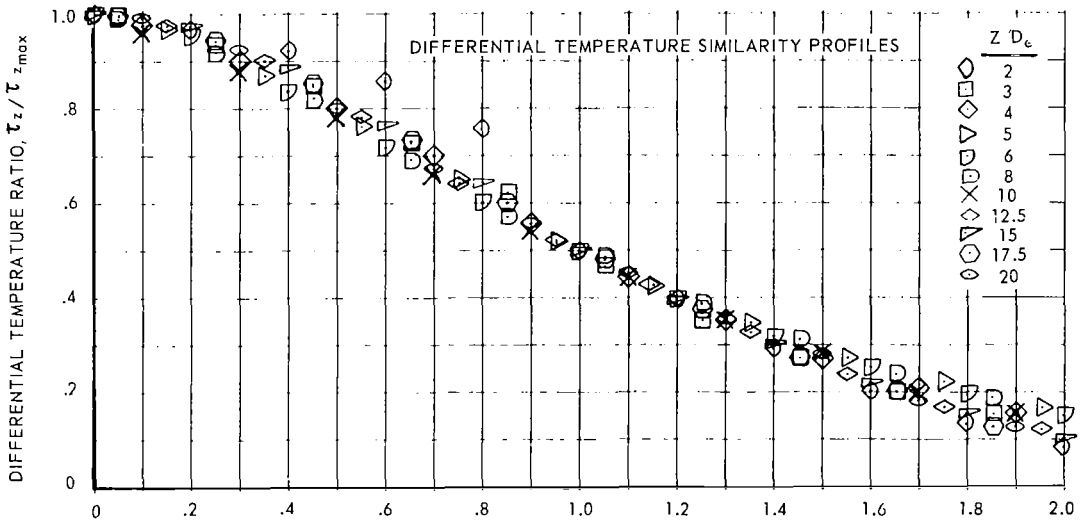

(b) CIRCULAR NOZZLE 1.1 – DIFFERENTIAL TEMPERATURE RATIO

Figure 29 - Continued

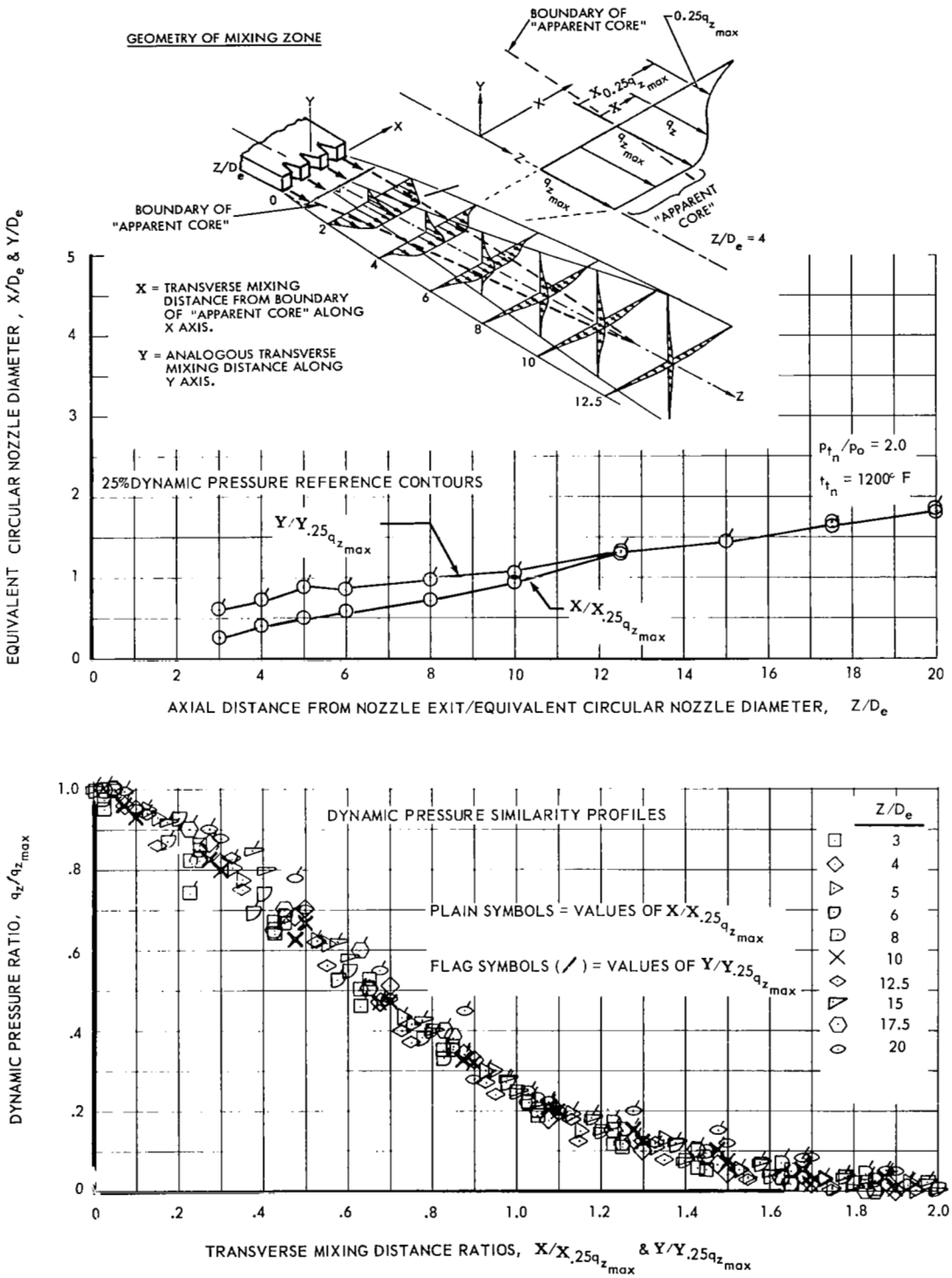

(c) NOZZLE 2.1 – DYNAMIC PRESSURE RATIO

Figure 29 – Continued

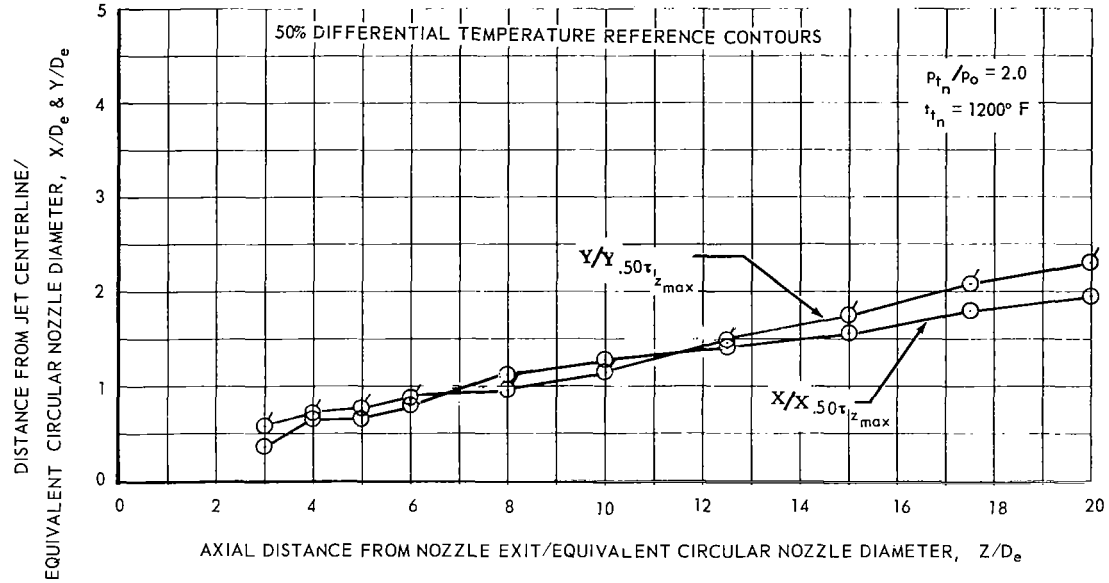

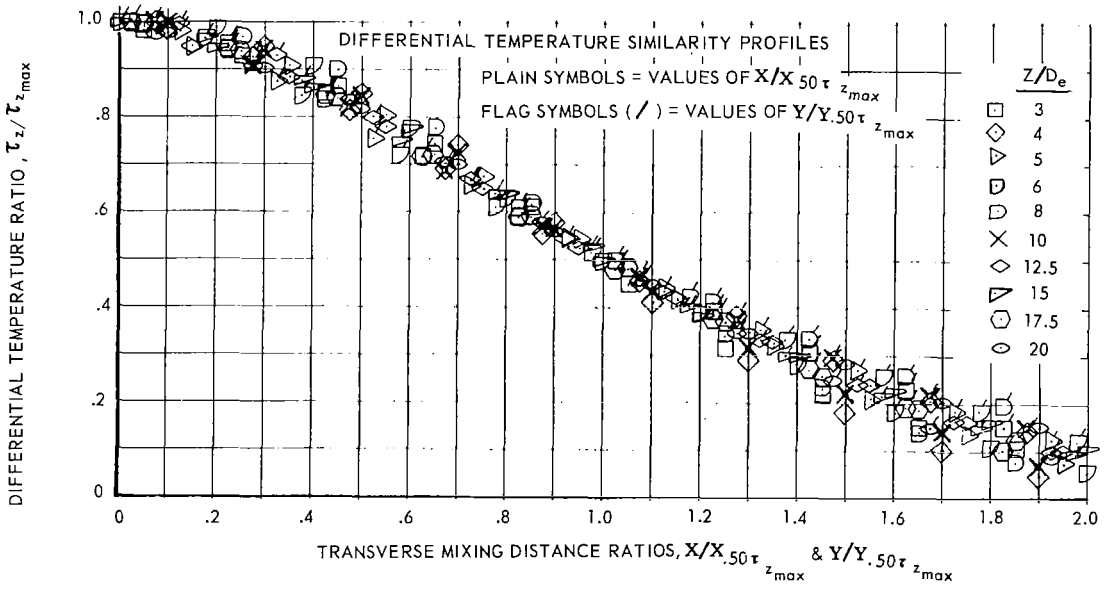

(d) NOZZLE 2.1 – DIFFERENTIAL TEMPERATURE RATIO

Figure 29 - Continued

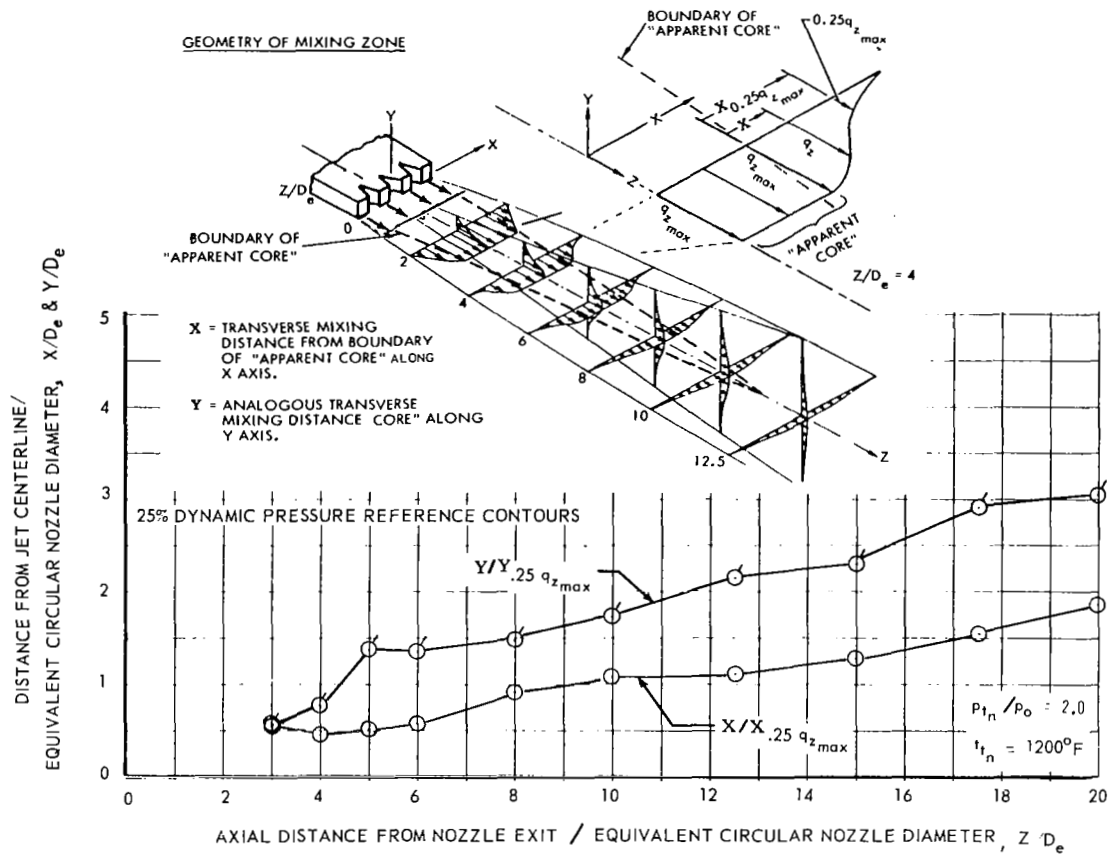

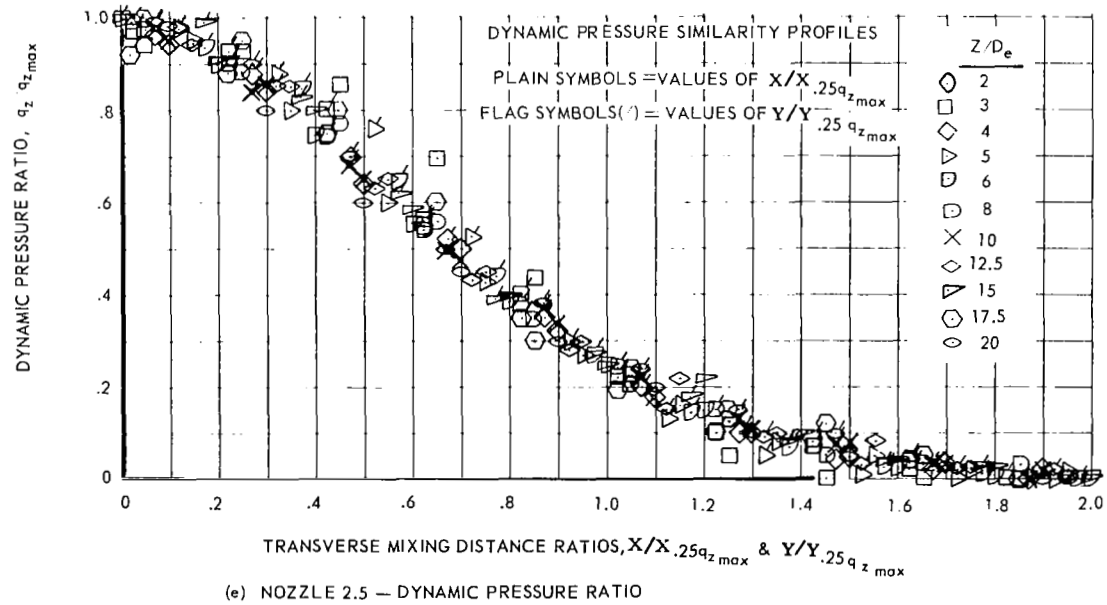

(e) NOZZLE 2.5 — DYNAMIC PRESSURE RATIO

Figure 29 - Continued

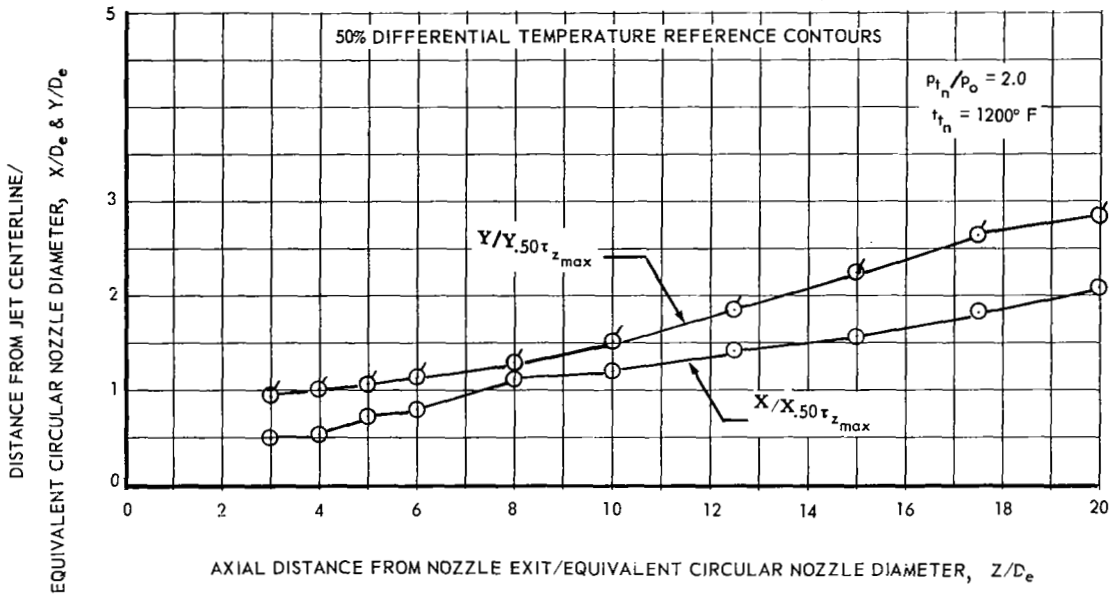

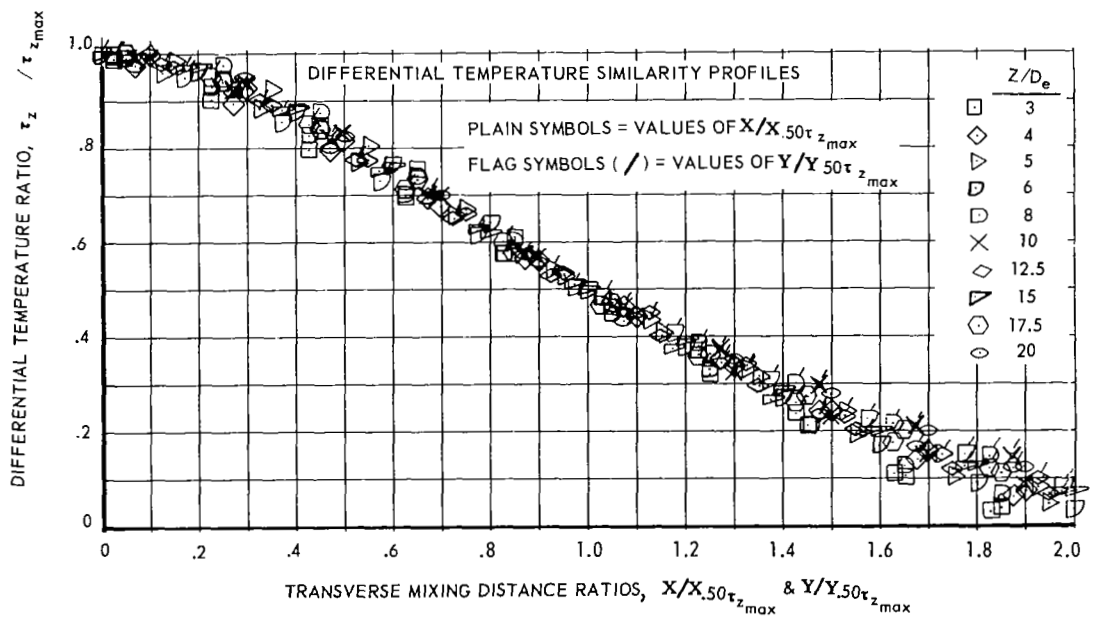

(f) NOZZLE 2.5 – DIFFERENTIAL TEMPERATURE RATIO

Figure 29 - Concluded

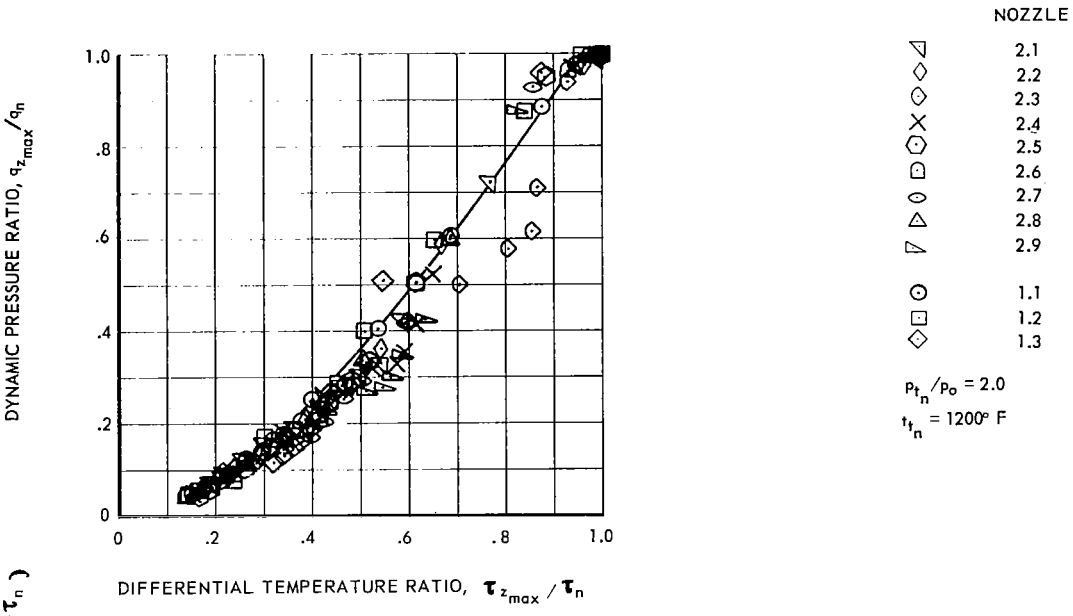

(a) DYNAMIC PRESSURE RATIO VERSUS DIFFERENTIAL TEMPERATURE RATIO

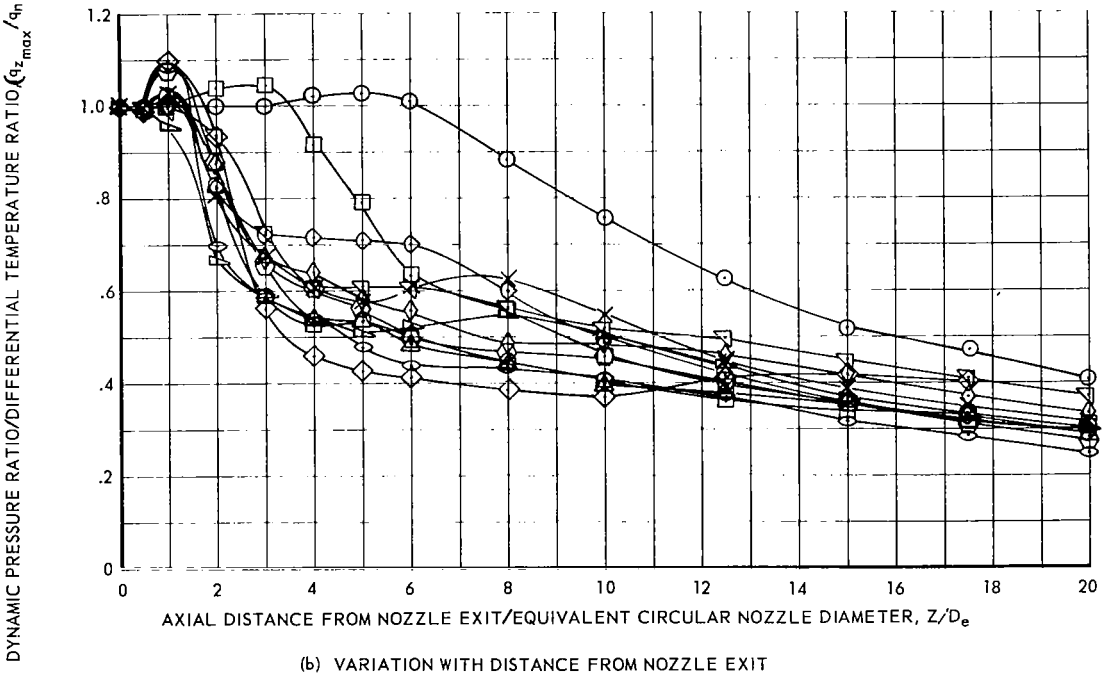

(b) VARIATION WITH DISTANCE FROM NOZZLE EXIT

Figure 30 - Comparison of dynamic pressure degradation with differential temperature degradation for all basic nozzles out of ground effect

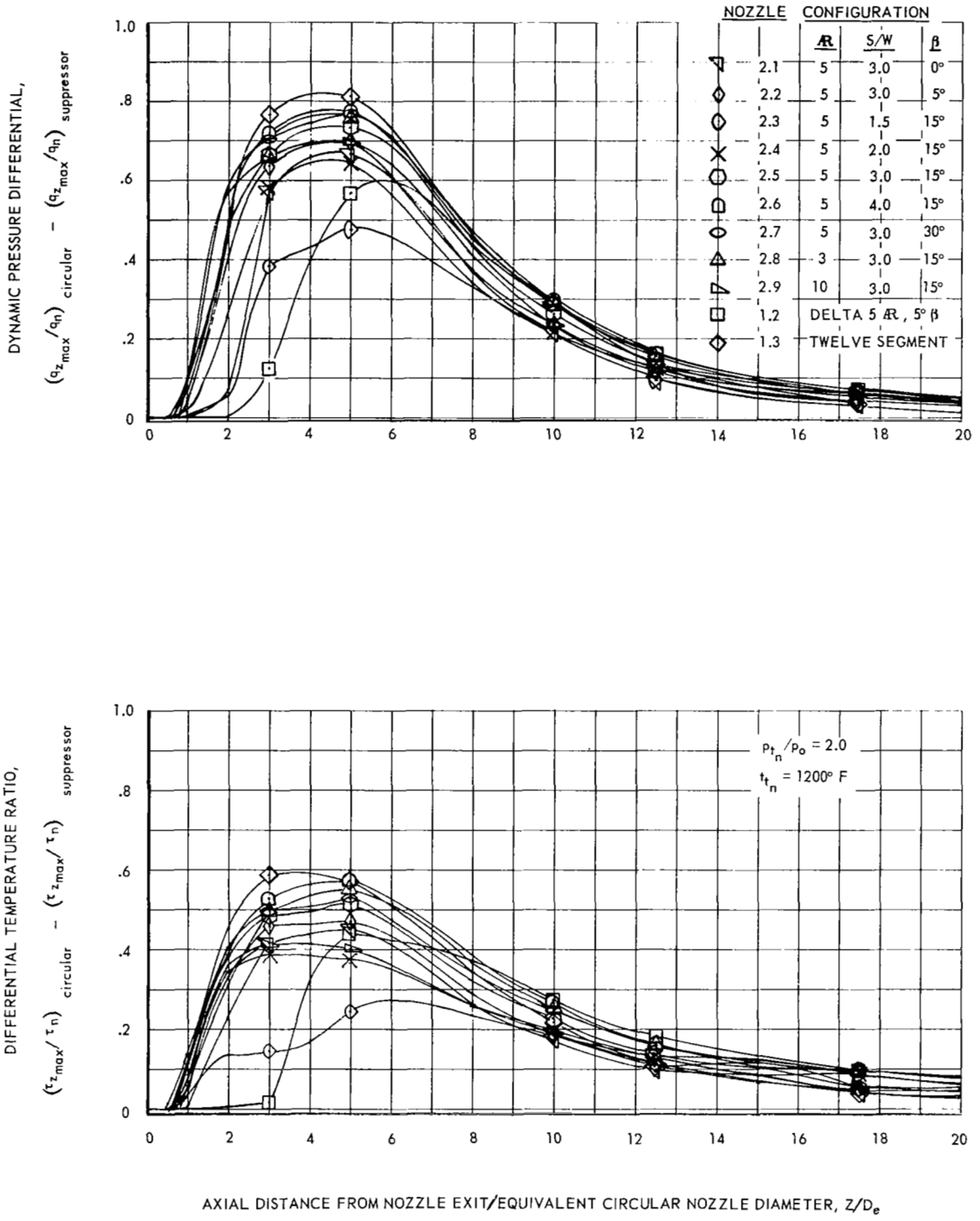

Figure 31 - Jet wake degradation characteristics of suppressor nozzles relative to the degradation characteristics of a circular nozzle for all basic nozzles out of ground effect

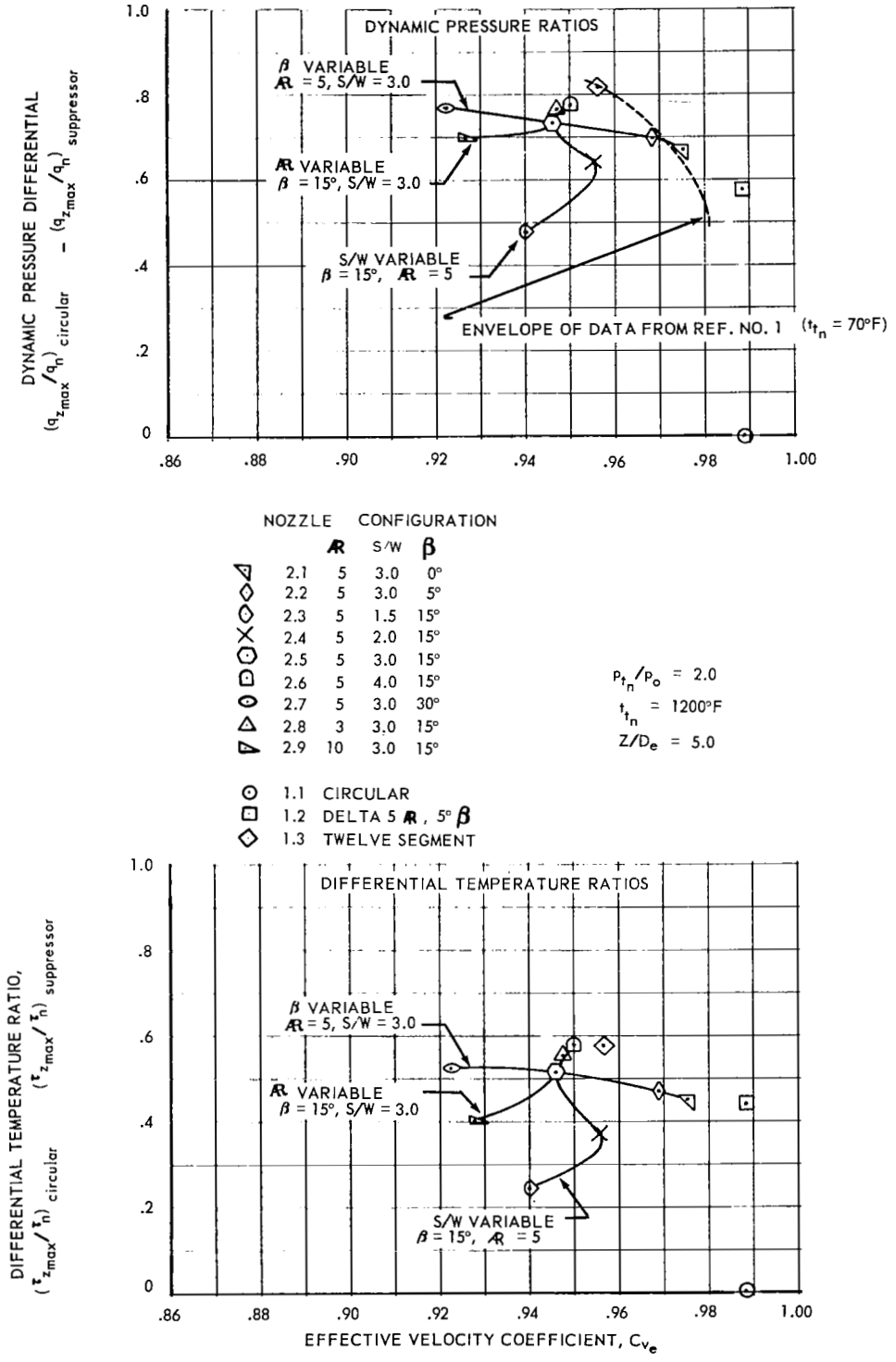

Figure 32 - Jet wake degradation versus thrust of basic nozzles for free jet tests

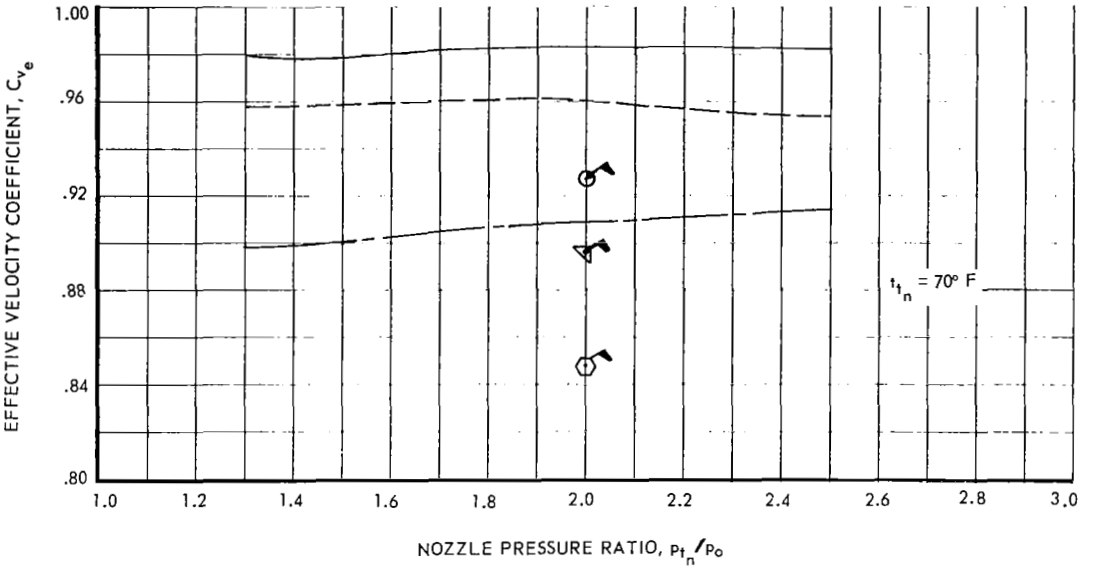

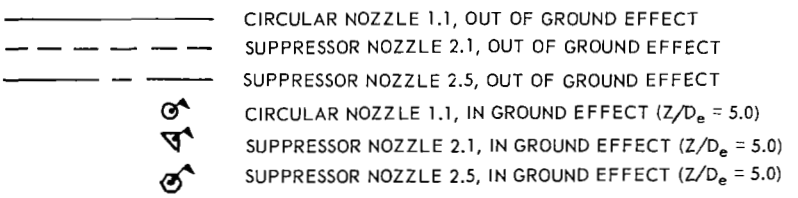

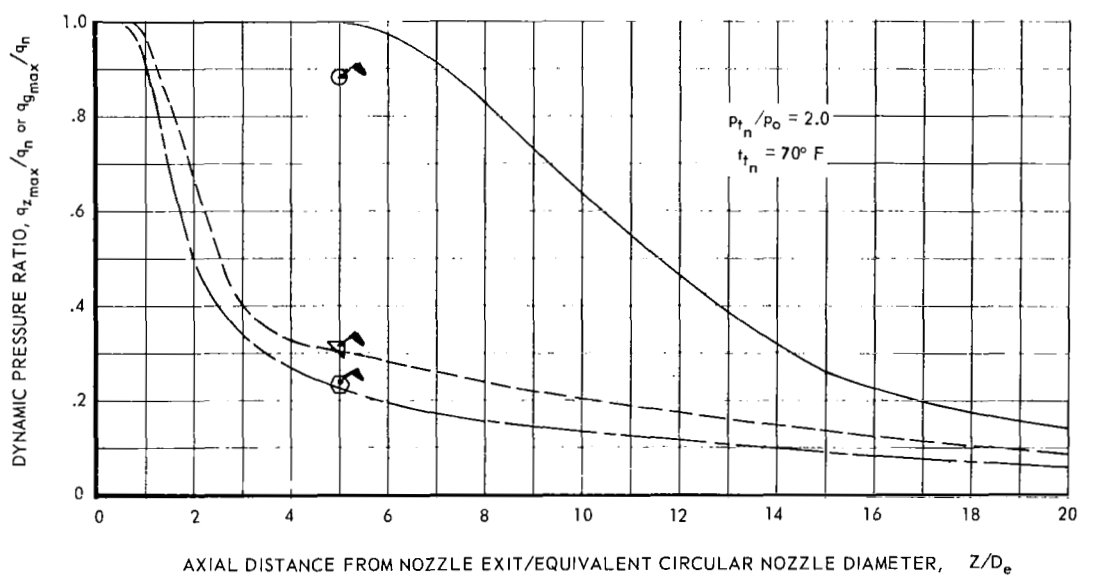

Figure 33 - Comparison of thrust and dynamic pressure degradation of nozzles 1.1, 2.1, and 2.5 with non-ventilated fuselage in and out of ground effect

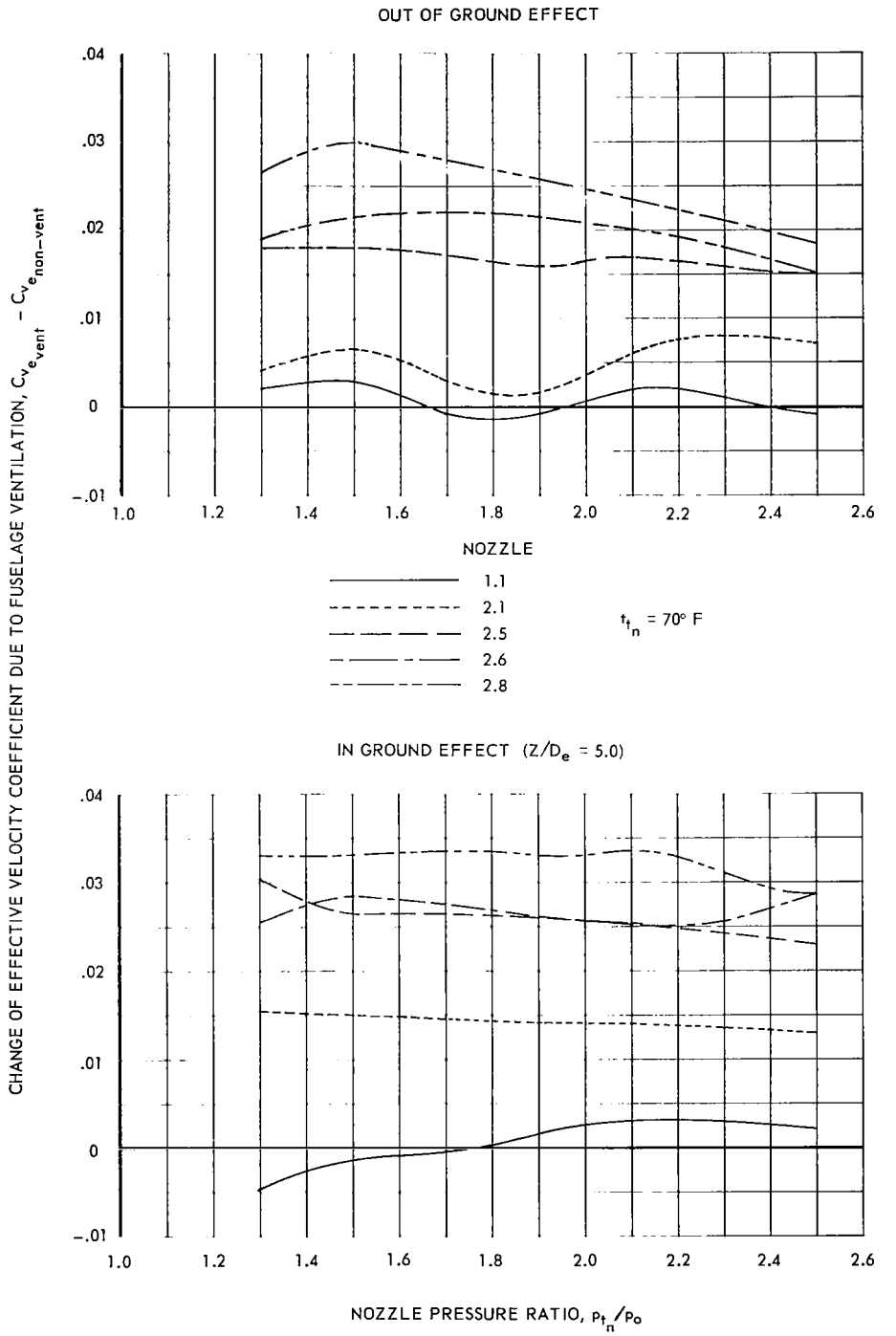

Figure 34 - Effect of fuselage ventilation on effective velocity coefficients for various nozzle and fuselage configurations

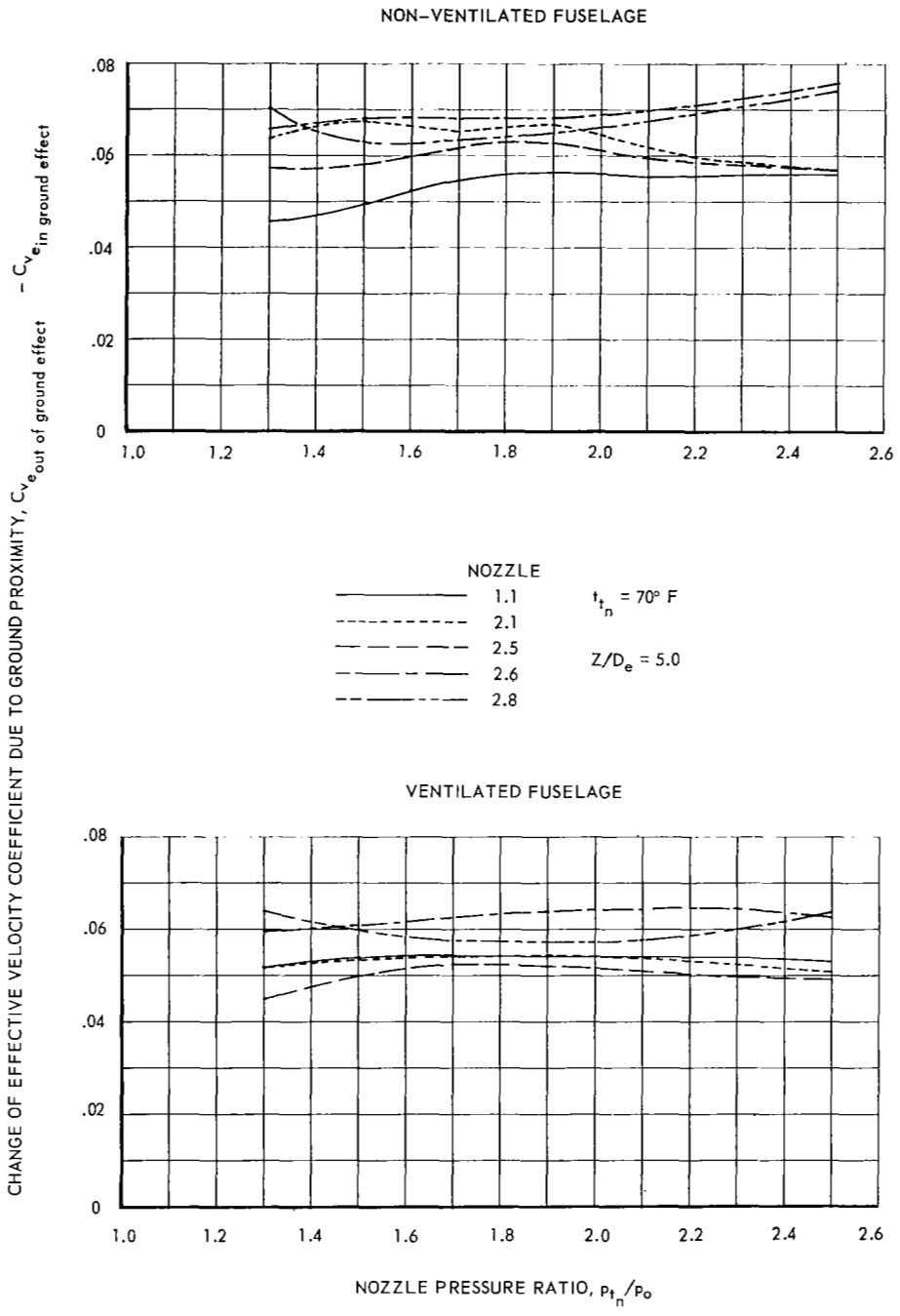

Figure 35 - Effect of ground proximity on effective velocity coefficients of various nozzle and fuselage configurations

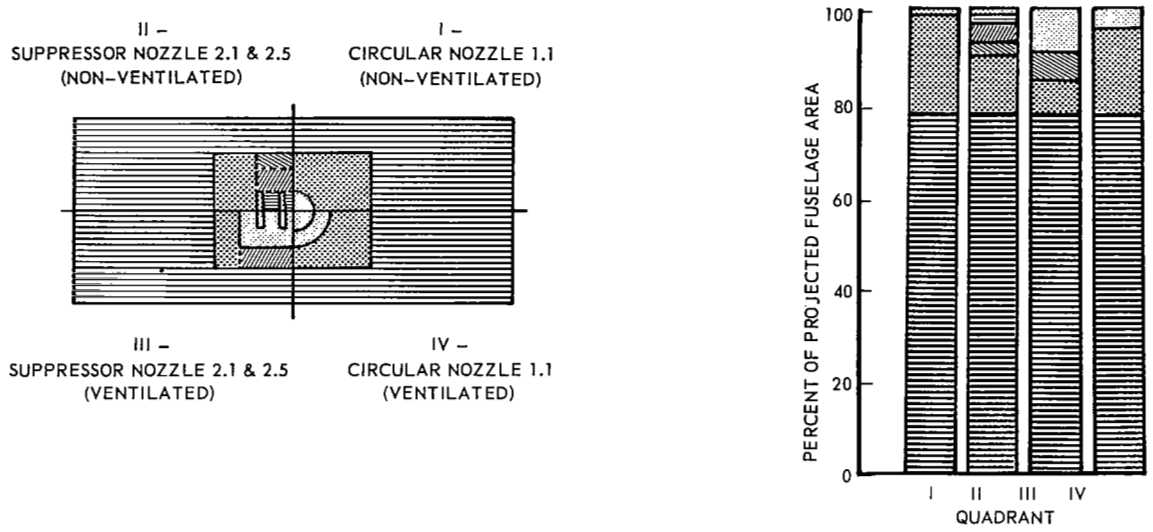

Figure 36 – Relative distribution of thrust losses for various nozzle and fuselage configurations

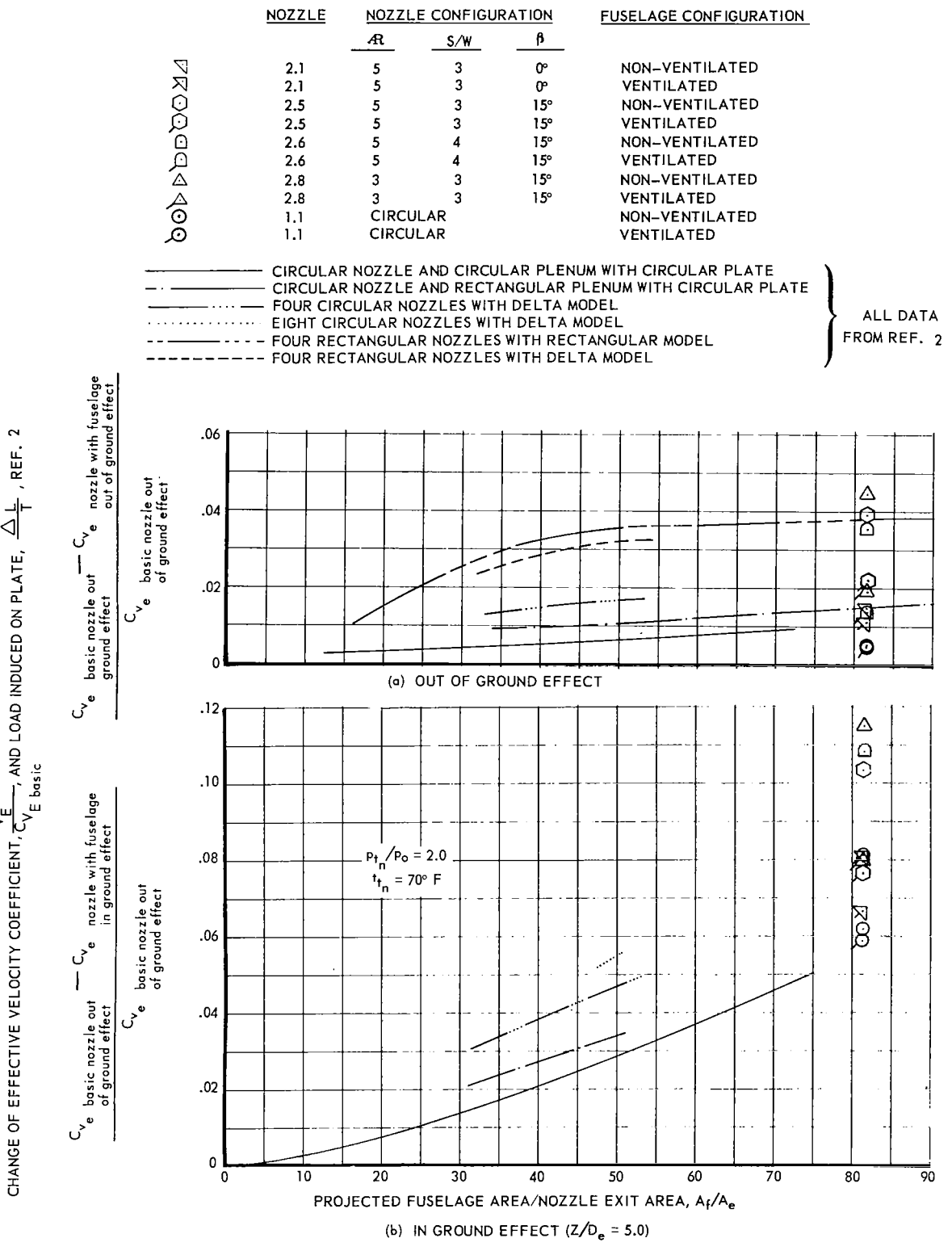

Figure 37 - Thrust losses attributed to the fuselage for various fuselage and nozzle configurations in and out of ground effect

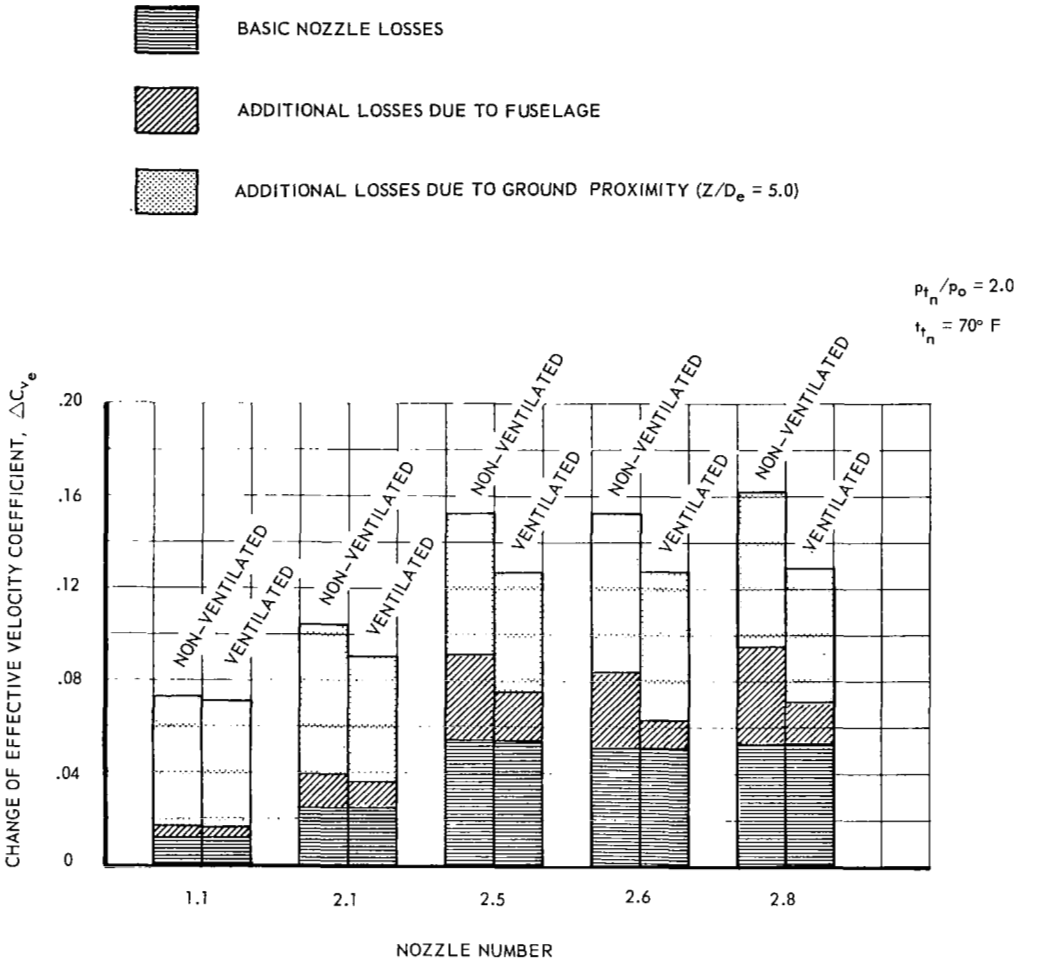

Figure 38 - Summary of thrust losses for various nozzle and fuselage configurations